Final Report
Grant NGR-01-002-036
August 31, 1968

BUREAU OF ENGINEERING RESEARCH

STUDY OF INEXACT MODELING TECHNIQUES

by

Dr. Harold Mott
Professor of Electrical Engineering
Project Director

Dr. David N. McQuiddy, Jr.
Research Associate

and

Dr. James E. Dudgeon
Research Associate

Prepared for

National Aeronautics and Space Administration

BER

COLLEGE OF ENGINEERING

THE UNIVERSITY OF ALABAMA 1831

UNIVERSITY OF ALABAMA

UNIVERSITY
ALABAMA

University of Alabama
Bureau of Engineering Research
University, Alabama

STUDY OF INEXACT MODELING TECHNIQUES

Final Report
Grant NGR-01-002-036
August 31, 1968

by

Dr. Harold Mott
Professor of Electrical Engineering
Project Director

Dr. David N. McQuiddy, Jr.
Research Associate

and

Dr. James E. Dudgeon
Research Associate

Prepared for

National Aeronautics and Space Administration

TABLE OF CONTENTS

ILLUSTRATIONS

ACKNOWLEDGEMENT

This report has been prepared for the National Aeronautics and Space Administration under NASA Grant NGR-01-002-036.

The authors wish to express their appreciation to Messrs. J. W. Harper, Paul Swindall, and Donald Stone of the Astrionics Division of George C. Marshall Space Flight Center for their interest and valuable advice.

The method of evaluating anechoic chambers discussed in Chapter 5 was suggested by Professor Walter R. Hanley. The authors are greatly indebted to Professor Hanley for this.

Mr. John J. Flood of the University of Alabama was most helpful in the construction of the antennas used for the conductivity experiments described in Chapter 3. The authors wish to acknowledge this valuable assistance.

ABSTRACT

This report discusses some of the major problems of making measurements on scaled models of antenna systems. A discussion of using models that are not exact likenesses of the full-size system is given, and measured results are given which might provide guidance about the effects of model inexactness.

Theoretical and experimental studies are discussed concerning the effect of conductivity and surface roughness of antenna models. A discussion on the validity of the range of frequency scale factor is also given.

Finally, a method of coding transmitted signals to evaluate, and to improve, the performance of an anechoic chamber for pattern measurements is presented.

Chapter 1

INTRODUCTION

In the experimental study of antennas for missile and airplane use it is almost always necessary to use models of the system rather than the full-scale system itself. To meet this need a theory of modeling has been established that accounts for exact models under optimum conditions, and procedures for carrying out measurements have been developed[1-4].

Practice has not followed theory in many cases, however. An exact model of an airplane or a large missile carrying many antennas would be difficult, time-consuming, and expensive to construct. As a consequence most antenna measurements are made on inexact models. These are inexact in varying ways and degrees. Conductivity in theory should be scaled according to the size and frequency scaling, but in practice this cannot be generally done. It is generally not practicable to scale connectors or coaxial conductors exactly. Finally, it is often economically infeasible to construct a complete model so only an arbitrarily chosen section of the full-scale system is modeled.

In this report some of the problems introduced by modeling inexactness are considered. In the second chapter an experimental study of reradiating objects in the primary field of an antenna is reported. An elementary theory concerned with the effects of reradiating objects in terms of their size, shape, and distance from the primary radiator is also presented. It is hoped that this can provide some guidance when questions arise about the effect of fins or other structural features

on a vehicle.

In Chapter 3 theoretical and experimental studies are presented which are concerned with the effect of conductivity on the frequency scaling of a typical antenna in the range of 5 GHz to 40 GHz. This chapter is also concerned with the range of validity of scaling an antenna in size and frequency.

In Chapter 4, the effect of surface roughness on antenna modeling is discussed. This subject has not been explored by anyone with the thoroughness needed, but we present here the thinking of some of the prominent investigators in this area.

Finally, Chapter 5 presents a technique for using binary-coded signals for studying antenna patterns in anechoic rooms or on outdoor pattern ranges. This coding process suppresses undesired reflected signals. A variation of the same process suppresses the direct ray from transmitter to receiver and allows the reflections in an anechoic room to be measured.

References for Chapter 1

1. G. Sinclair, "Theory of Models of Electromagnetic Systems," Proc. IRE, vol. 36, no. 11, pp. 1364-1370, November 1948.

2. G. Sinclair, et al, "Measurement of Aircraft Antenna Patterns Using Models," Proc. IRE, vol. 35, no. 12, pp. 1451-1462, December 1947.

3. H. Jasik, "Antenna Engineering Handbook," McGraw-Hill Book Company, New York, 1961, p. 2-51.

4. J. A. Stratton, "Electromagnetic Theory," McGraw-Hill Book Company, New York, 1961, pp. 488-490.

Chapter 2

PATTERN EFFECT OF RERADIATING OBJECTS

Introduction

Consider a reradiating object in the field of a primary radiator, as shown in Fig. 2.1. The "object" may be physical, such as a conducting structure or fin, or it may be an abrupt change in the slope of a ground plane, or it may be the edge of a ground plane.

The current induced in the object by the field of the primary radiator will depend on the strength of the primary radiator field, on the size, shape, and composition of the object, and on its distance from the primary radiator. In particular if the object is in the far-field of the primary antenna the induced current will vary inversely with the distance from the source. The reradiated field from the object or discontinuity will then be given by

$$E_o(\theta,\phi) = K(\theta,\phi)/D \qquad (2.1)$$

where the factor K depends on the size, shape, orientation, and composition of the object, and upon its direction from the primary radiator. As a particular object is moved along a straight line drawn from the primary antenna, K will be constant. In (2.1) θ and ϕ are coordinate angles.

Let the radiation pattern of the primary radiator be $E(\theta,\phi)$, where we consider E and E_o to be amplitudes. The total field will then be

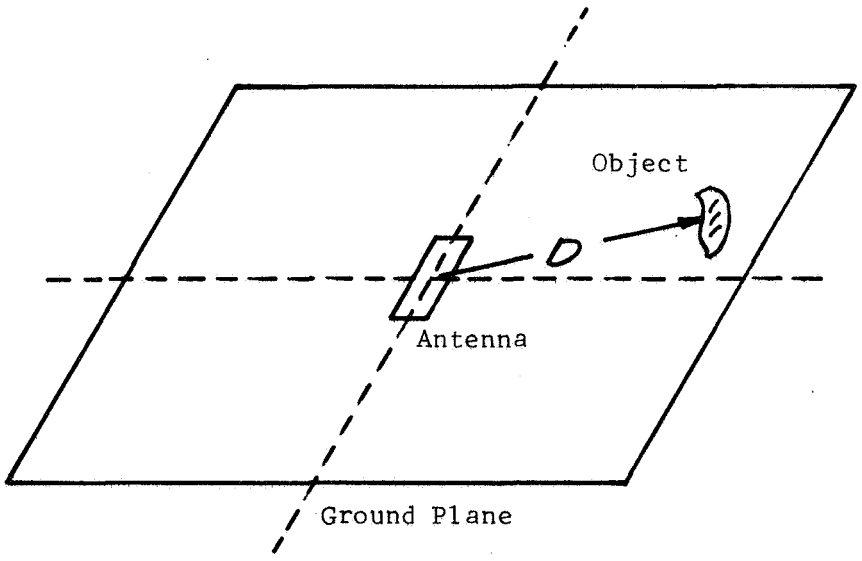

Fig. 2.1

Reradiating Object in Antenna Field

given by

$$E_T(\theta,\phi) = E(\theta,\phi) + E_o(\theta,\phi)\varepsilon^{i\alpha} \tag{2.2}$$

where α is some phase angle. We here assume that in the region of interest the polarizations of the direct and reradiated fields are substantially the same.

At some point, or points, in space the fields will add directly to give a maximum resultant, and at other points they will subtract to give a minimum. These are

$$E_{T\ max} = E(\theta^+,\phi^+) + E_o(\theta^+,\phi^+) \tag{2.3}$$

$$E_{T\ min} = \left|E(\theta^-,\phi^-) - E_o(\theta^-,\phi^-)\right| \tag{2.4}$$

Now

$$E(\theta,\phi) = E_m\ U(\theta,\phi) \tag{2.5}$$

where E_m is a maximum field and $U(\theta,\phi)$ is a normalized pattern factor with limits

$$0 \leq U(\theta,\phi) \leq 1 \tag{2.6}$$

We may then write

$$E_{T\ max} = E_m\ U(\theta^+,\phi^+) + K(\theta^+,\phi^+)/D \tag{2.7}$$

$$E_{T\ min} = \left|E_m\ U(\theta^-,\phi^-) - K(\theta^-,\phi^-)/D\right| \tag{2.8}$$

where all terms are real, and the magnitude is taken in (2.8) to eliminate possible negative values.

Let us define pattern disturbance factors by ratios of reradiated to direct fields

$$Q^{+} = \frac{E_o(\theta^{+},\phi^{+})}{E(\theta^{+},\phi^{+})} = \frac{K(\theta^{+},\phi^{+})/D}{E_m\, U(\theta^{+},\phi^{+})} \tag{2.9}$$

$$Q^{-} = \frac{E_o(\theta^{-},\phi^{-})}{E(\theta^{-},\phi^{-})} = \frac{K(\theta^{-},\phi^{-})/D}{E_m\, U(\theta^{-},\phi^{-})} \tag{2.10}$$

At points in space where the fields add directly (2.9) effectively gives the disturbance to the pattern caused by the reradiating object or discontinuity. Where the fields subtract (2.10) gives the disturbance.

Superficial study of (2.9) or (2.10) would apprear to indicate that the disturbance factors will be improved (decreased) if D is increased. However, further thought will show that a change in D may change the values of θ^{+},ϕ^{+} and θ^{-},ϕ^{-}, where the fields add or subtract, because the relative phase of E_o depends on D. Thus the obvious conclusion cannot be made.

Consider, however, a specialization valid if the pattern of the disturbing object is substantially isotropic in the region of interest. Then we have

$$Q^{+} = \frac{K/D}{E_m\, U(\theta^{+},\phi^{+})} \tag{2.11}$$

$$Q^{-} = \frac{K/D}{E_m\, U(\theta^{-},\phi^{-})} \tag{2.12}$$

with K constant. We then see that the disturbance of the original pattern will be greatest wherever $U(\theta^{+},\phi^{+})$ or $U(\theta^{-},\phi^{-})$ is smallest. Since U is a normalized pattern it follows that reradiation by an obstacle

near a primary source will have its greatest effect if the primary source has a highly directive pattern, and this effect will be most significant in regions where the primary field is small. This of course confirms our intuitive feelings about the situation.

Next, let us specialize further to the case where both the primary radiator and the disturbing object are substantially isotropic radiators in the region of interest. Then

$$U(\theta^+,\phi^+) \approx U(\theta^-,\phi^-) \approx 1 \tag{2.13}$$

and

$$Q = Q^+ = Q^- = \frac{K}{E_m D} \tag{2.14}$$

The position of the maximum and minimum fields may change as D is varied, but nevertheless we see that the pattern disturbance varies inversely with D, the distance of the disturbing object from the source.

Pattern Measurements

Pattern measurements of a slot antenna in a ground phase with a disturbing post mounted on the ground plane have been made in order to verify the results of the preceding analysis and to give experience in the magnitude of the disturbance effect for typical pattern-disturbing objects. These measurements were carried out at a frequency of 10.975 GHz. The ground plane was 3' x 3' copper with an X-band waveguide slot opening into it. E-plane patterns only were made. The conducting cylindrical posts ranged in size from a diameter of 0.0625" to 0.1875" and a height of 0.269" to 0.975". The posts were mounted along a line perpendicular to the long edge of the slot and passing through the center of the slot

(in the E plane). Distance from the center of the post to the nearest edge of the slot ranged from 0.370" to 5.75". The distance from transmitter to ground plane was 20'.

The measured patterns are shown in Figs. 2.2 through 2.60. Each figure is marked with post diameter, height, and distance from edge of slot. Reference for angle of rotation θ is $\theta = 0$ when the post is located between the slot and the transmitting horn. Those figures marked "No Post" were made as control patterns for those patterns immediately following and were made during the same period of time and under the same conditions as the following patterns. Three calibration points for each pattern are also shown.

The pattern ripples occurring with an approximate average period of 5° were caused by edge effects of the ground plane. A study of the patterns most affected by the conducting posts (those patterns with large posts close to the slot) show a periodicity with a much longer period, typically two periods in the pattern.

From (2.7) and (2.8) we see that if the primary source pattern and the disturbing object pattern are both isotropic, then

$$E_{T\ max} - E_{T\ min} = 2K/D \qquad (2.15)$$

The measured patterns were studied in an attempt to verify this relation. This analysis was handicapped by the presence of the edge-effect ripples which made it difficult to measure accurately the difference between $E_{T\ max}$ and $E_{T\ min}$. In addition, while the E-plane pattern of the slot is reasonably isotropic, the pattern of the vertical conducting post in the same plane, particularly for the thinner posts, is definitely not isotropic.

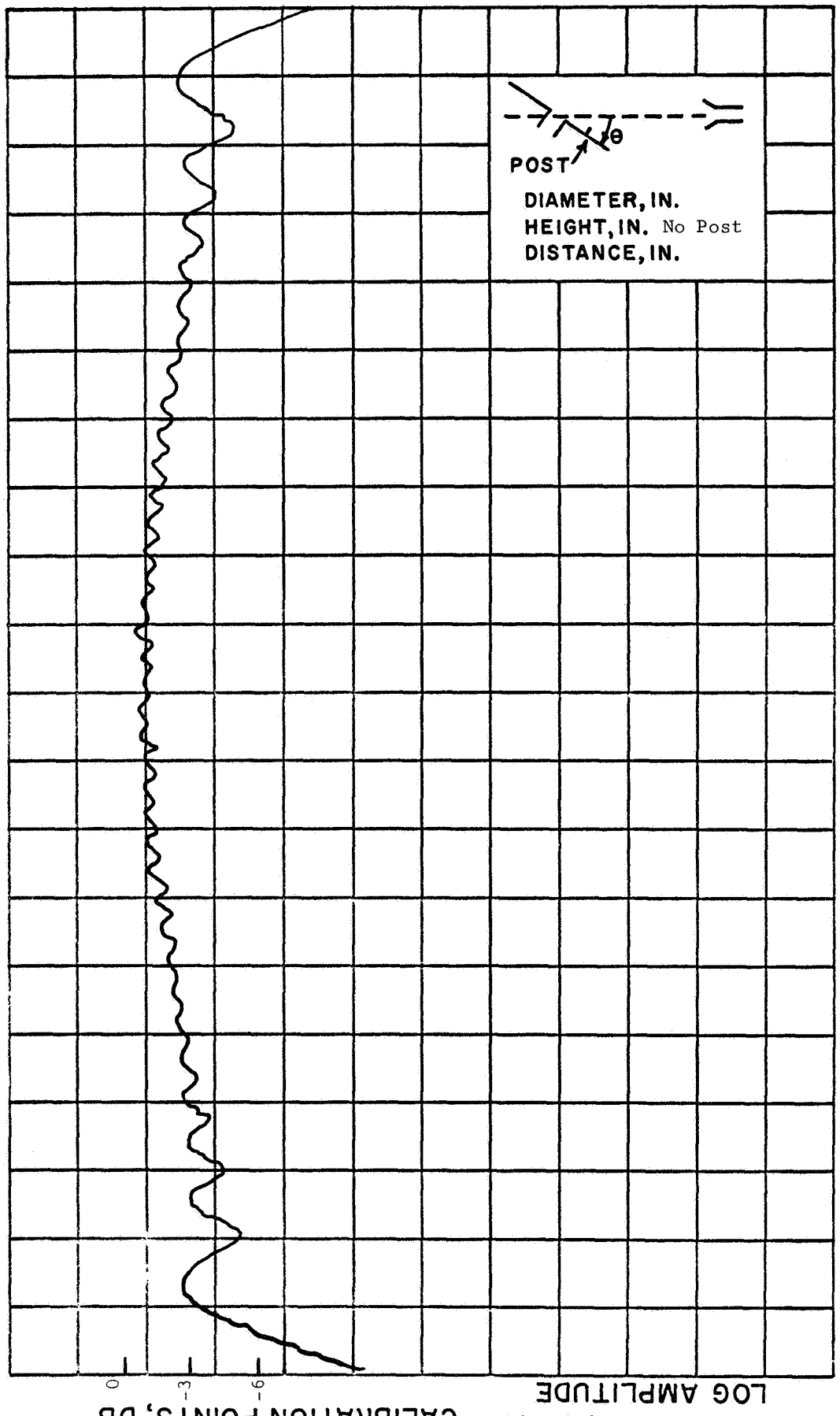
θ
POST
DIAMETER, IN.
HEIGHT, IN. No Post
DISTANCE, IN.
180
90
0
θ, DEGREES
LOG AMPLITUDE
0
-3
-6
CALIBRATION POINTS, DB

Fig. 2.2

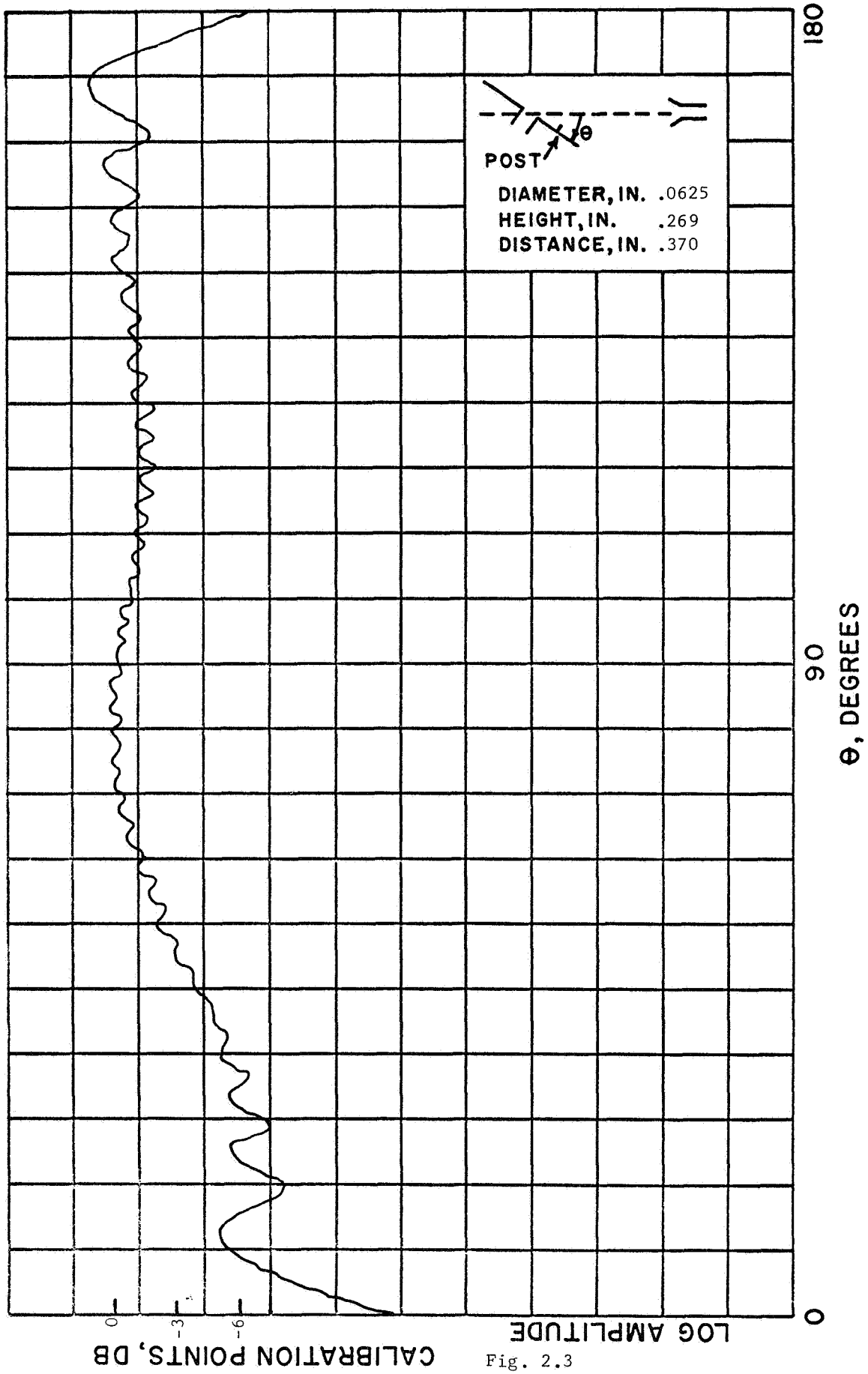
θ
POST
DIAMETER, IN. .0625
HEIGHT, IN. .269
DISTANCE, IN. .370
180
90
0
θ, DEGREES
LOG AMPLITUDE
0
-3
-6
CALIBRATION POINTS, DB

Fig. 2.3

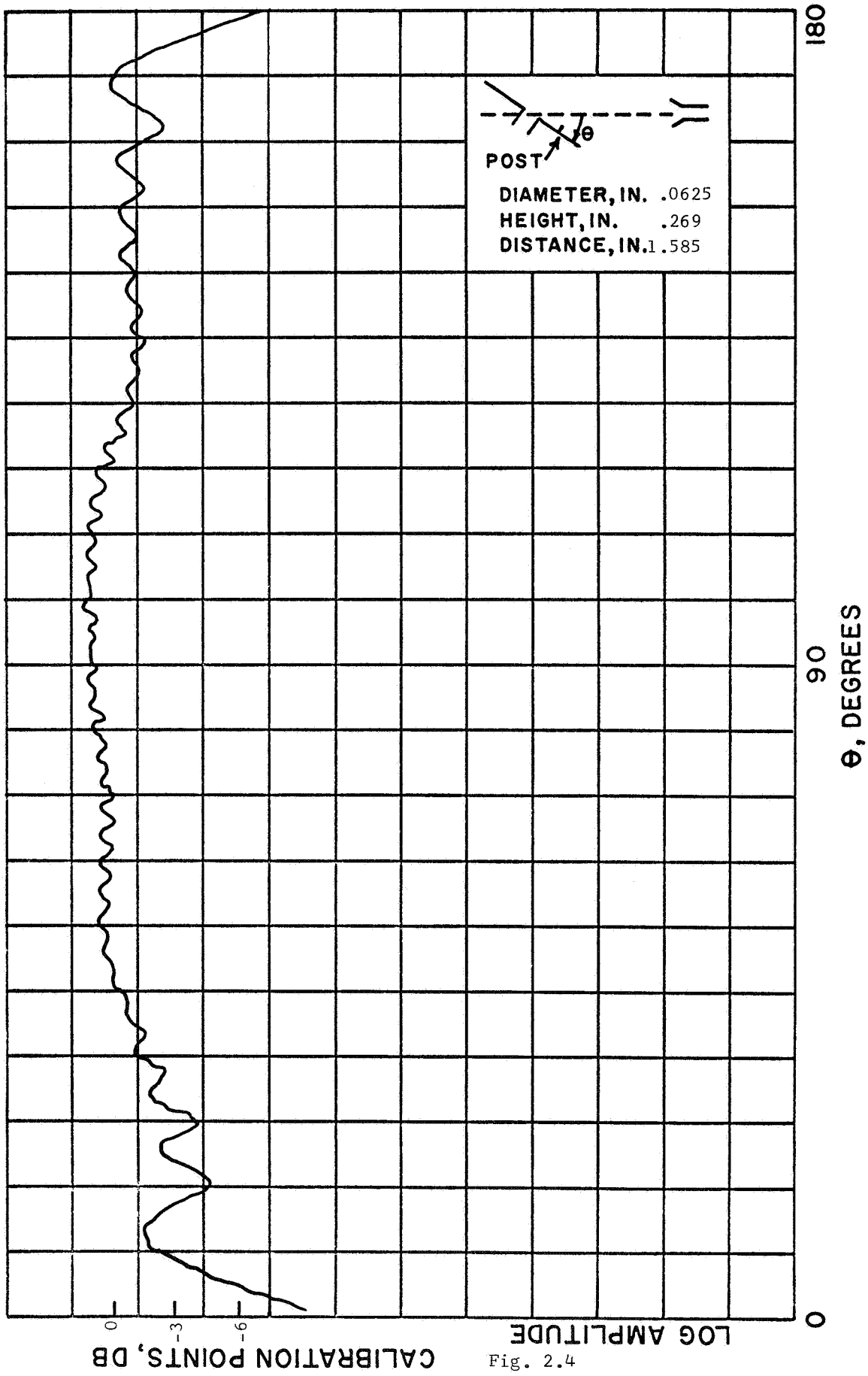
θ
POST
DIAMETER, IN. .0625
HEIGHT, IN. .269
DISTANCE, IN. 1.585
180
90
0
θ, DEGREES
LOG AMPLITUDE
0
-3
-6
CALIBRATION POINTS, DB

Fig. 2.4

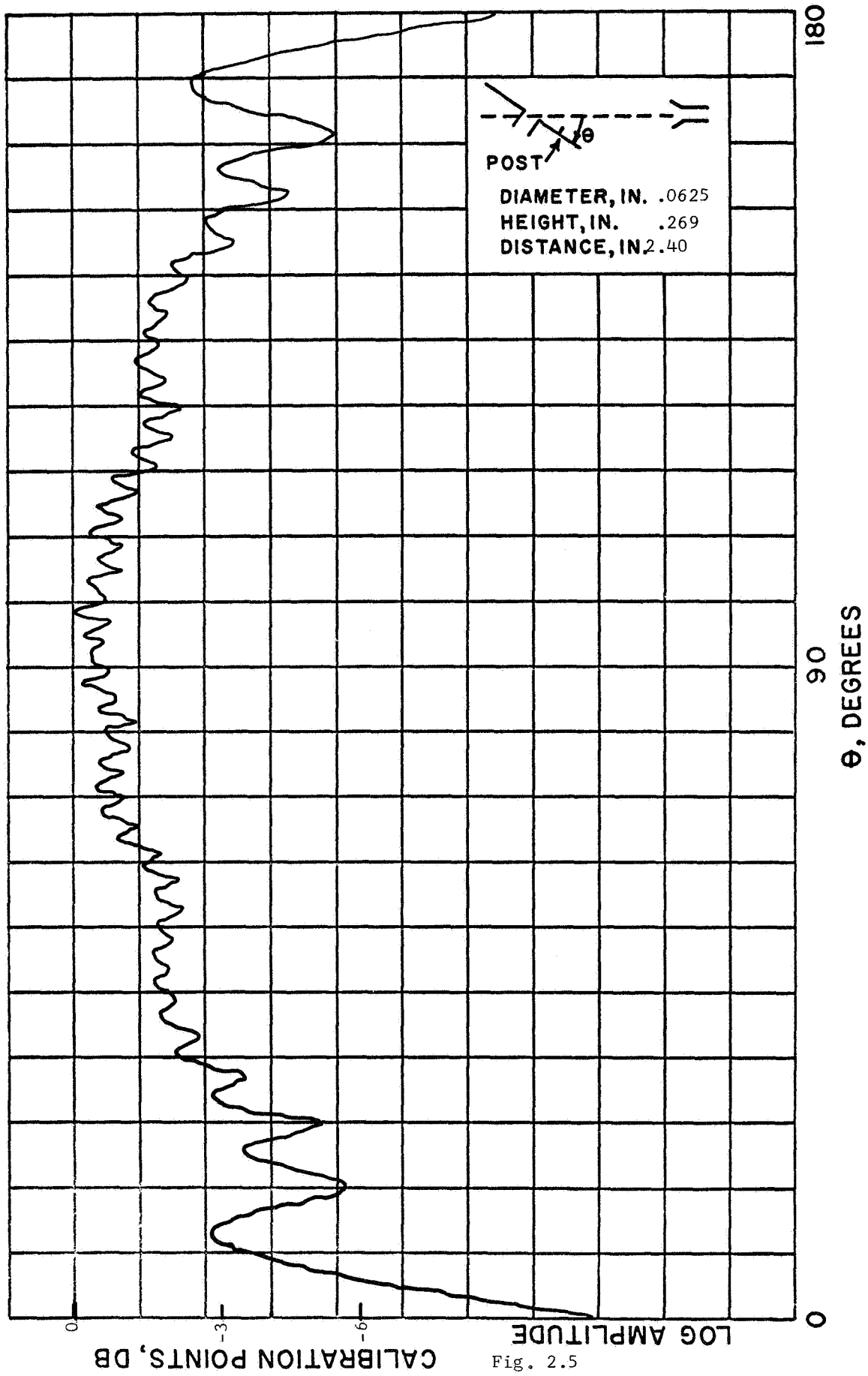
θ
POST
DIAMETER, IN. .0625
HEIGHT, IN. .269
DISTANCE, IN. 2.40
180
90
0
θ, DEGREES
LOG AMPLITUDE
0
-3
-6
CALIBRATION POINTS, DB

Fig. 2.5

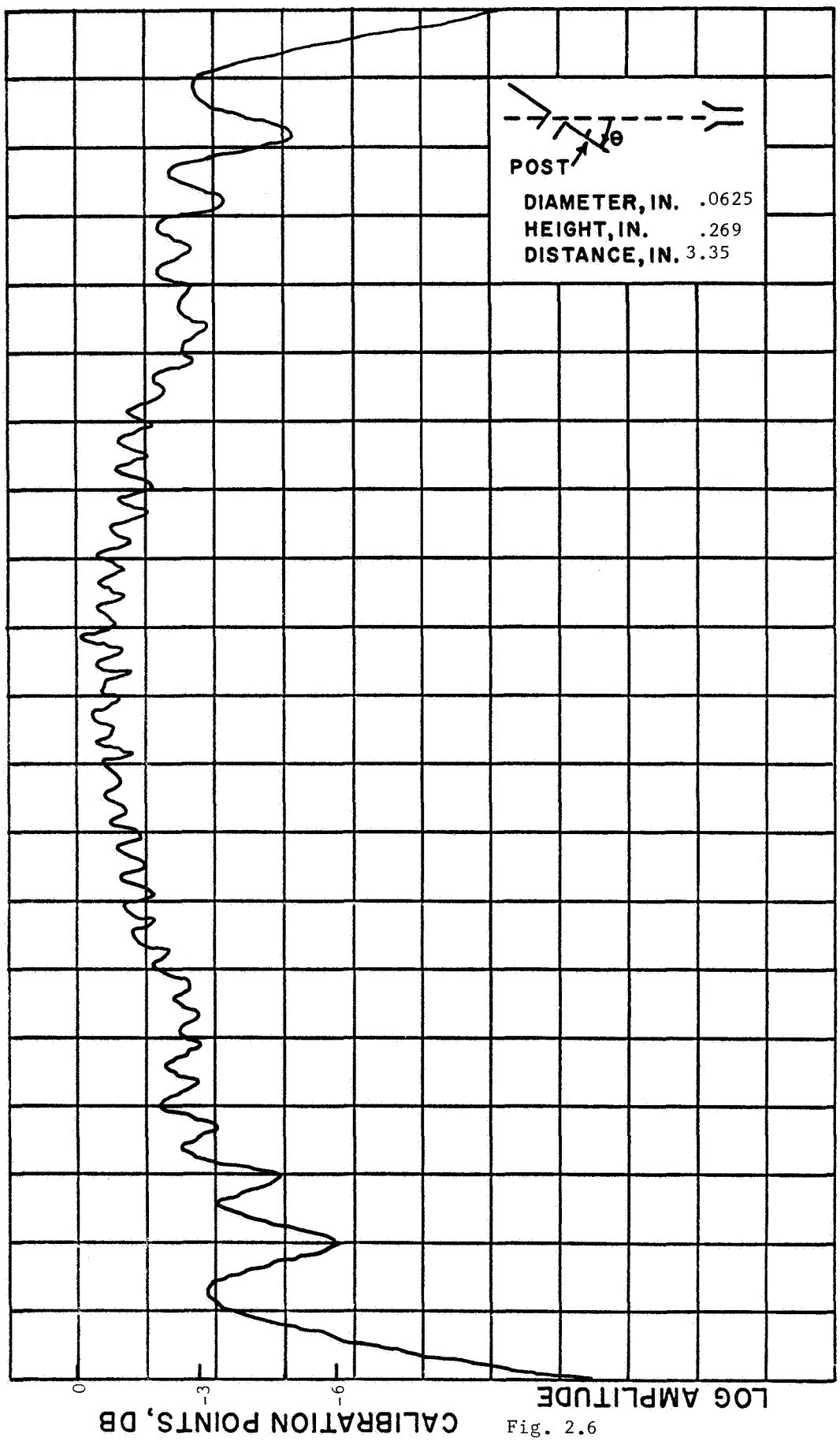
θ
POST
DIAMETER, IN. .0625
HEIGHT, IN. .269
DISTANCE, IN. 3.35
180
90
0
θ, DEGREES
LOG AMPLITUDE
0
-3
-6
CALIBRATION POINTS, DB

Fig. 2.6

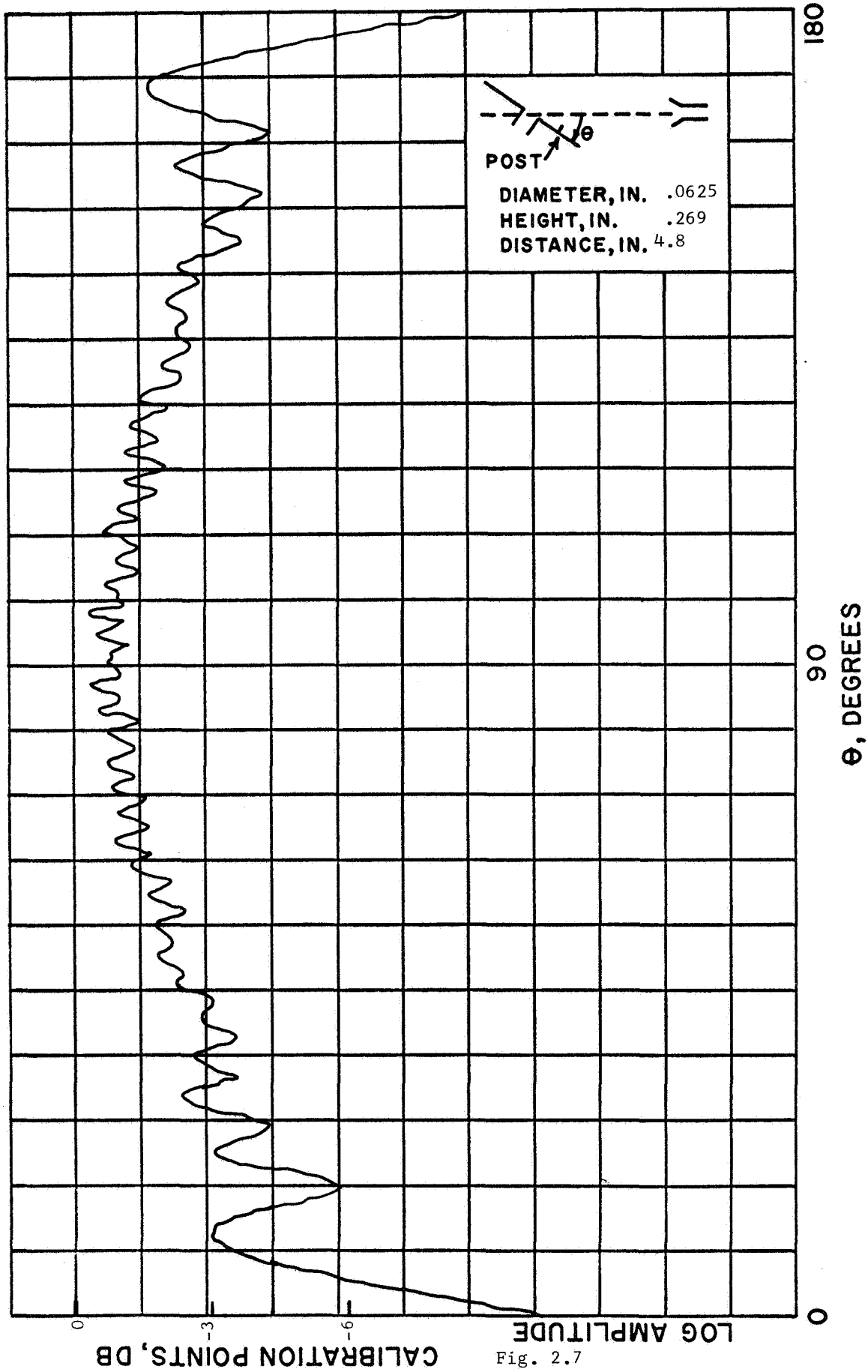
θ
POST
DIAMETER, IN. .0625
HEIGHT, IN. .269
DISTANCE, IN. 4.8
180
90
0
θ, DEGREES
LOG AMPLITUDE
0
-3
-6
CALIBRATION POINTS, DB

Fig. 2.7

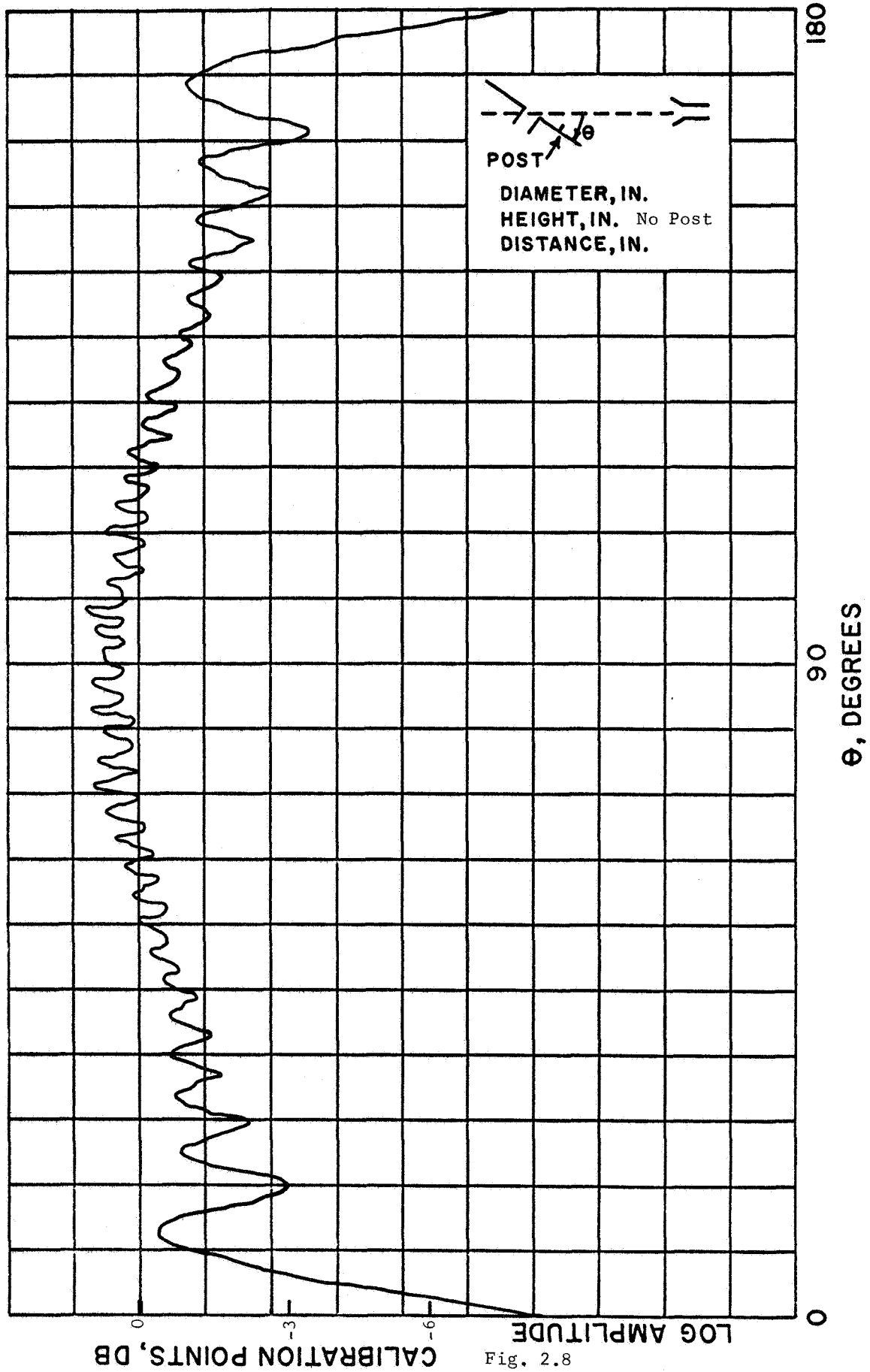
180
θ
POST
DIAMETER, IN.
HEIGHT, IN. No Post
DISTANCE, IN.
90
θ, DEGREES
0
LOG AMPLITUDE
0
-3
-6
CALIBRATION POINTS, DB

Fig. 2.8

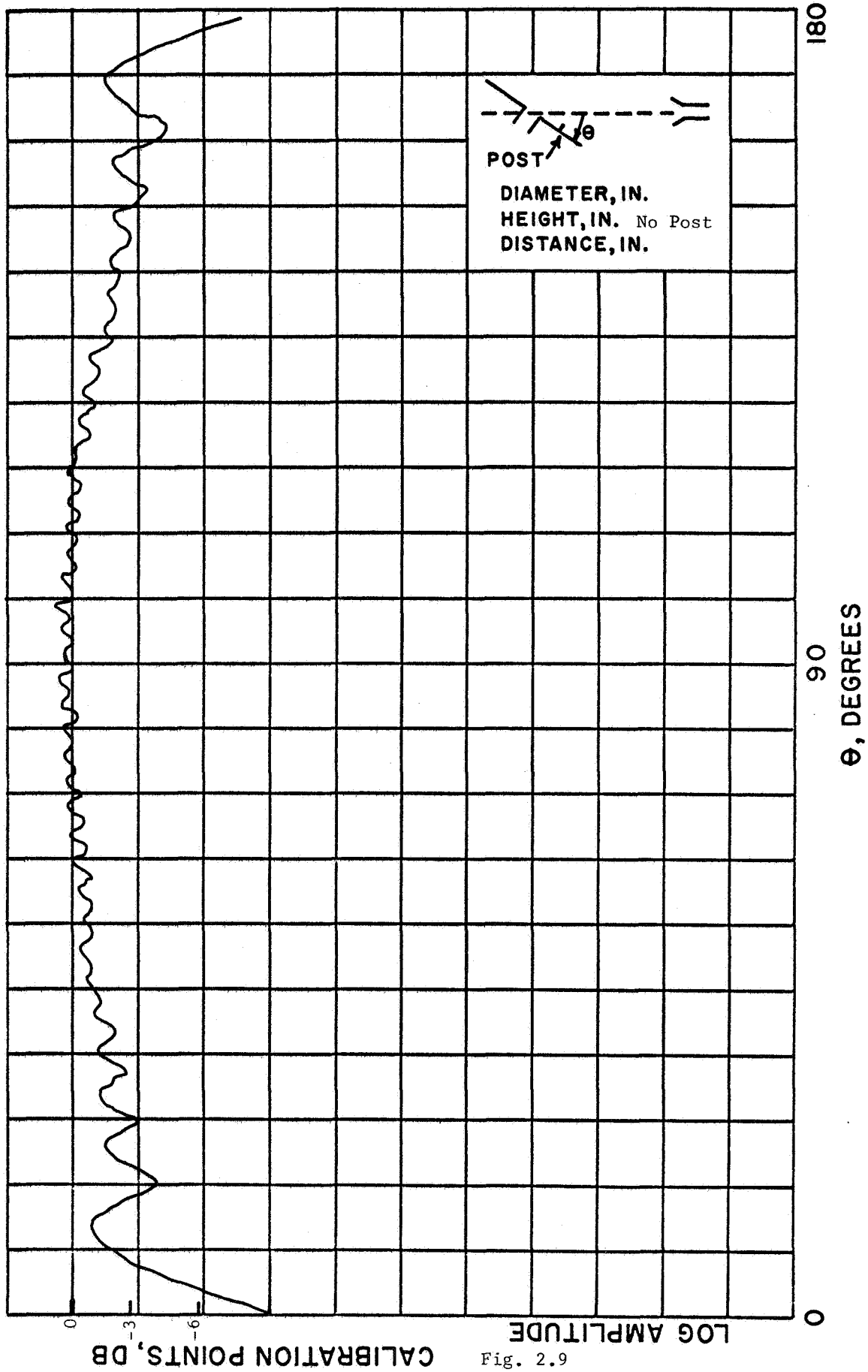
θ
POST
DIAMETER, IN.
HEIGHT, IN. No Post
DISTANCE, IN.
180
90
0
θ, DEGREES
LOG AMPLITUDE
0
-3
-6
CALIBRATION POINTS, DB

Fig. 2.9

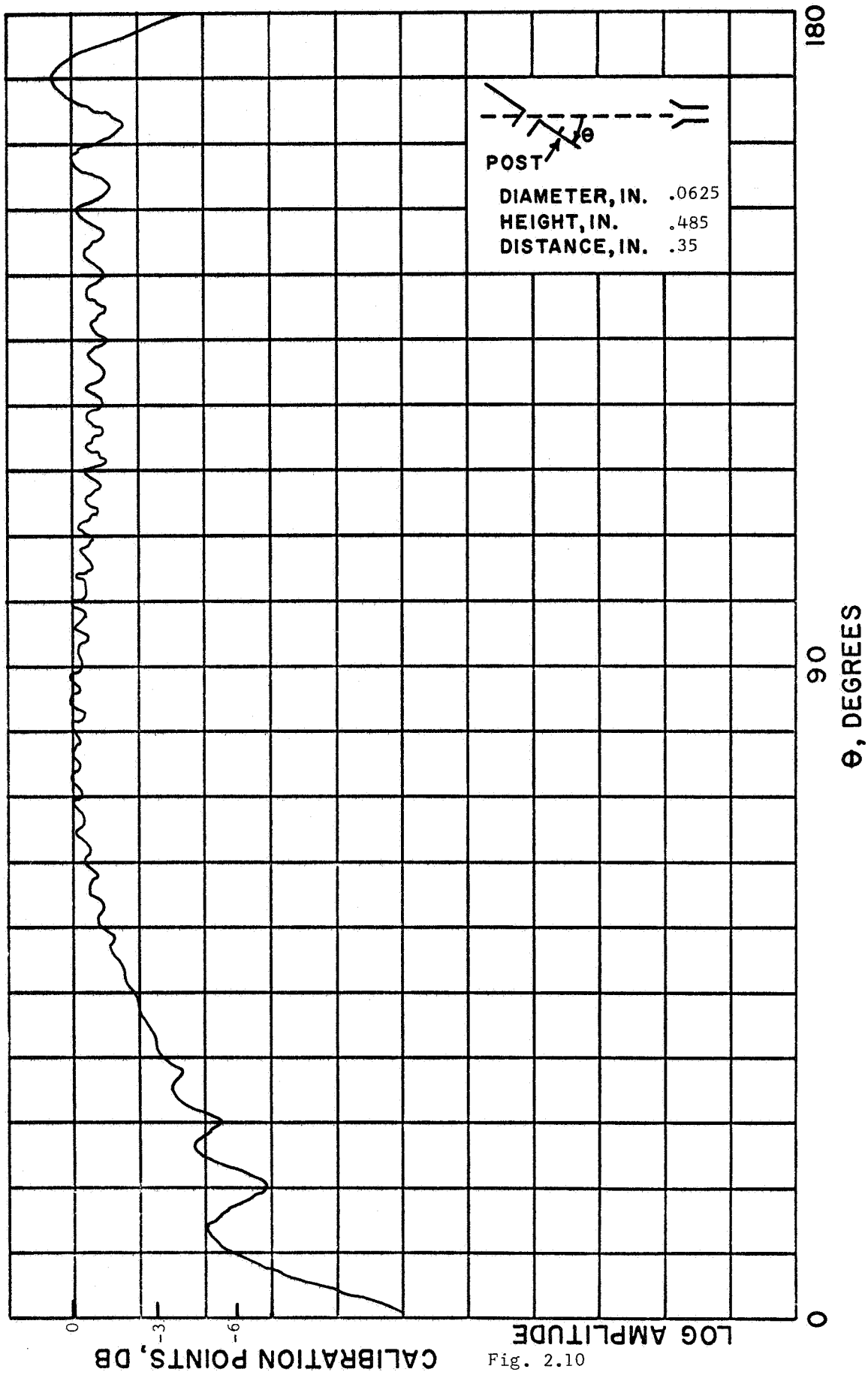
θ
POST
DIAMETER, IN. .0625
HEIGHT, IN. .485
DISTANCE, IN. .35
180
90
0
θ, DEGREES
LOG AMPLITUDE
0
-3
-6
CALIBRATION POINTS, DB

Fig. 2.10

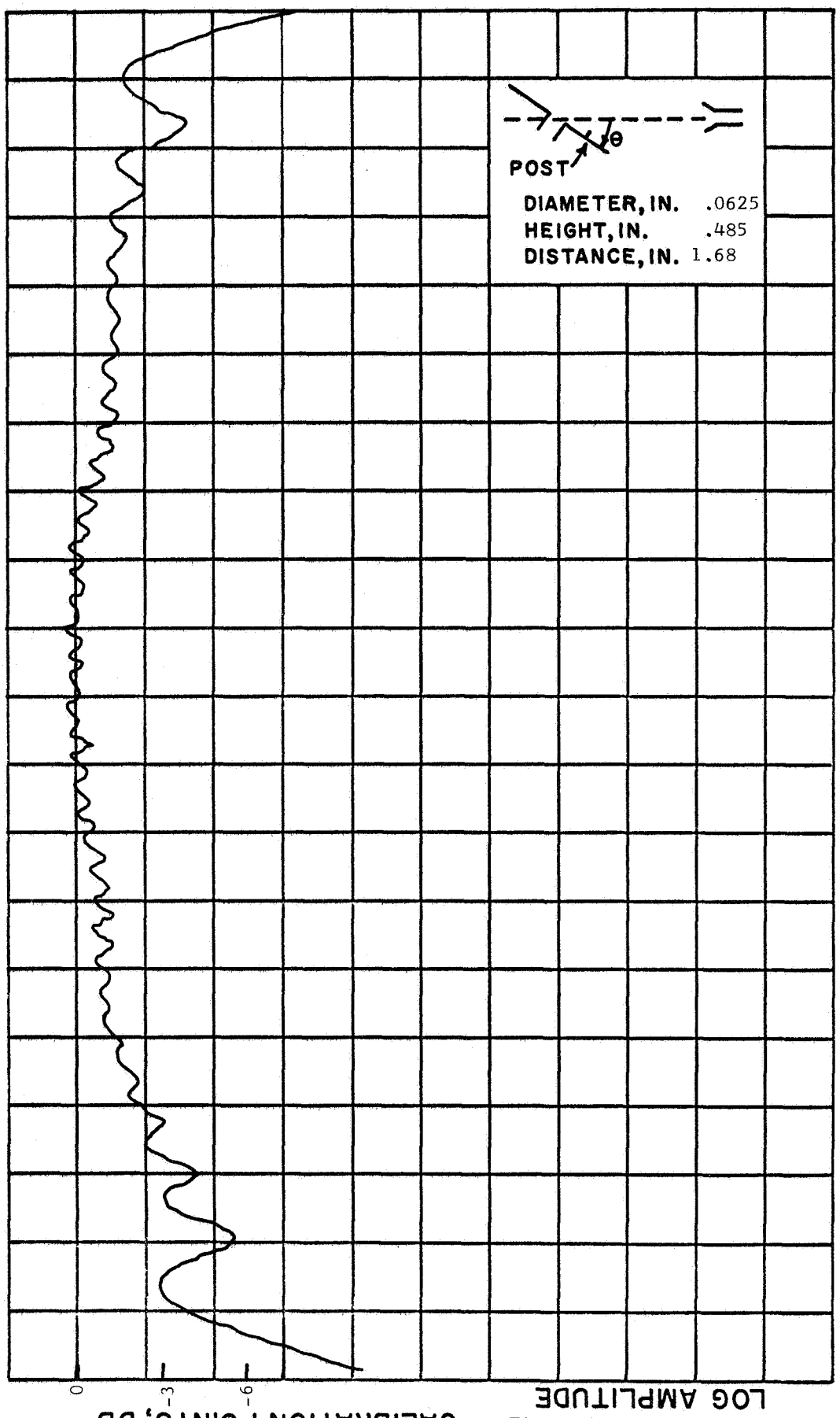
POST
θ
DIAMETER, IN. .0625
HEIGHT, IN. .485
DISTANCE, IN. 1.68
180
90
0
θ, DEGREES
LOG AMPLITUDE
0
-3
-6
CALIBRATION POINTS, DB

Fig. 2.11

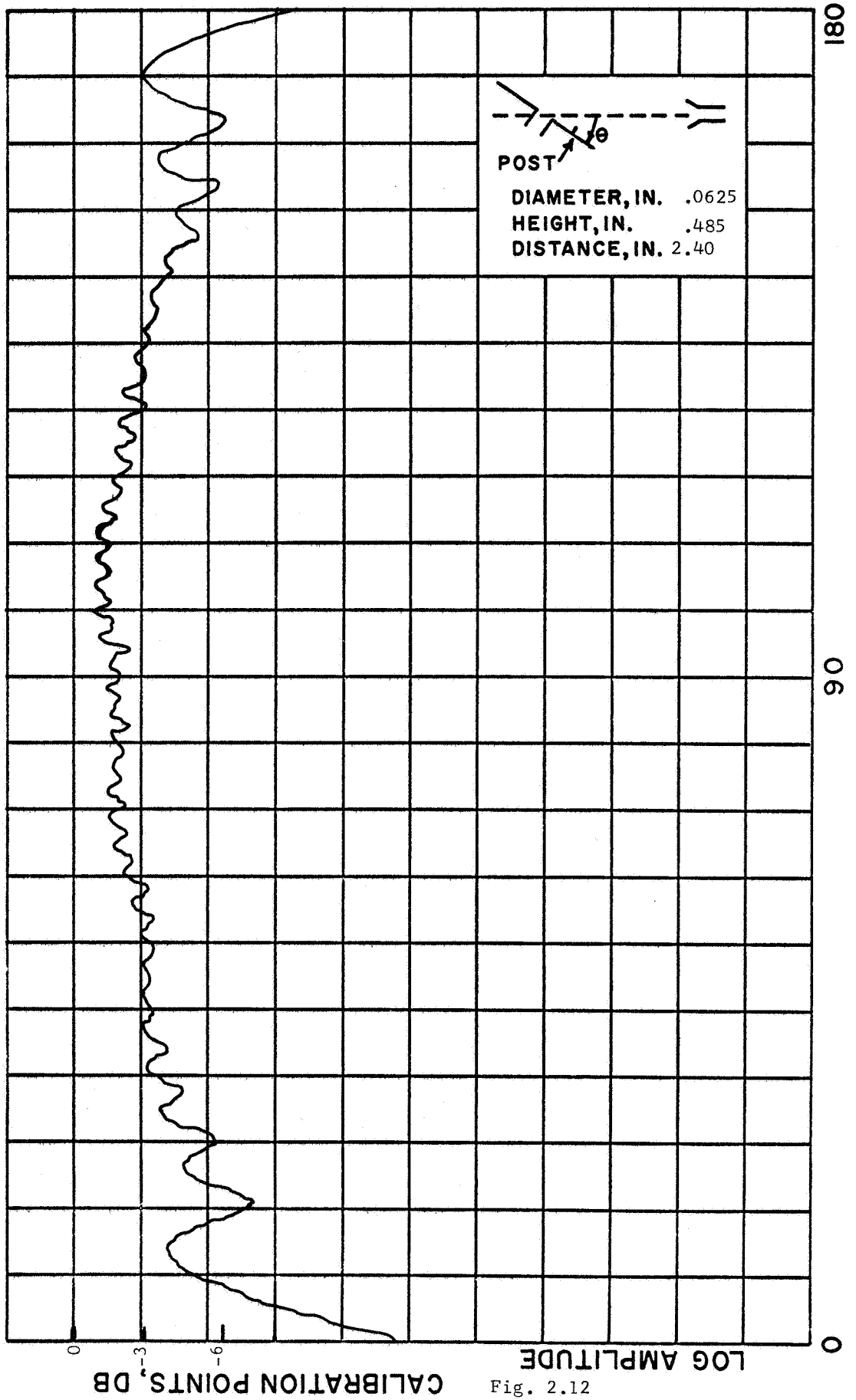
θ
POST
DIAMETER, IN. .0625
HEIGHT, IN. .485
DISTANCE, IN. 2.40
180
90
0
θ, DEGREES
LOG AMPLITUDE
0
-3
-6
CALIBRATION POINTS, DB

Fig. 2.12

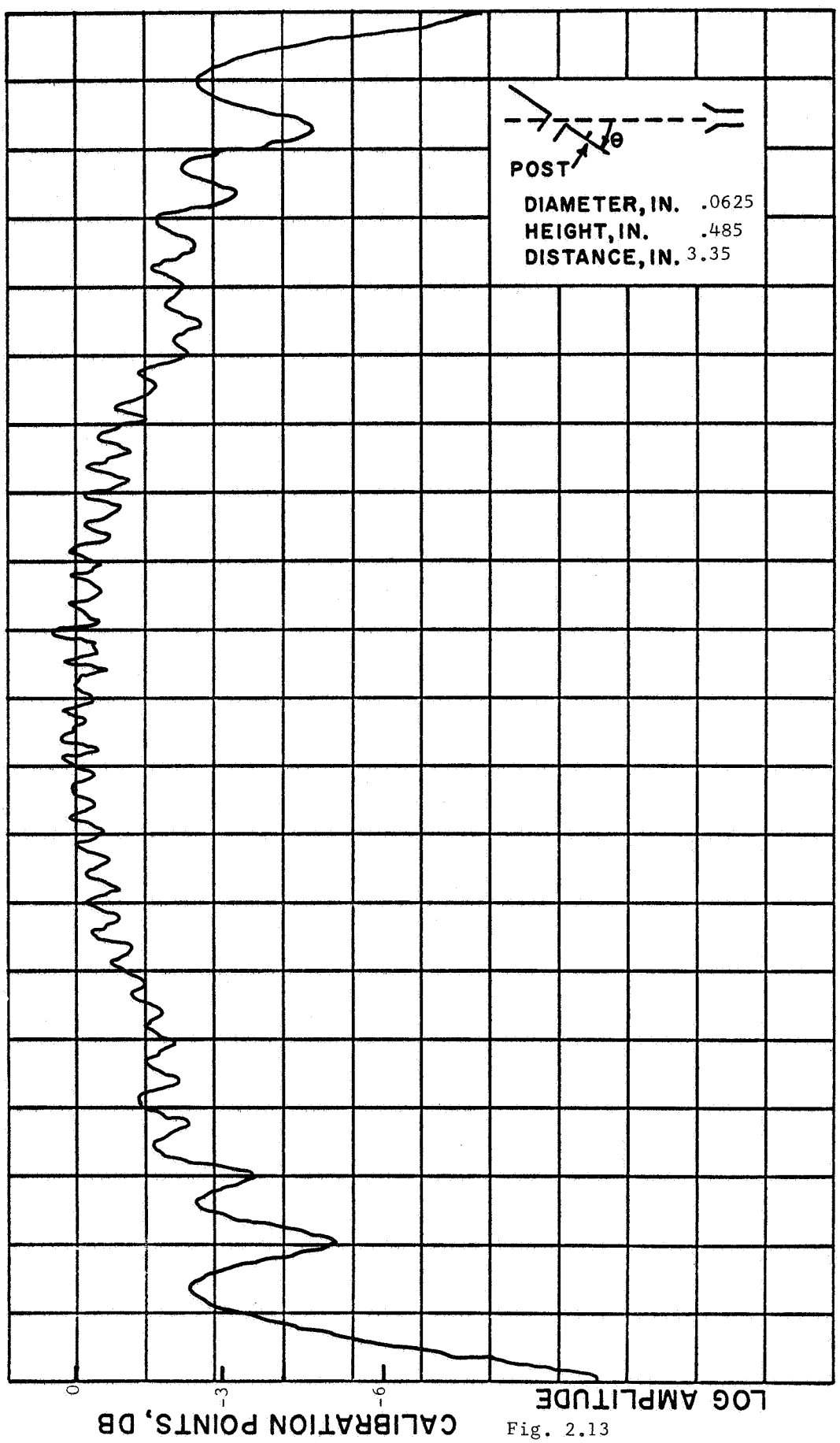
POST
DIAMETER, IN. .0625
HEIGHT, IN. .485
DISTANCE, IN. 3.35
θ
180
90
0
θ, DEGREES
LOG AMPLITUDE
0
-3
-6
CALIBRATION POINTS, DB

Fig. 2.13

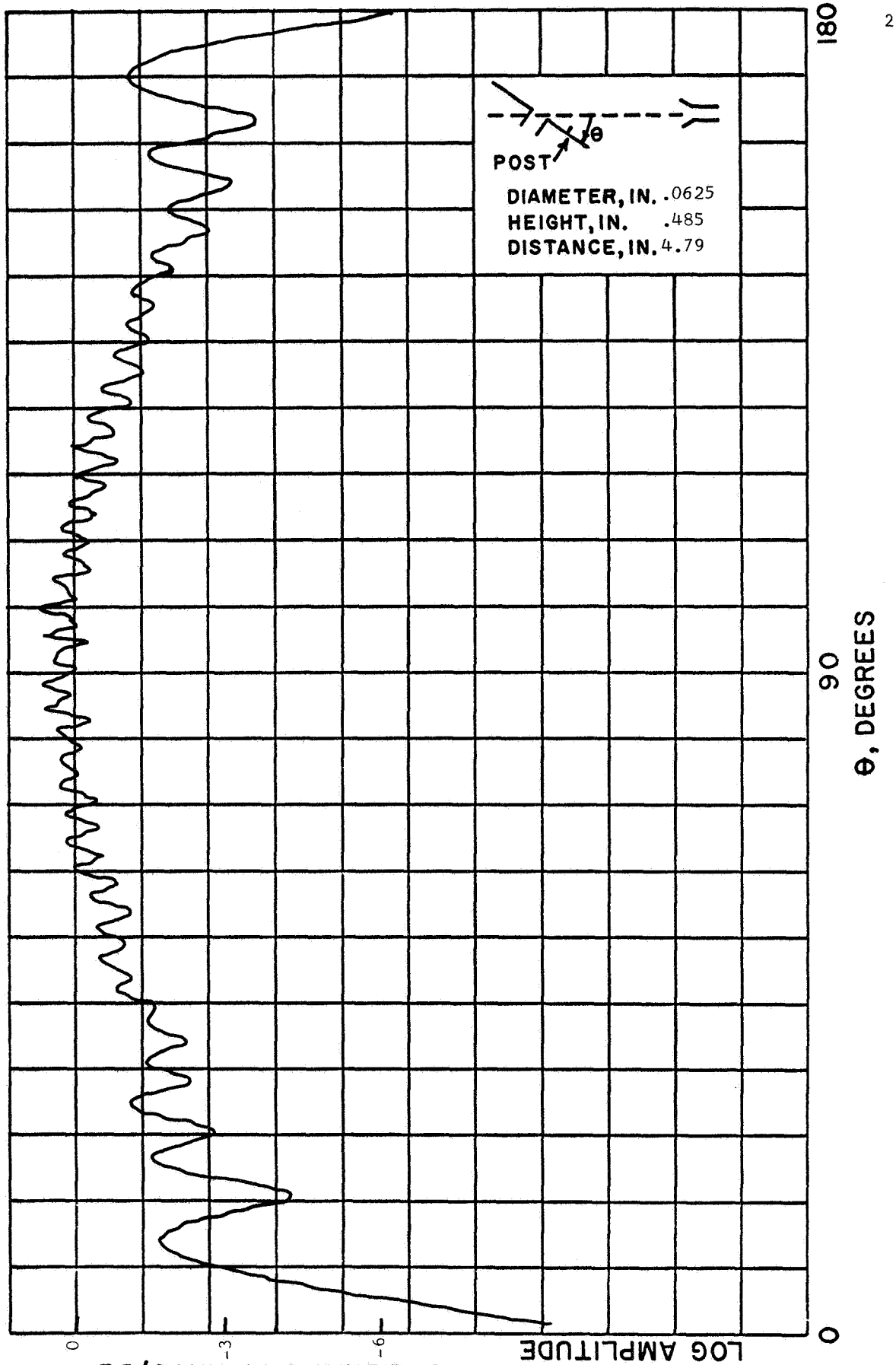
θ
POST
DIAMETER, IN. .0625
HEIGHT, IN. .485
DISTANCE, IN. 4.79
180
90
0
θ, DEGREES
LOG AMPLITUDE
0
-3
-6
CALIBRATION POINTS, DB

Fig. 2.14

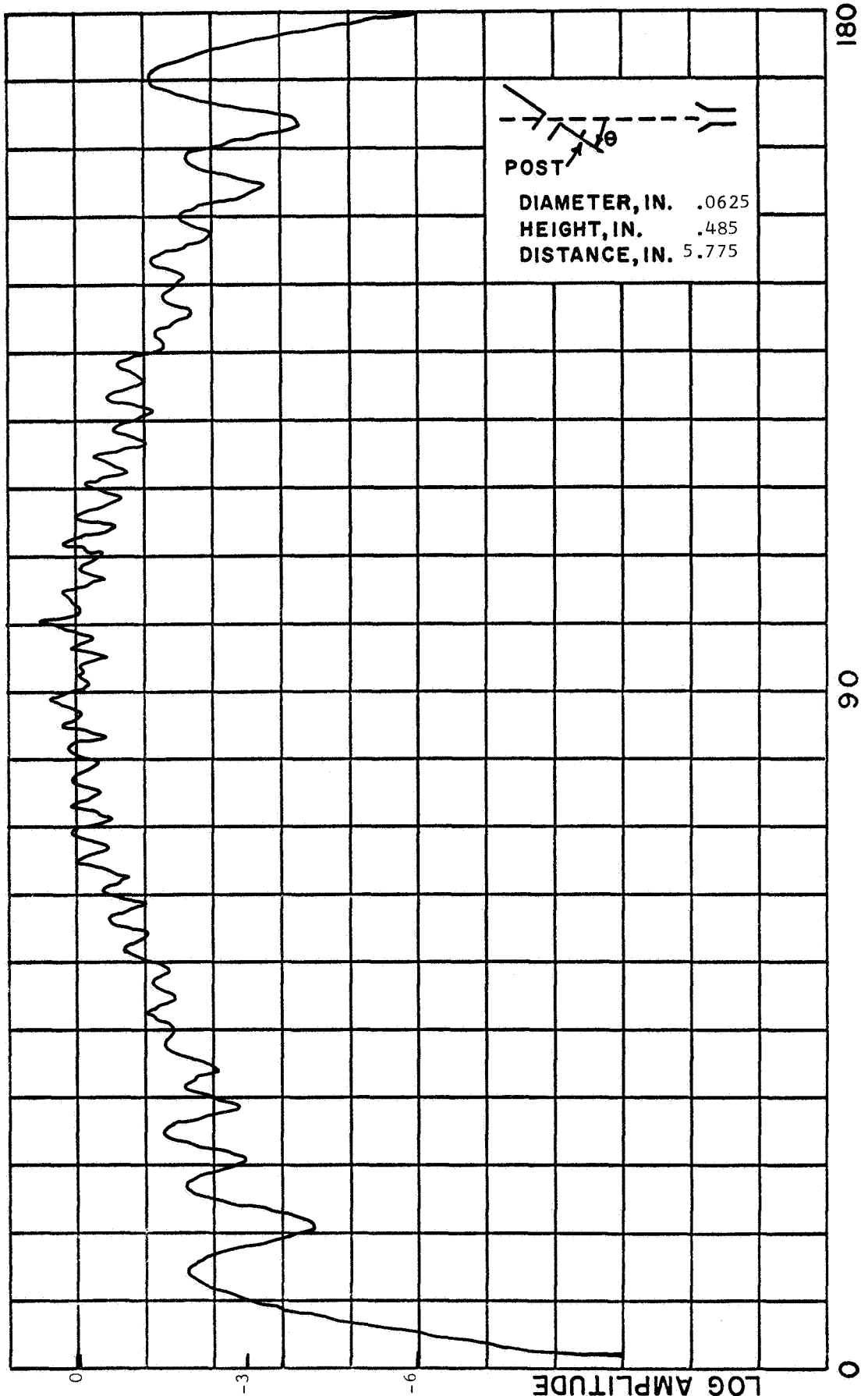
θ
POST
DIAMETER, IN. .0625
HEIGHT, IN. .485
DISTANCE, IN. 5.775
180
90
0
θ, DEGREES
LOG AMPLITUDE
0
-3
-6
CALIBRATION POINTS, DB

Fig. 2.15

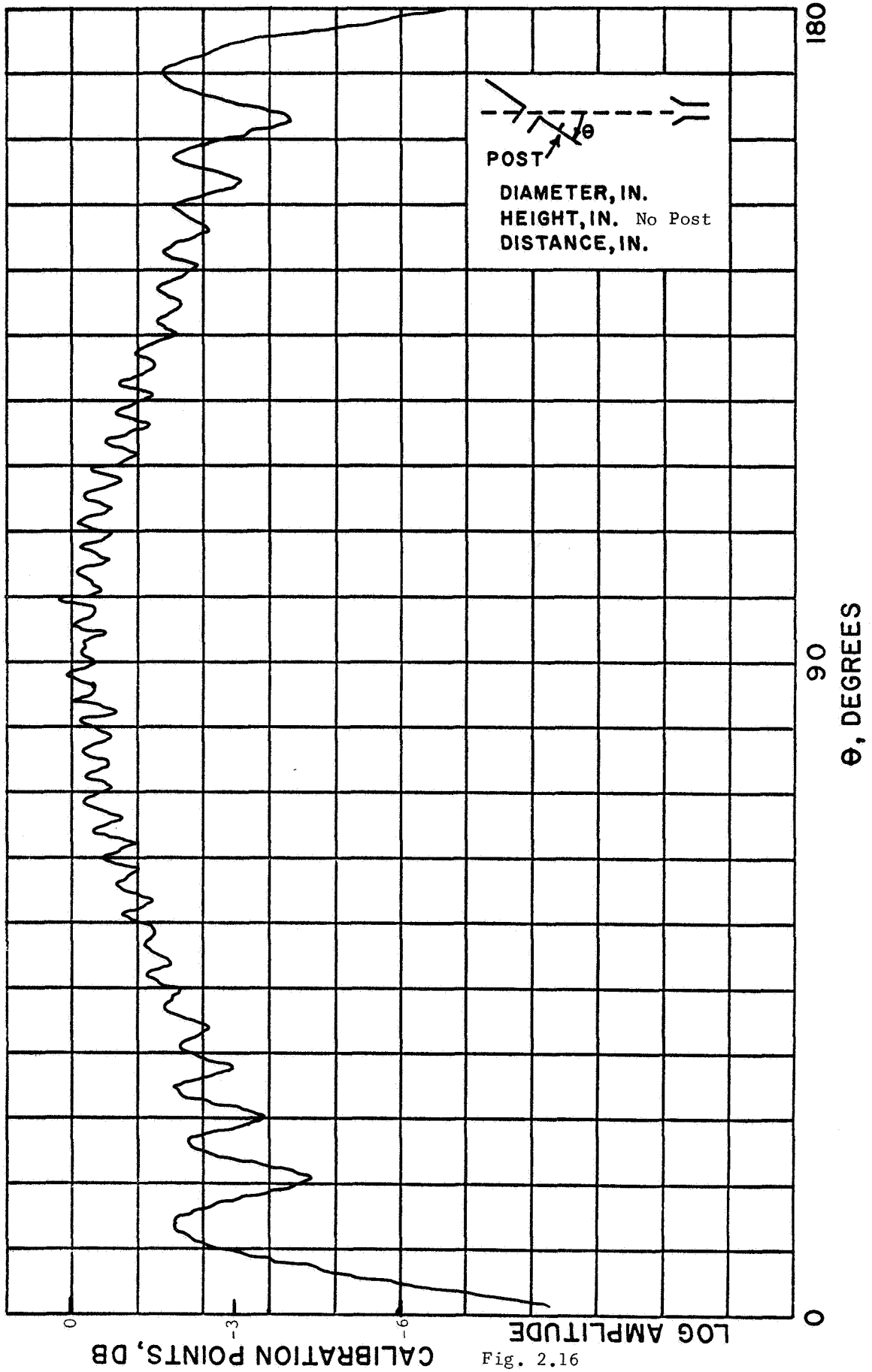
POST
DIAMETER, IN.
HEIGHT, IN. No Post
DISTANCE, IN.
θ
180
90
0
θ, DEGREES
LOG AMPLITUDE
0
-3
-6
CALIBRATION POINTS, DB

Fig. 2.16

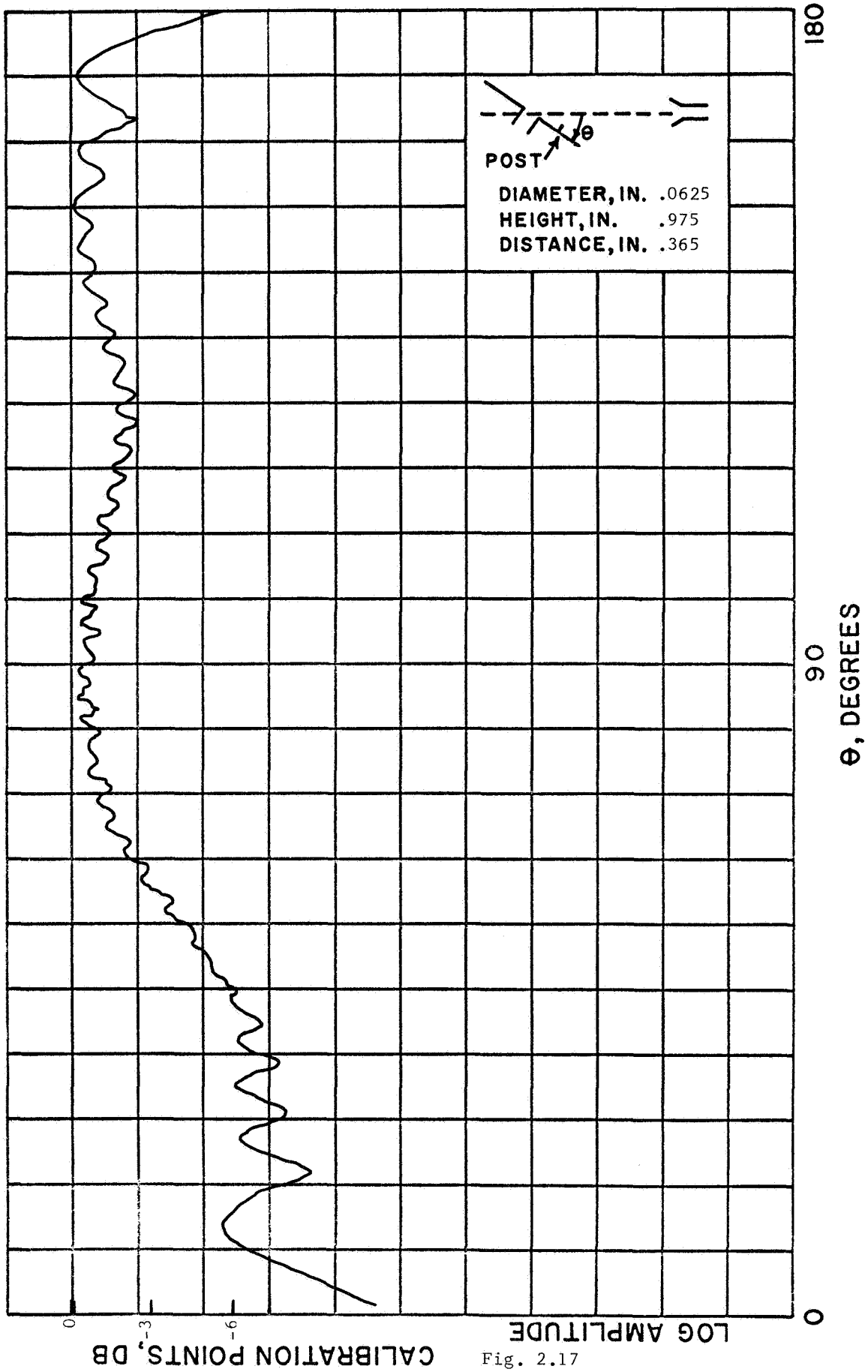
θ
POST
DIAMETER, IN. .0625
HEIGHT, IN. .975
DISTANCE, IN. .365
180
90
0
θ, DEGREES
LOG AMPLITUDE
0
-3
-6
CALIBRATION POINTS, DB

Fig. 2.17

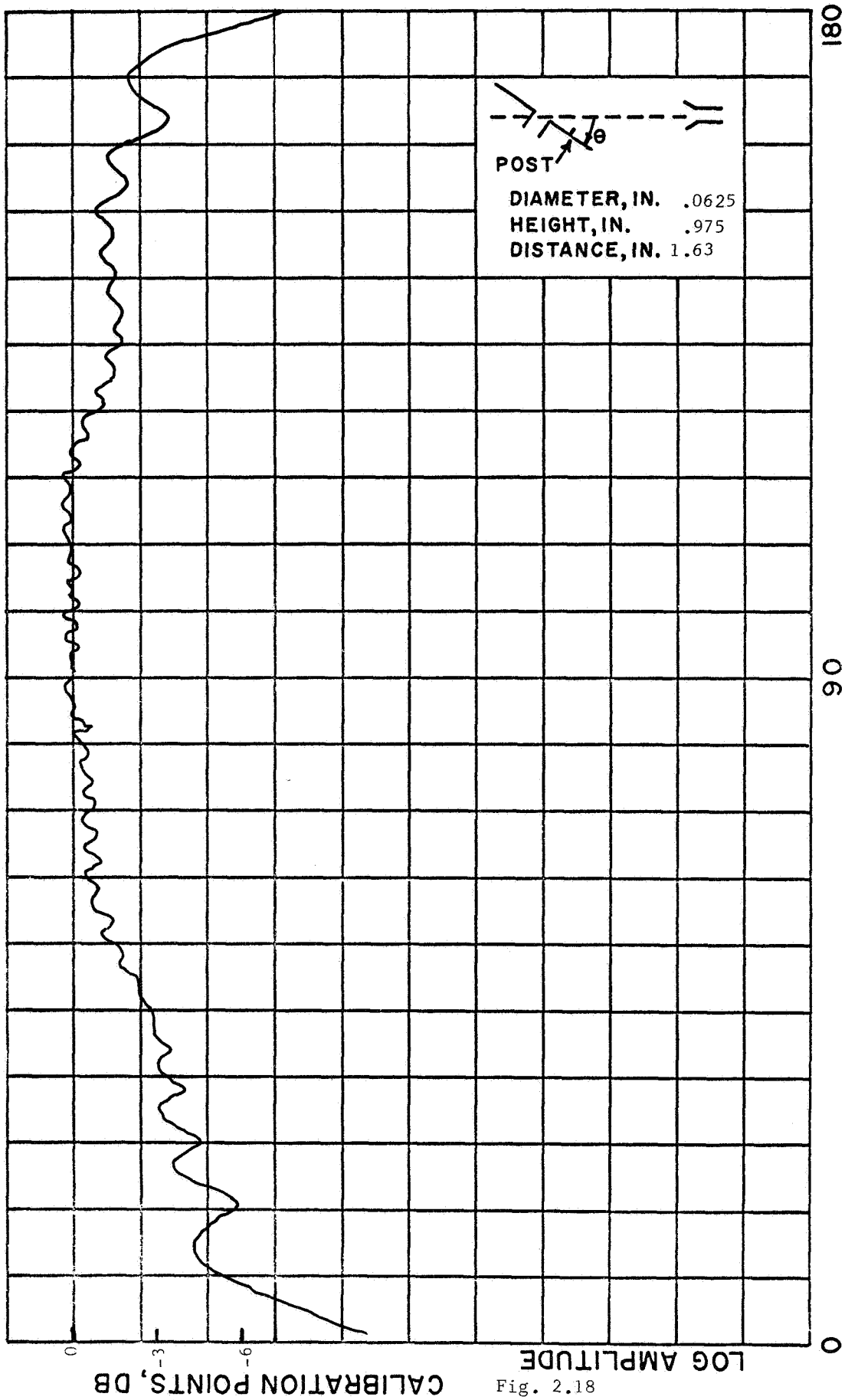
θ
POST
DIAMETER, IN. .0625
HEIGHT, IN. .975
DISTANCE, IN. 1.63
180
90
0
θ, DEGREES
LOG AMPLITUDE
0
-3
-6
CALIBRATION POINTS, DB

Fig. 2.18

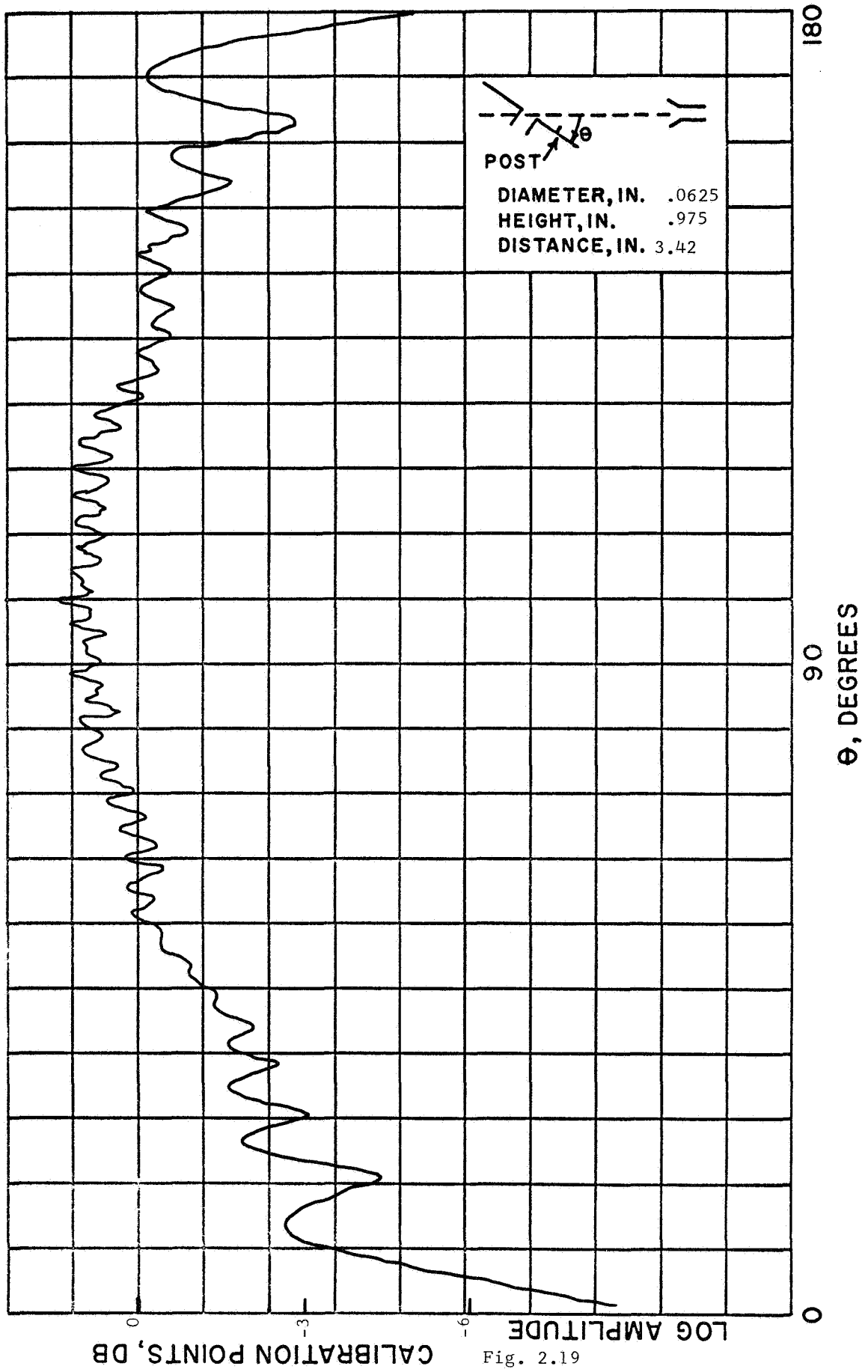
POST
θ
DIAMETER, IN. .0625
HEIGHT, IN. .975
DISTANCE, IN. 3.42
180
90
0
θ, DEGREES
LOG AMPLITUDE
0
-3
-6
CALIBRATION POINTS, DB

Fig. 2.19

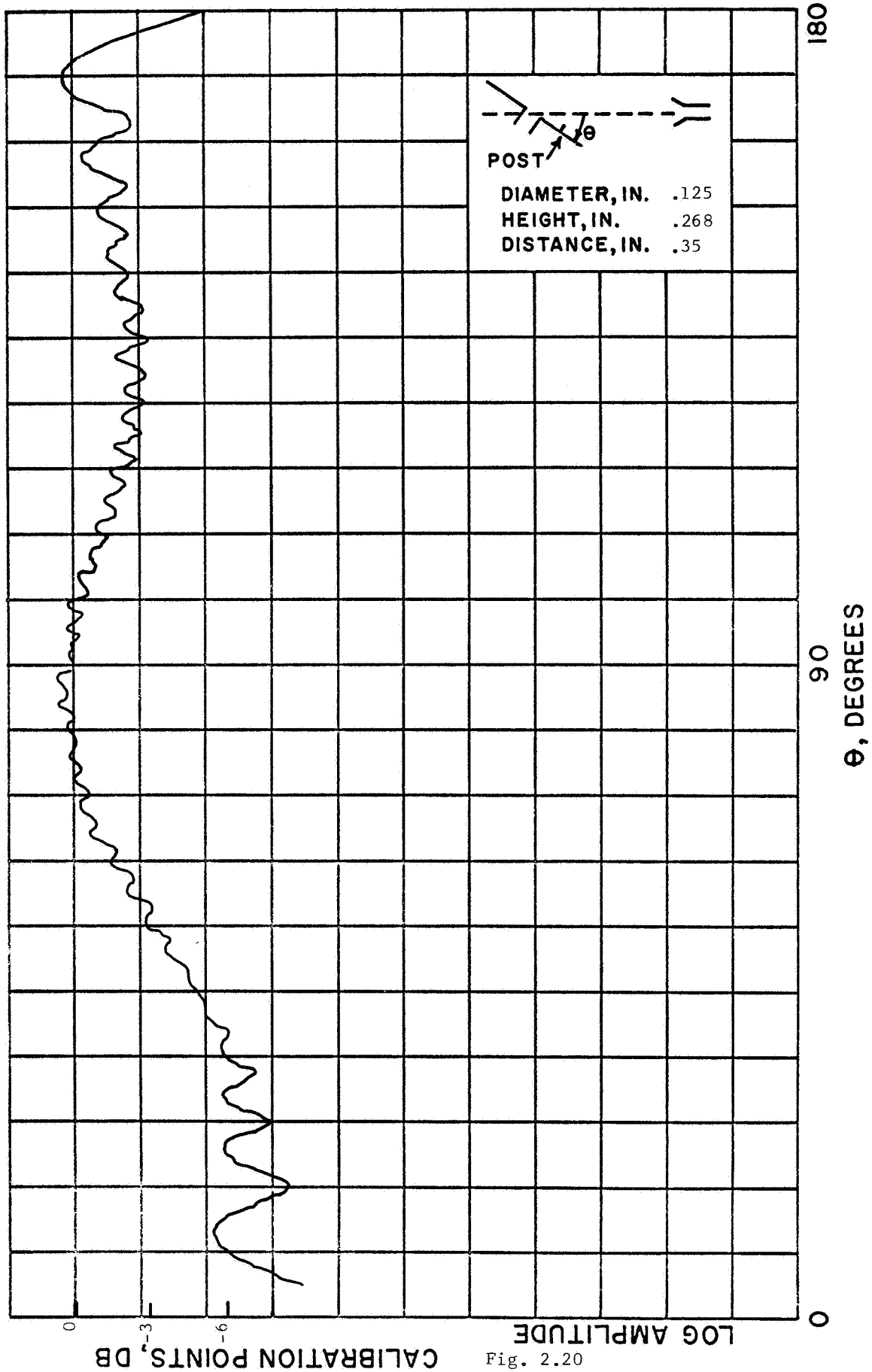
θ
POST
DIAMETER, IN. .125
HEIGHT, IN. .268
DISTANCE, IN. .35
180
90
0
θ, DEGREES
LOG AMPLITUDE
0
-3
-6
CALIBRATION POINTS, DB

Fig. 2.20

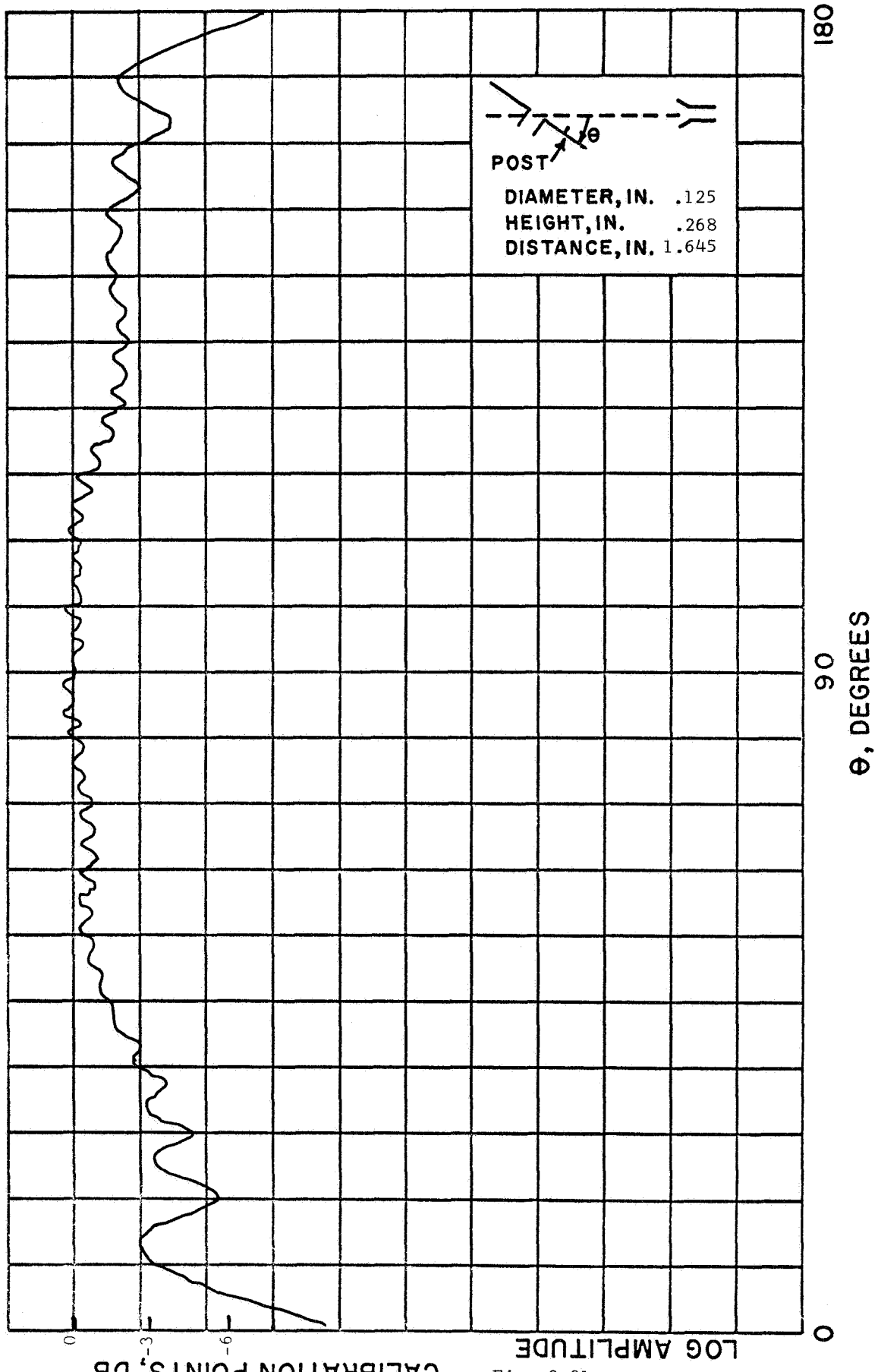
θ
POST
DIAMETER, IN. .125
HEIGHT, IN. .268
DISTANCE, IN. 1.645
180
90
0
θ, DEGREES
LOG AMPLITUDE
0
-3
-6
CALIBRATION POINTS, DB

Fig. 2.21

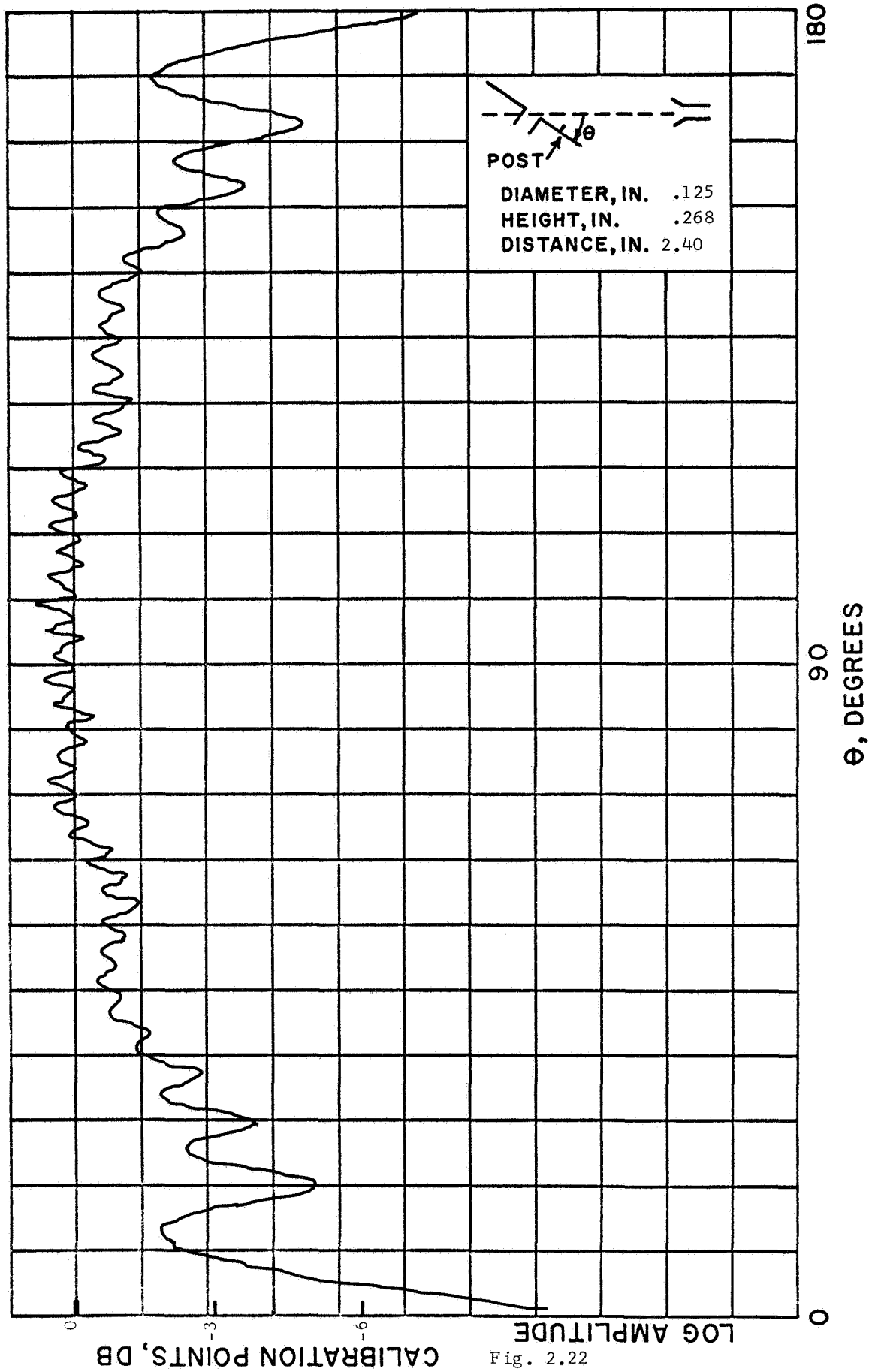
POST
DIAMETER, IN. .125
HEIGHT, IN. .268
DISTANCE, IN. 2.40
θ
180
90
0
θ, DEGREES
LOG AMPLITUDE
0
-3
-6
CALIBRATION POINTS, DB

Fig. 2.22

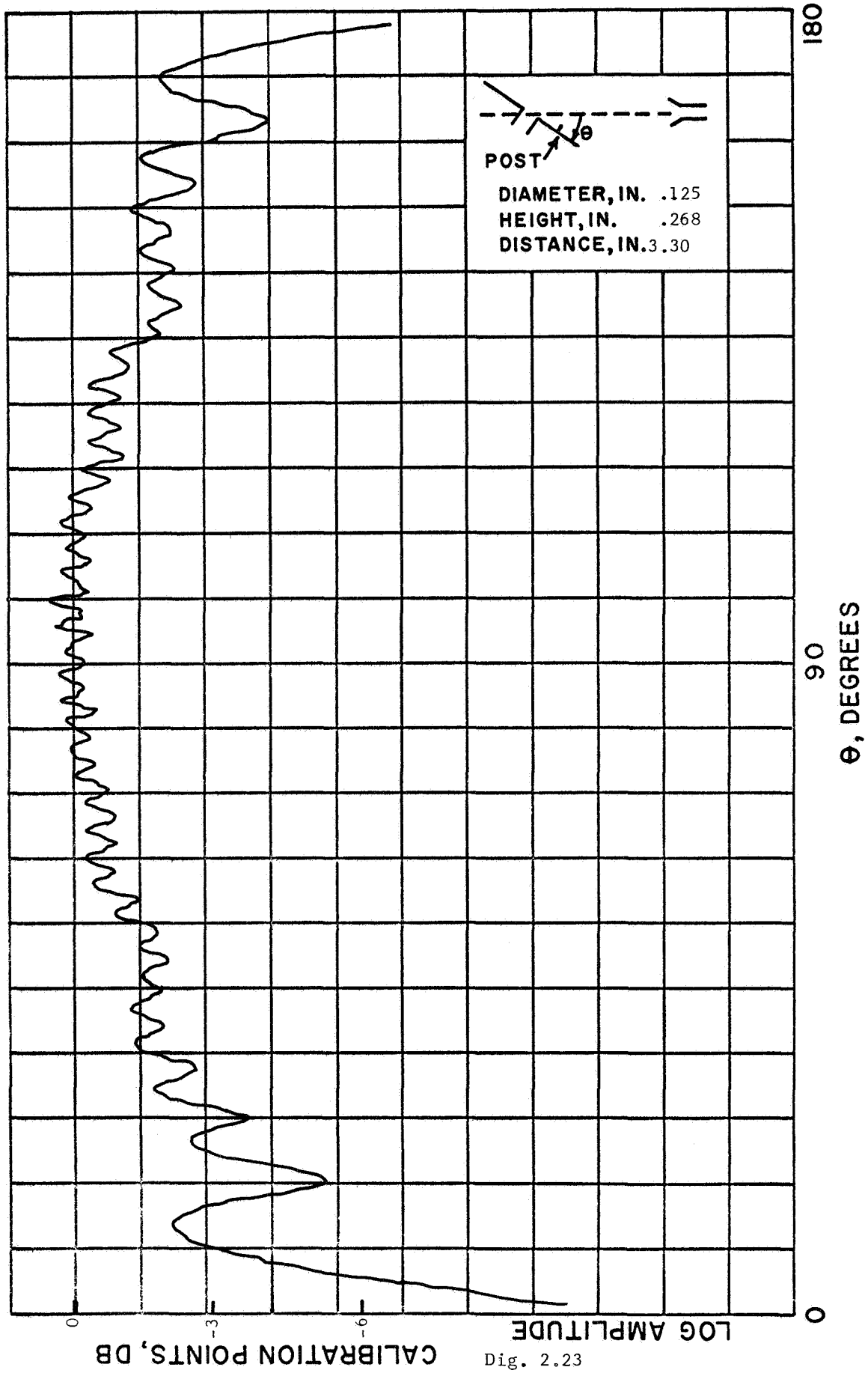
θ
POST
DIAMETER, IN. .125
HEIGHT, IN. .268
DISTANCE, IN. 3.30
180
90
0
θ, DEGREES
LOG AMPLITUDE
0
-3
-6
CALIBRATION POINTS, DB

Dig. 2.23

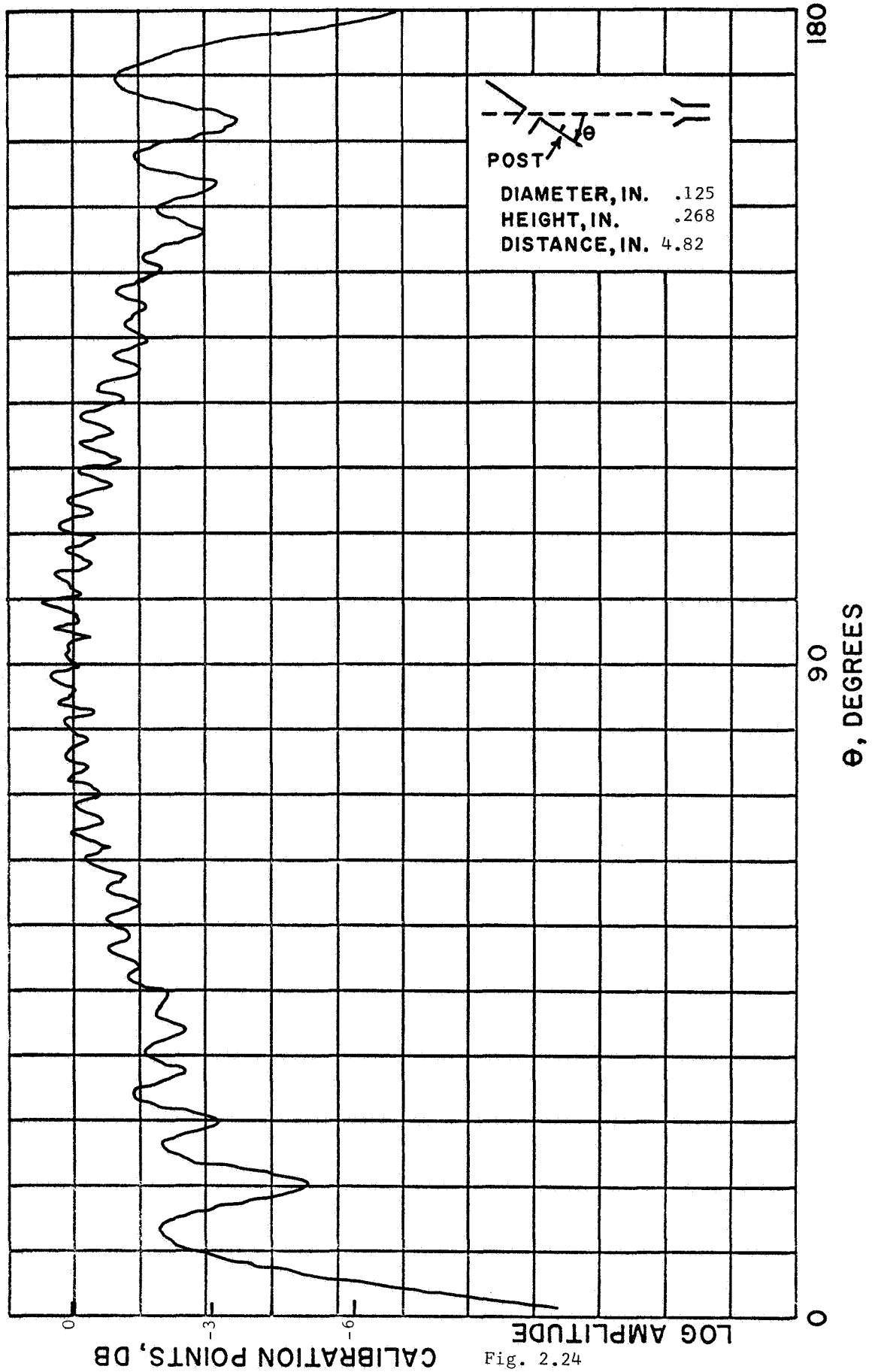
POST
θ
DIAMETER, IN. .125
HEIGHT, IN. .268
DISTANCE, IN. 4.82
180
90
0
θ, DEGREES
LOG AMPLITUDE
0
-3
-6
CALIBRATION POINTS, DB

Fig. 2.24

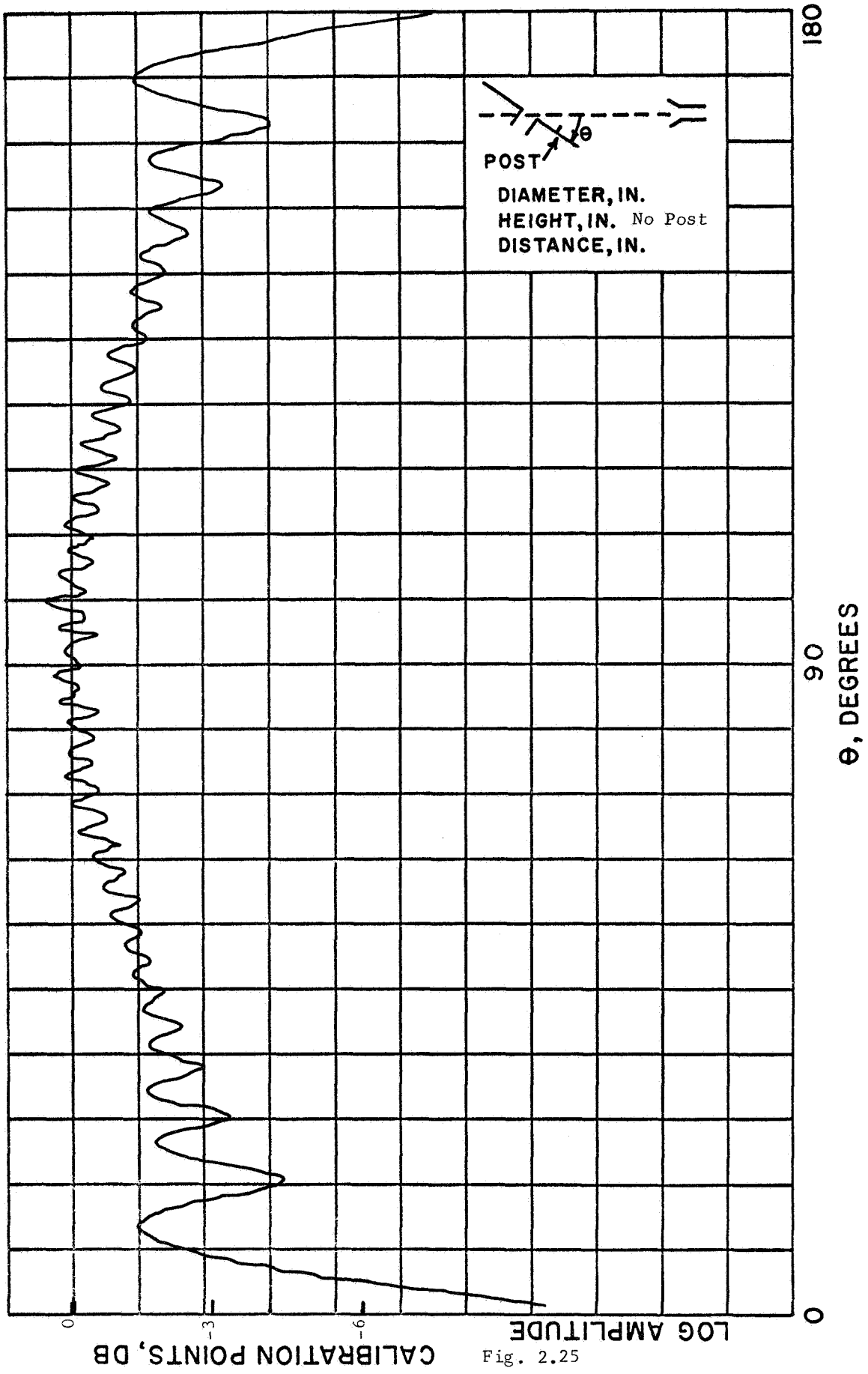
θ
POST
DIAMETER, IN.
HEIGHT, IN. No Post
DISTANCE, IN.
180
90
0
θ, DEGREES
LOG AMPLITUDE
0
-3
-6
CALIBRATION POINTS, DB

Fig. 2.25

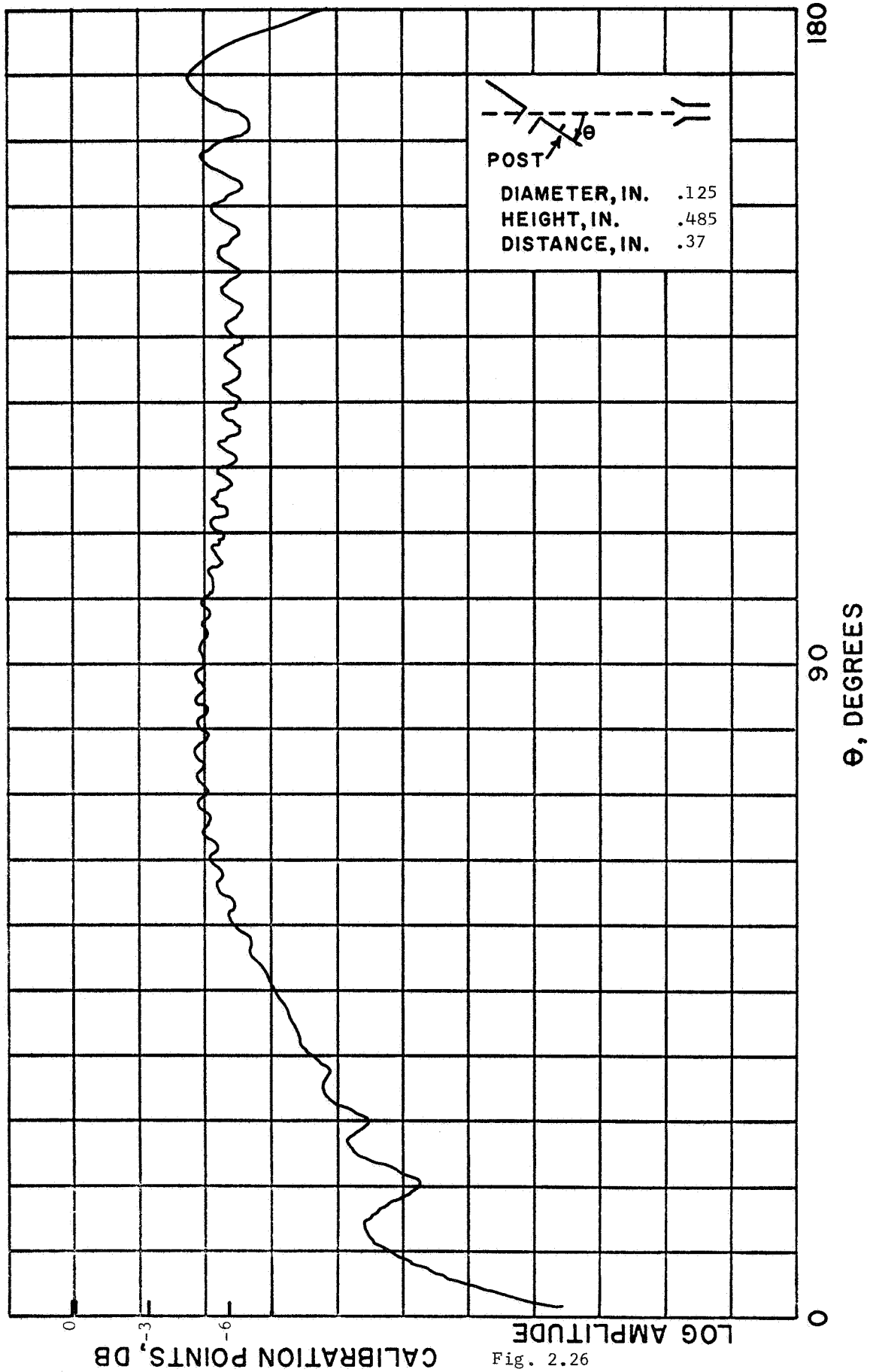
θ
POST
DIAMETER, IN. .125
HEIGHT, IN. .485
DISTANCE, IN. .37
180
90
0
θ, DEGREES
LOG AMPLITUDE
0
-3
-6
CALIBRATION POINTS, DB

Fig. 2.26

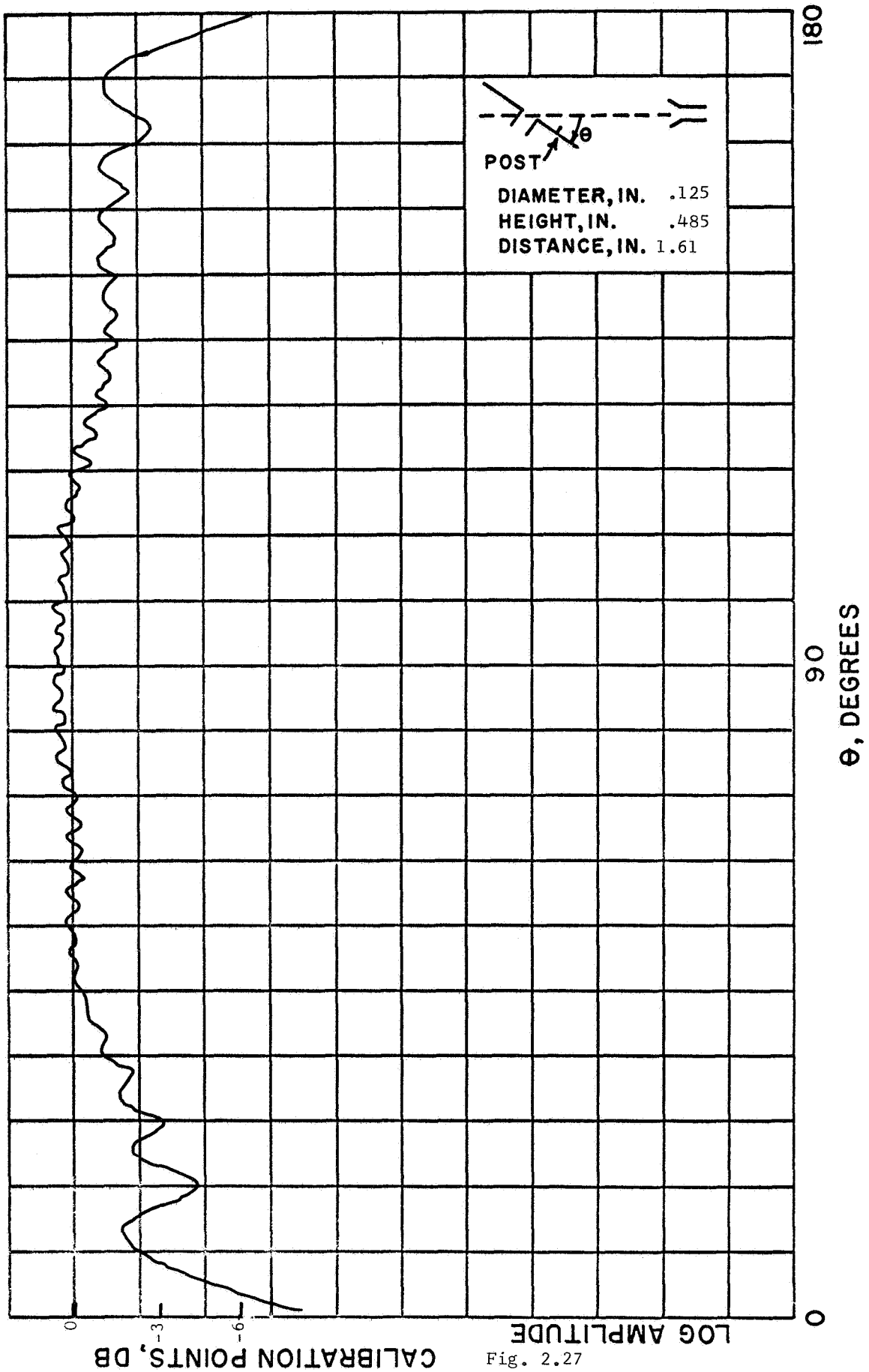
θ
POST
DIAMETER, IN. .125
HEIGHT, IN. .485
DISTANCE, IN. 1.61
180
90
0
θ, DEGREES
LOG AMPLITUDE
0
-3
-6
CALIBRATION POINTS, DB

Fig. 2.27

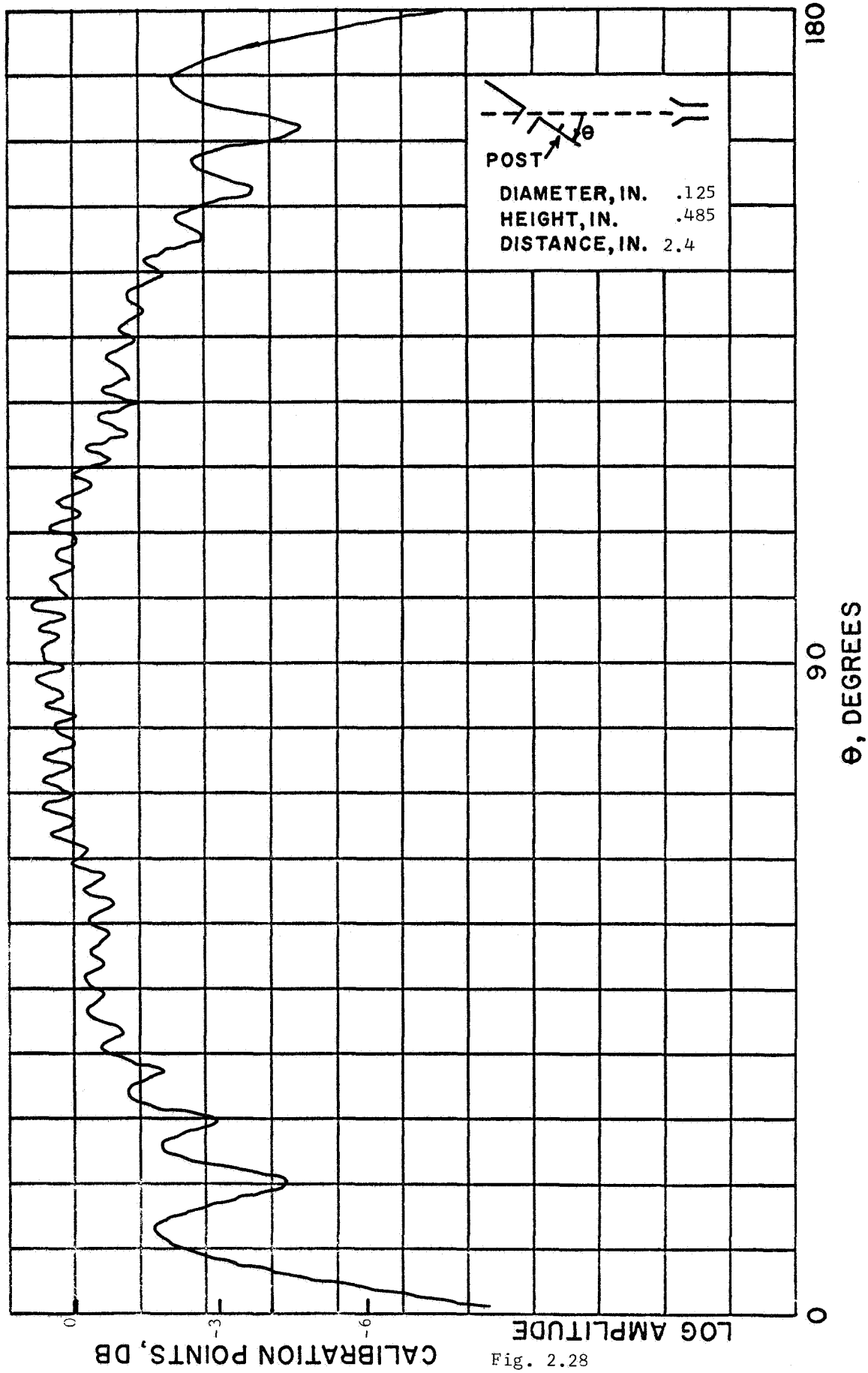
θ
POST
DIAMETER, IN. .125
HEIGHT, IN. .485
DISTANCE, IN. 2.4
180
90
0
θ, DEGREES
LOG AMPLITUDE
0
-3
-6
CALIBRATION POINTS, DB

Fig. 2.28

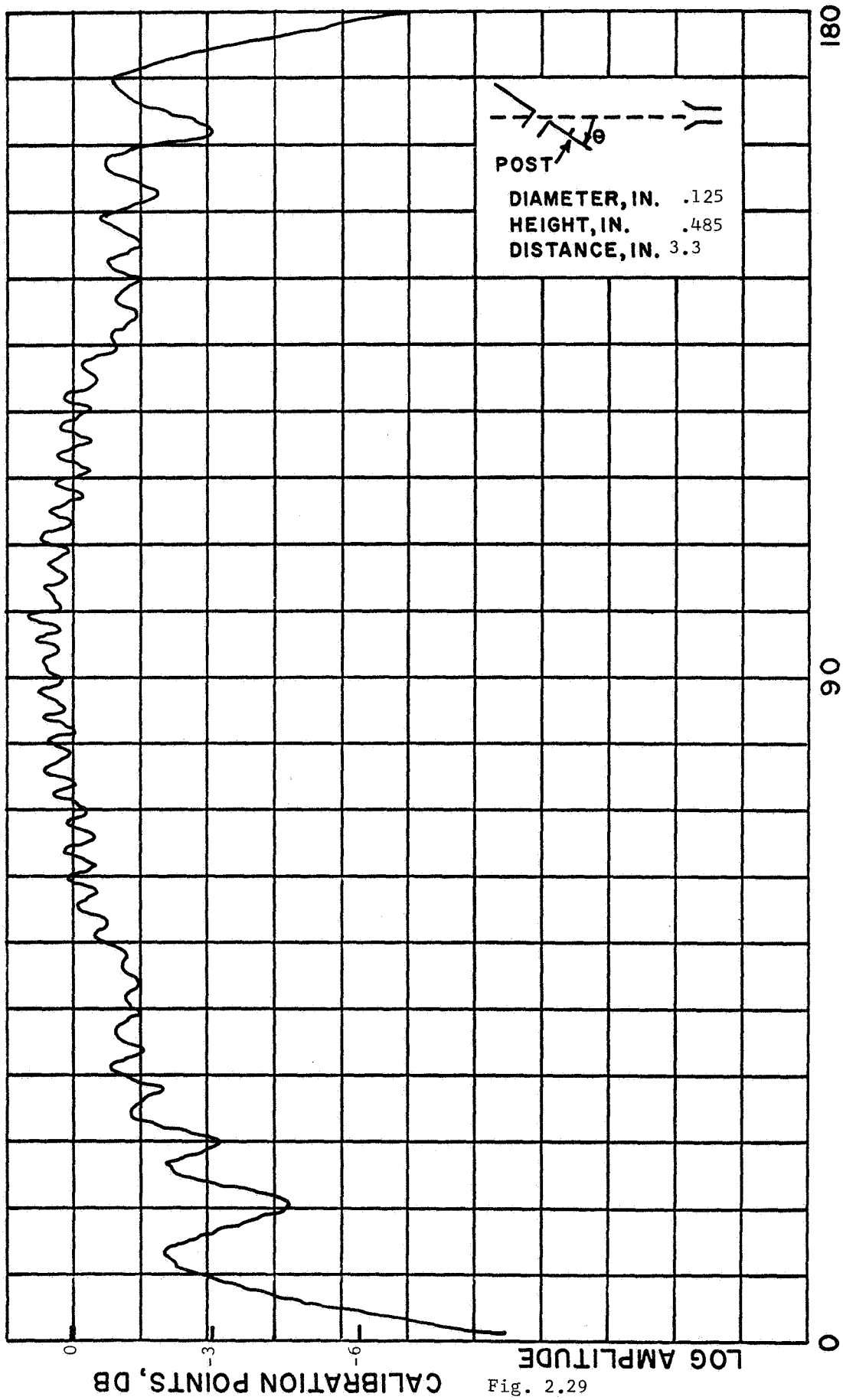
θ
POST
DIAMETER, IN. .125
HEIGHT, IN. .485
DISTANCE, IN. 3.3
180
90
0
θ, DEGREES
LOG AMPLITUDE
0
-3
-6
CALIBRATION POINTS, DB

Fig. 2.29

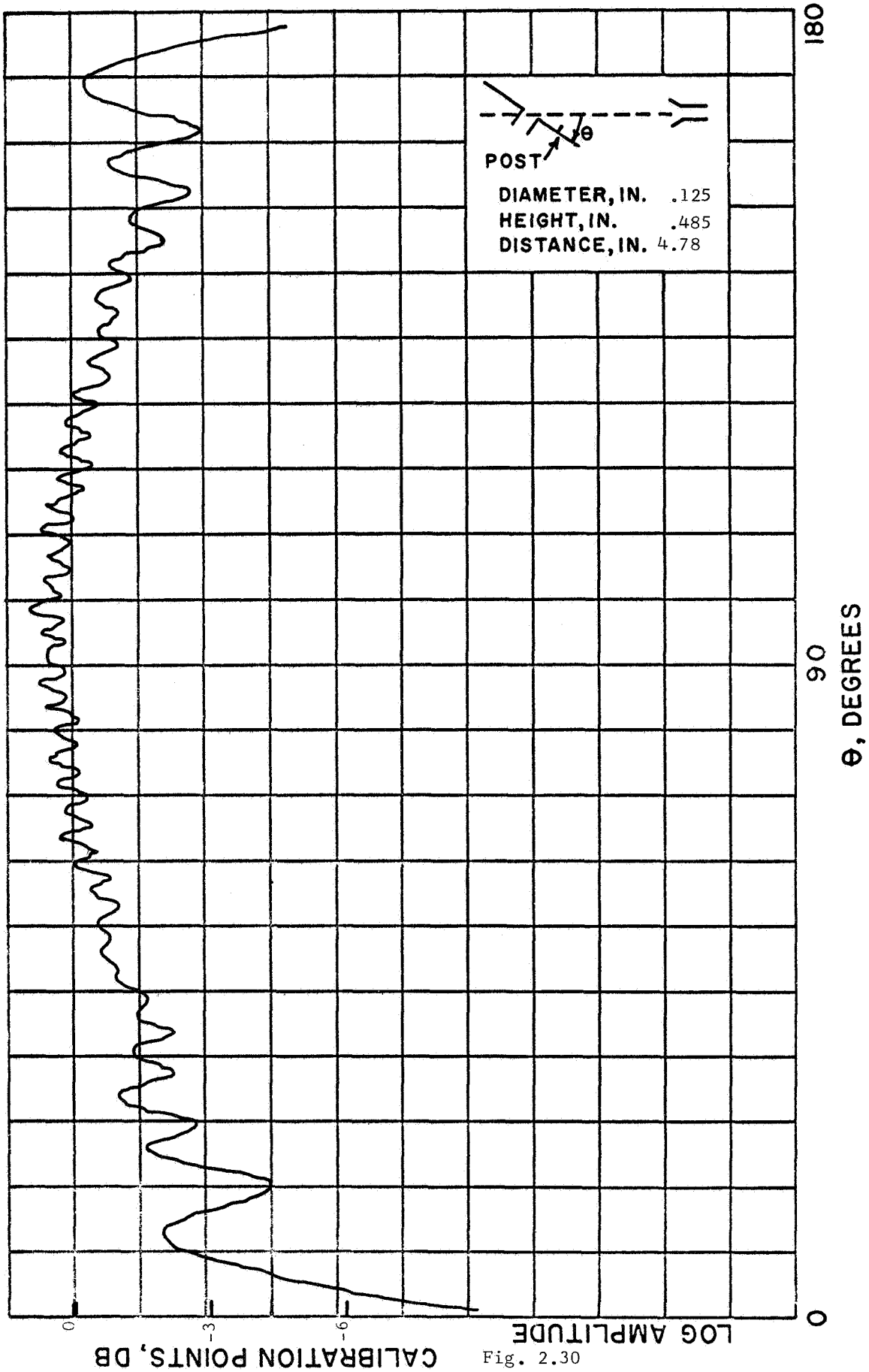
θ
POST
DIAMETER, IN. .125
HEIGHT, IN. .485
DISTANCE, IN. 4.78
180
90
0
θ, DEGREES
LOG AMPLITUDE
0
-3
-6
CALIBRATION POINTS, DB

Fig. 2.30

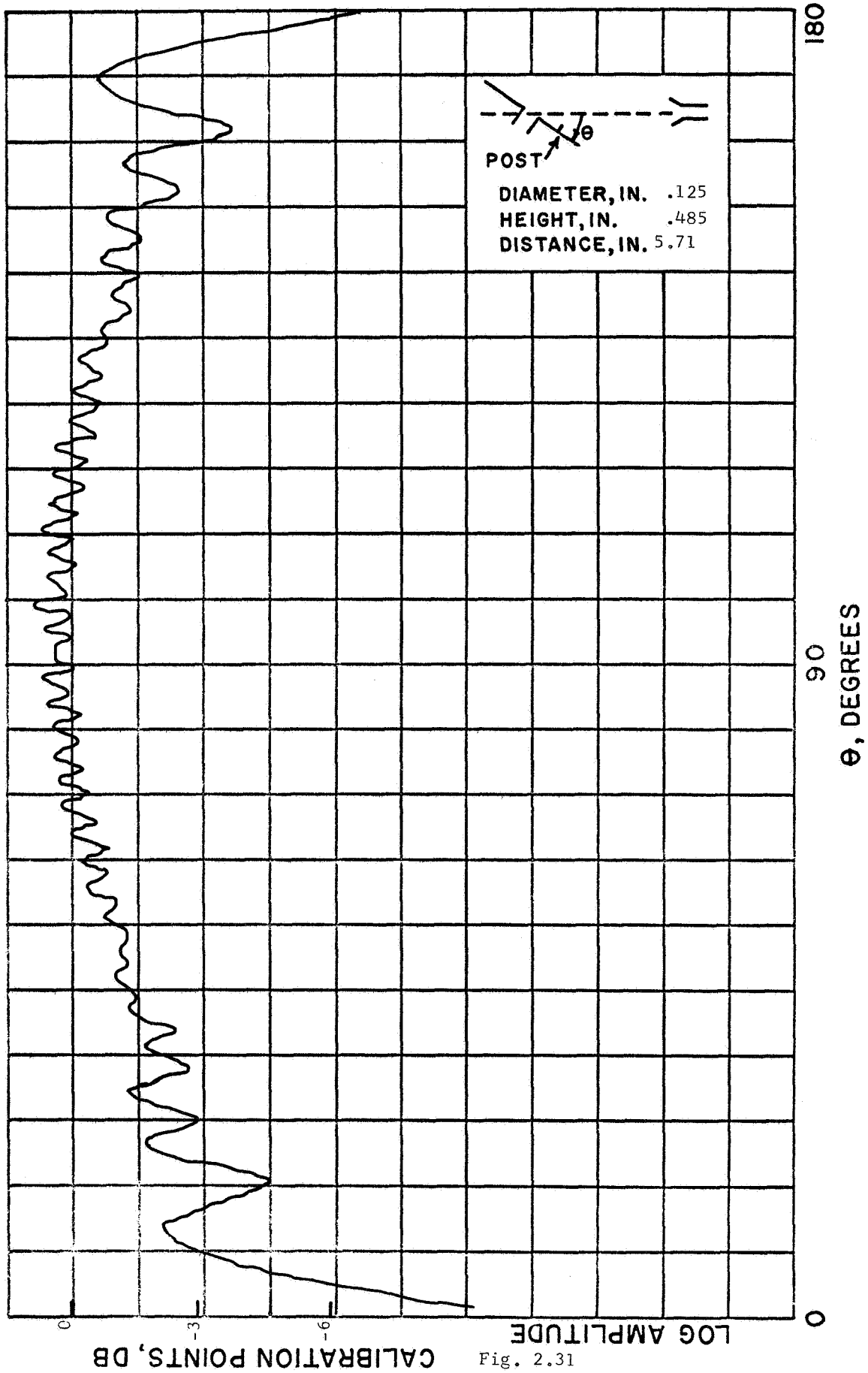
POST
θ
DIAMETER, IN. .125
HEIGHT, IN. .485
DISTANCE, IN. 5.71
180
90
0
θ, DEGREES
LOG AMPLITUDE
0
-3
-6
CALIBRATION POINTS, DB

Fig. 2.31

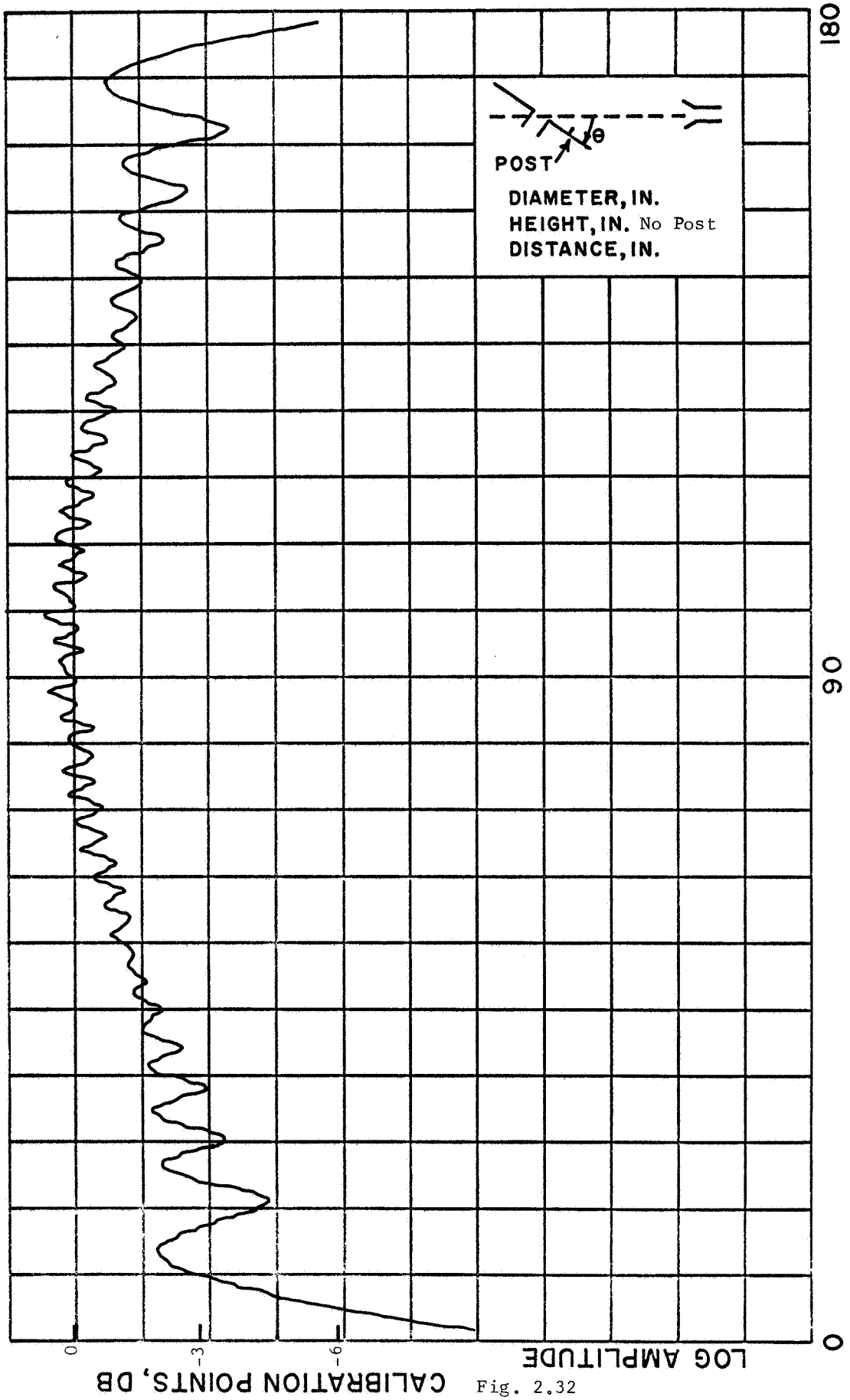
θ
POST
DIAMETER, IN.
HEIGHT, IN. No Post
DISTANCE, IN.
180
90
0
θ, DEGREES
LOG AMPLITUDE
0
-3
-6
CALIBRATION POINTS, DB

Fig. 2.32

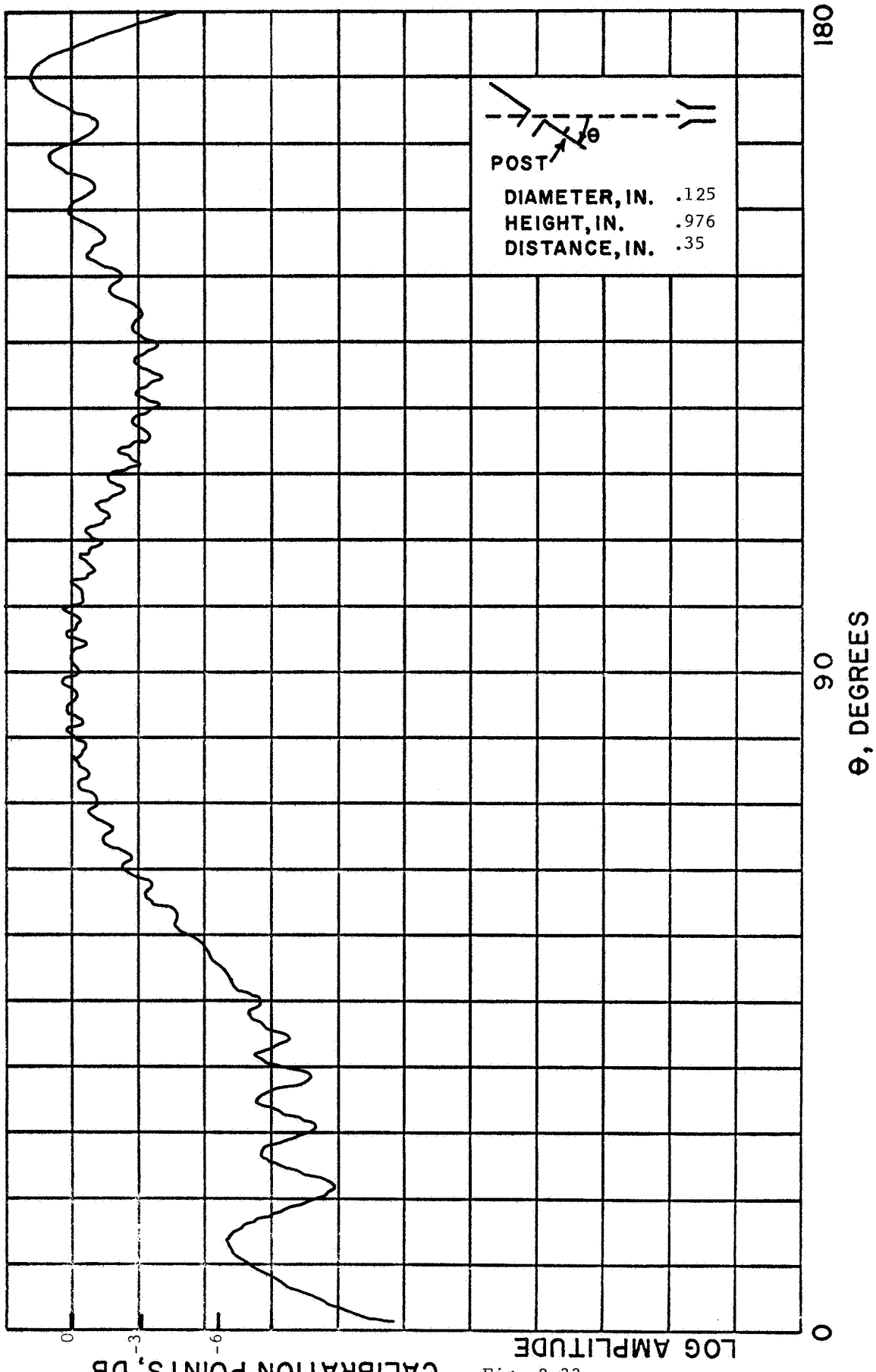
θ
POST
DIAMETER, IN. .125
HEIGHT, IN. .976
DISTANCE, IN. .35
180
90
0
θ, DEGREES
LOG AMPLITUDE
0
-3
-6
CALIBRATION POINTS, DB

Fig. 2.33

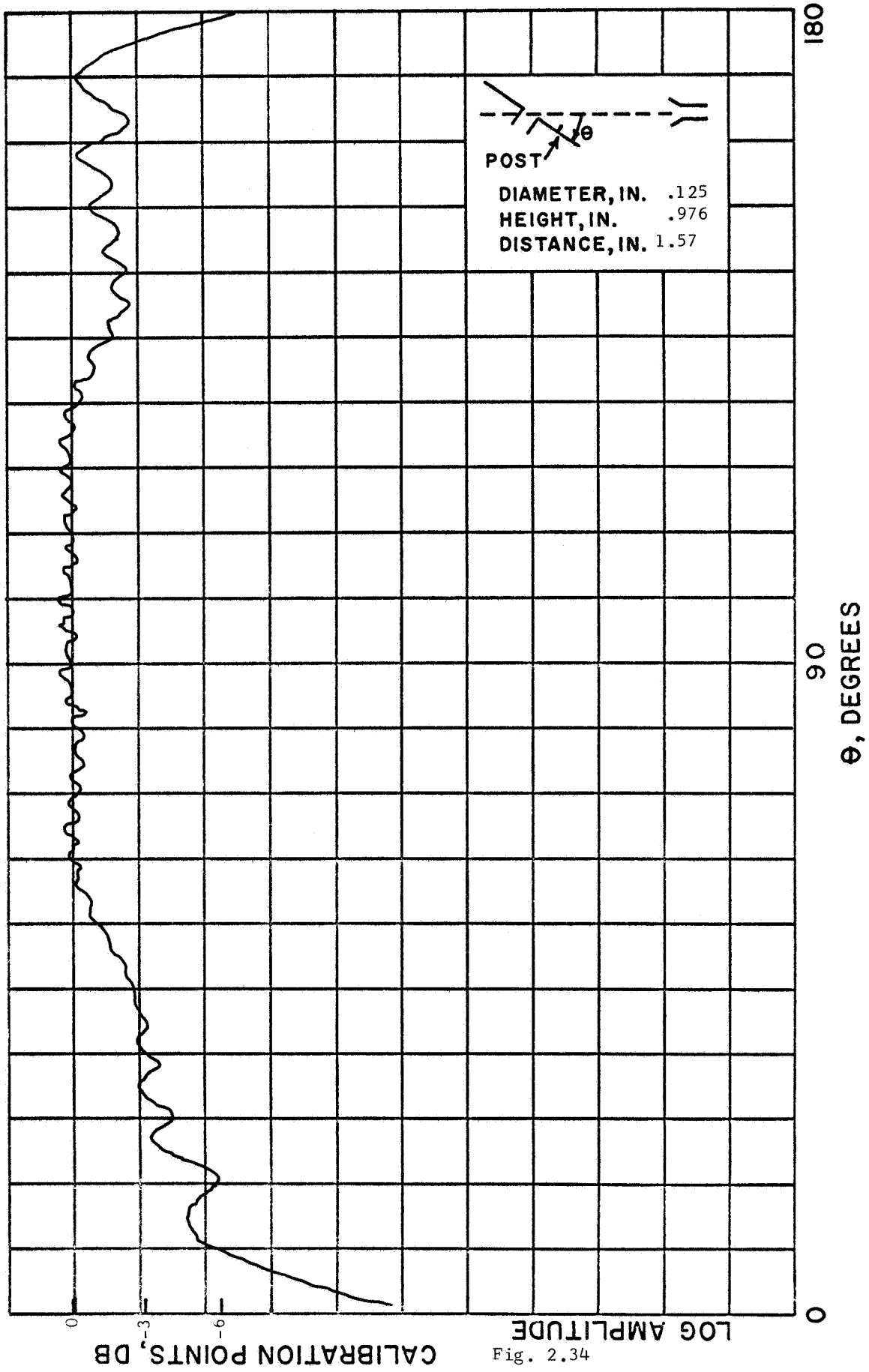
POST
θ
DIAMETER, IN. .125
HEIGHT, IN. .976
DISTANCE, IN. 1.57
180
90
0
θ, DEGREES
LOG AMPLITUDE
0
-3
-6
CALIBRATION POINTS, DB

Fig. 2.34

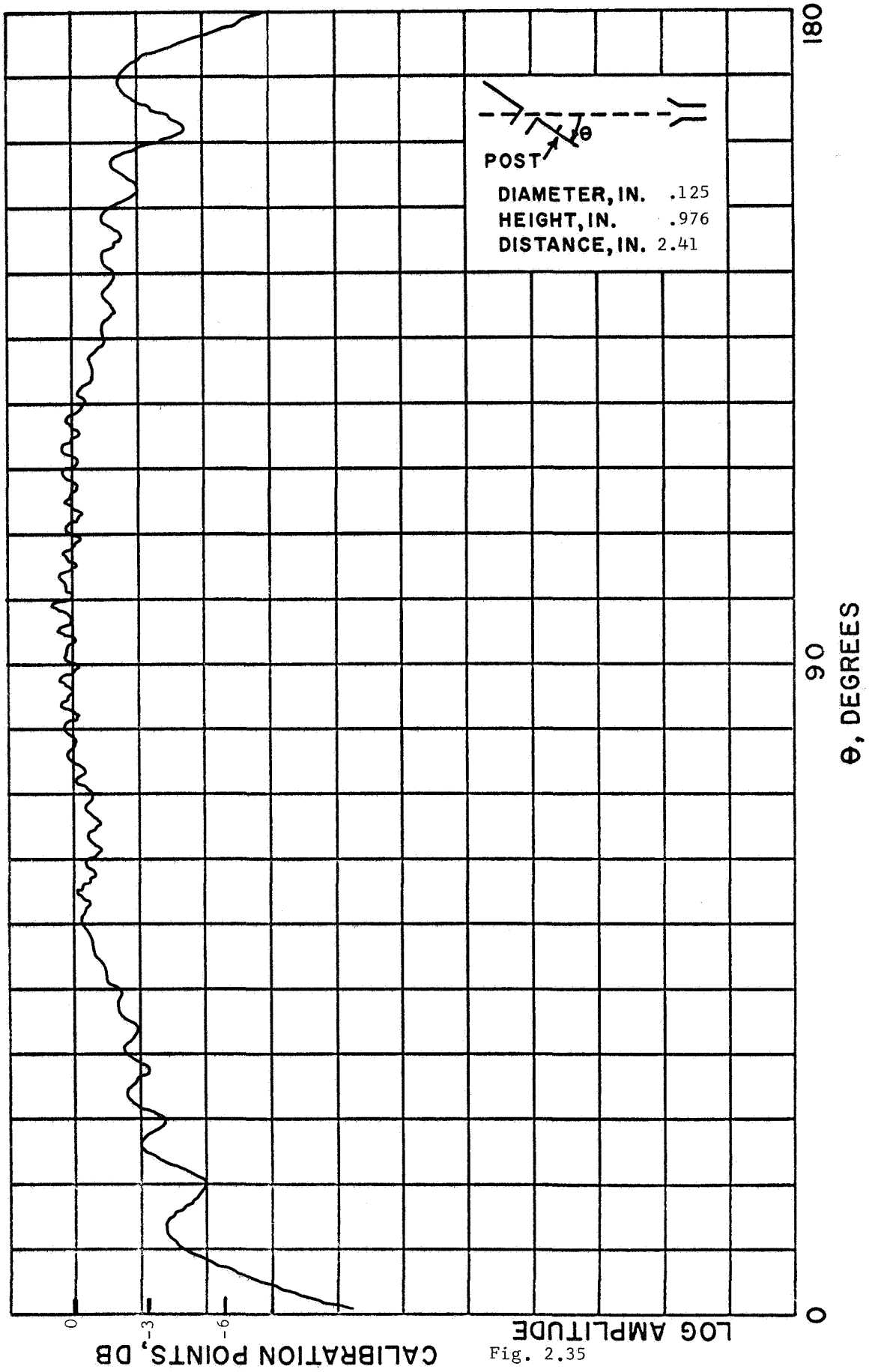
θ
POST
DIAMETER, IN. .125
HEIGHT, IN. .976
DISTANCE, IN. 2.41
180
90
0
θ, DEGREES
LOG AMPLITUDE
0
-3
-6
CALIBRATION POINTS, DB

Fig. 2.35

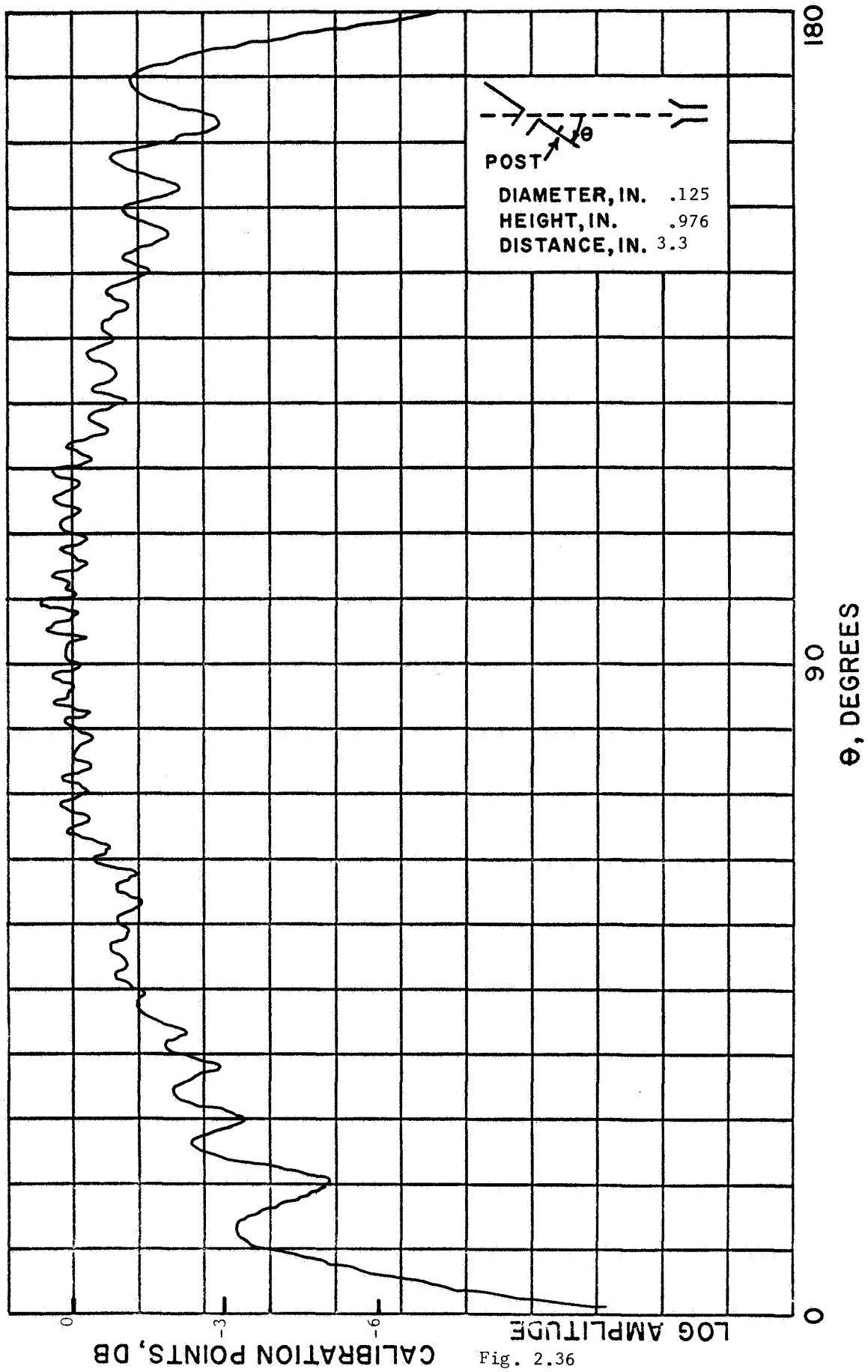
θ
POST
DIAMETER, IN. .125
HEIGHT, IN. .976
DISTANCE, IN. 3.3
180
90
0
θ, DEGREES
LOG AMPLITUDE
0
-3
-6
CALIBRATION POINTS, DB

Fig. 2.36

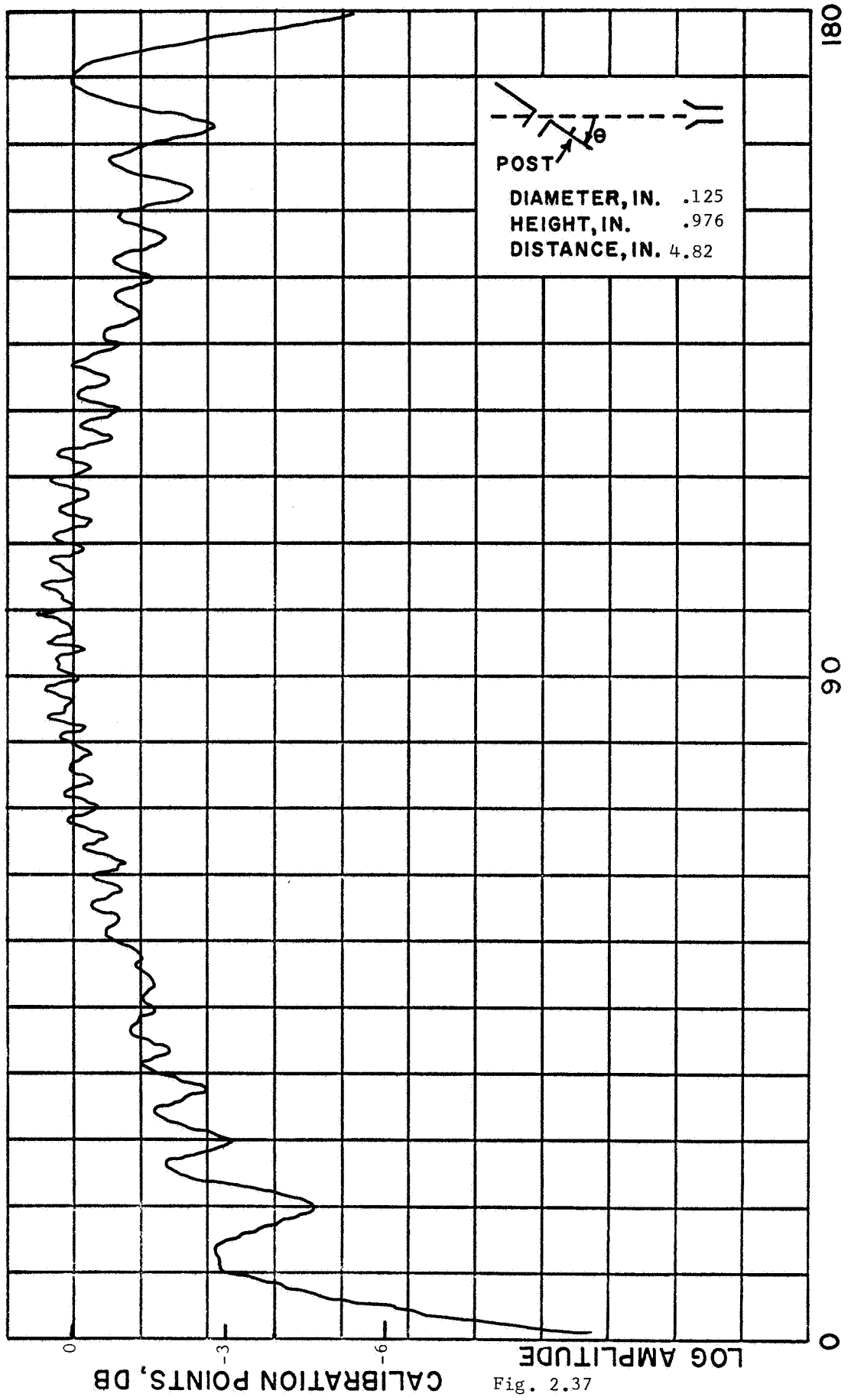
θ
POST
DIAMETER, IN. .125
HEIGHT, IN. .976
DISTANCE, IN. 4.82
180
90
0
θ, DEGREES
LOG AMPLITUDE
0
-3
-6
CALIBRATION POINTS, DB

Fig. 2.37

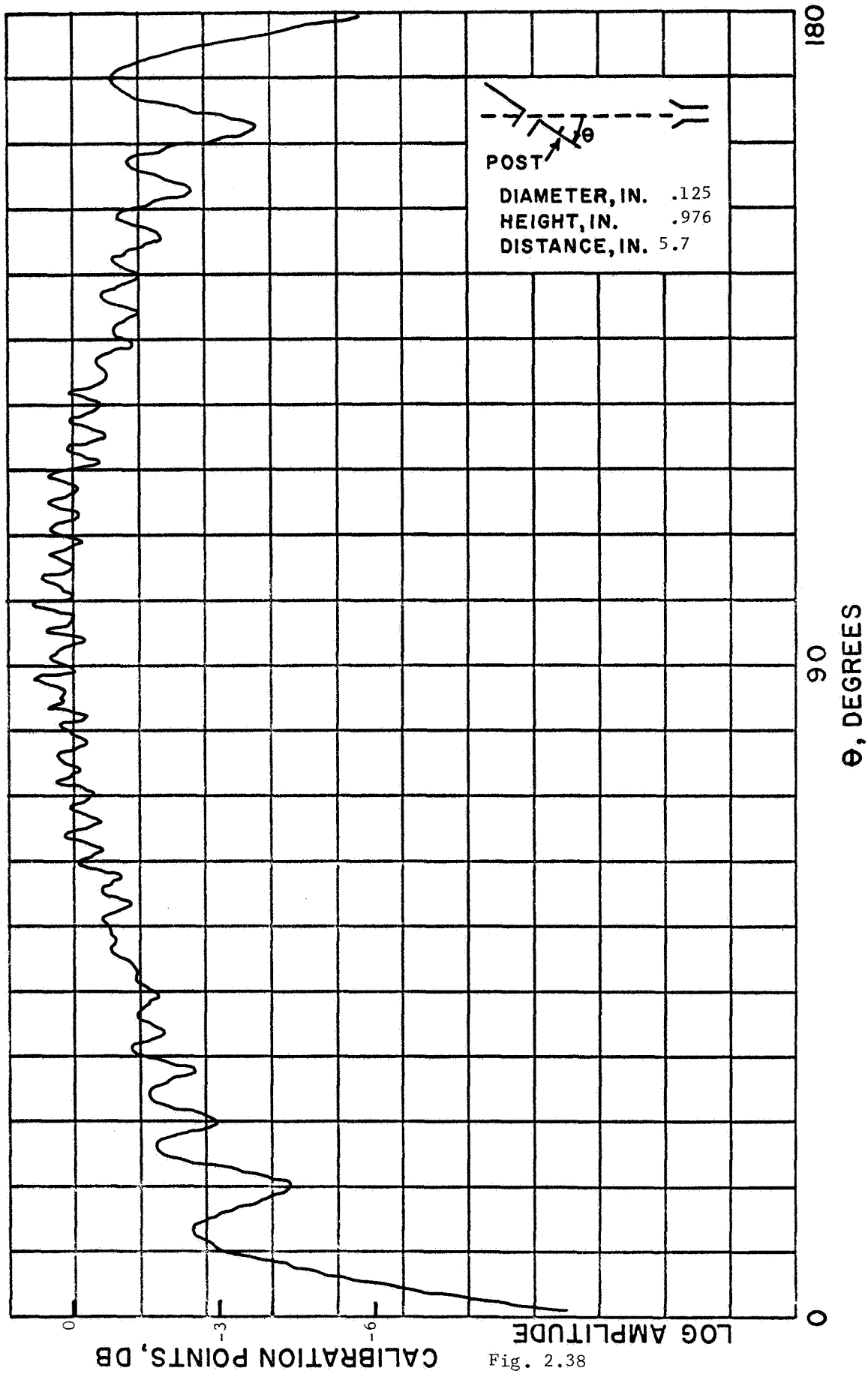
θ
POST
DIAMETER, IN. .125
HEIGHT, IN. .976
DISTANCE, IN. 5.7
180
90
0
θ, DEGREES
LOG AMPLITUDE
0
-3
-6
CALIBRATION POINTS, DB

Fig. 2.38

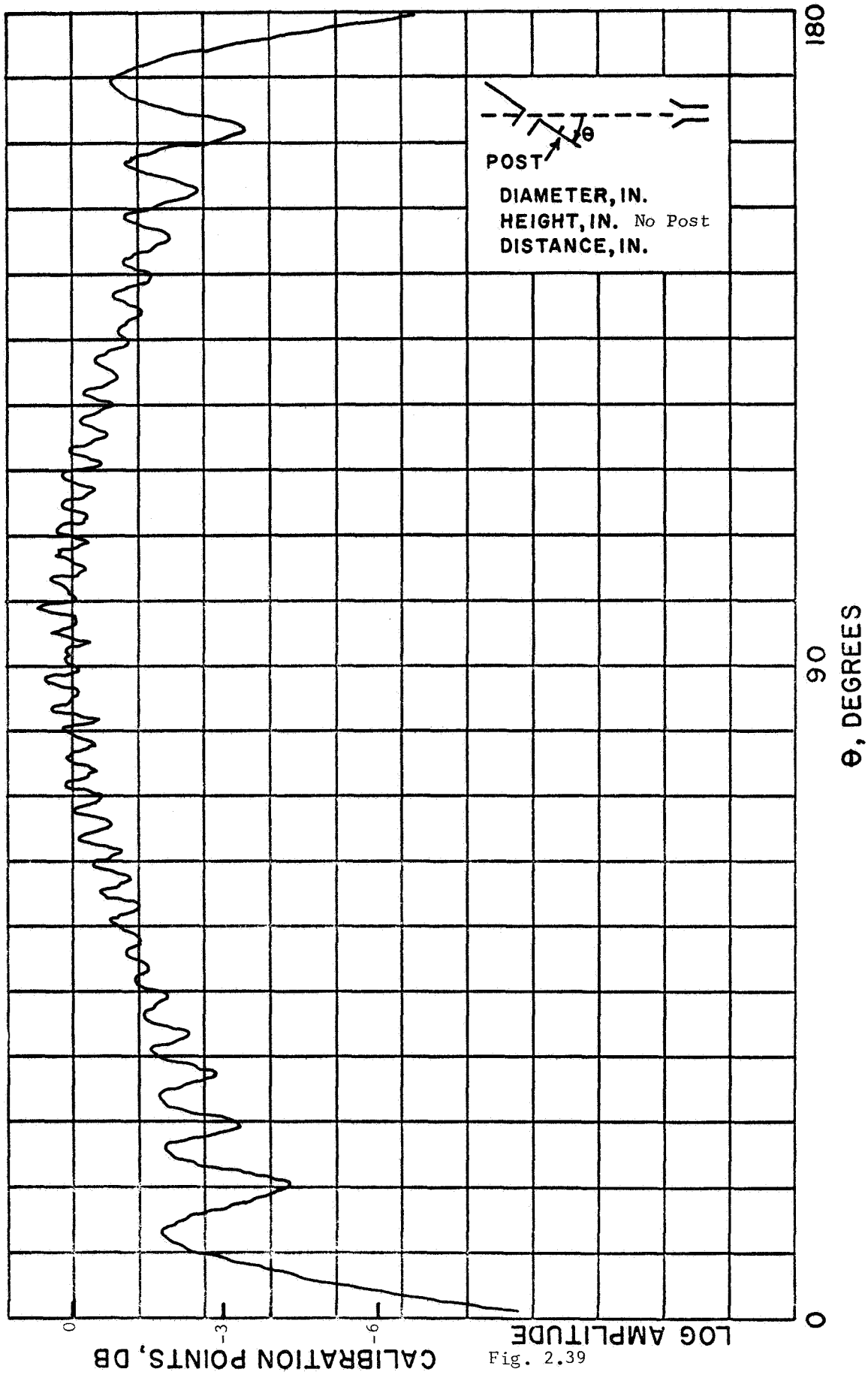
θ
POST
DIAMETER, IN.
HEIGHT, IN. No Post
DISTANCE, IN.
180
90
0
θ, DEGREES
LOG AMPLITUDE
0
-3
-6
CALIBRATION POINTS, DB

Fig. 2.39

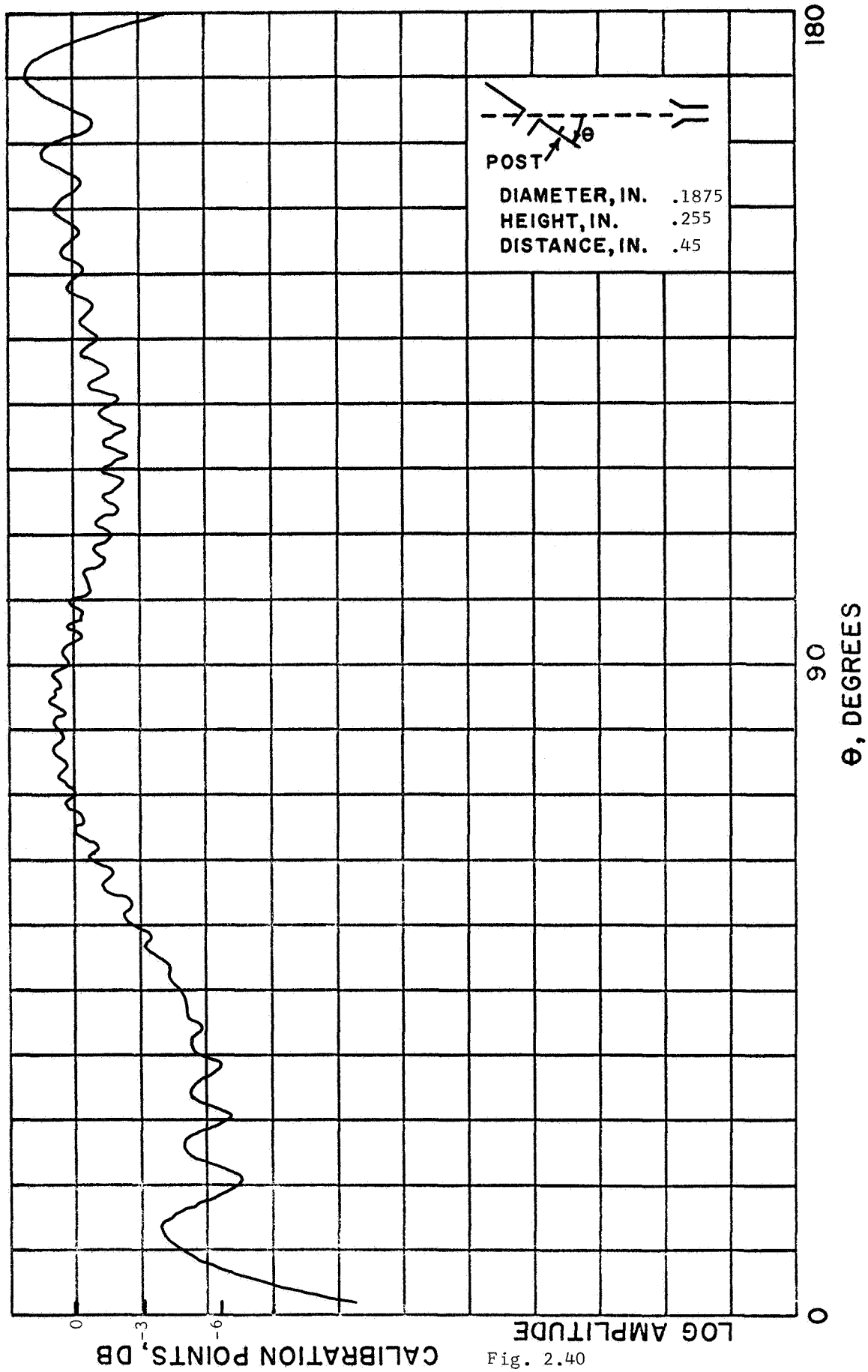
θ
POST
DIAMETER, IN. .1875
HEIGHT, IN. .255
DISTANCE, IN. .45
180
90
0
θ, DEGREES
LOG AMPLITUDE
0
-3
-6
CALIBRATION POINTS, DB

Fig. 2.40

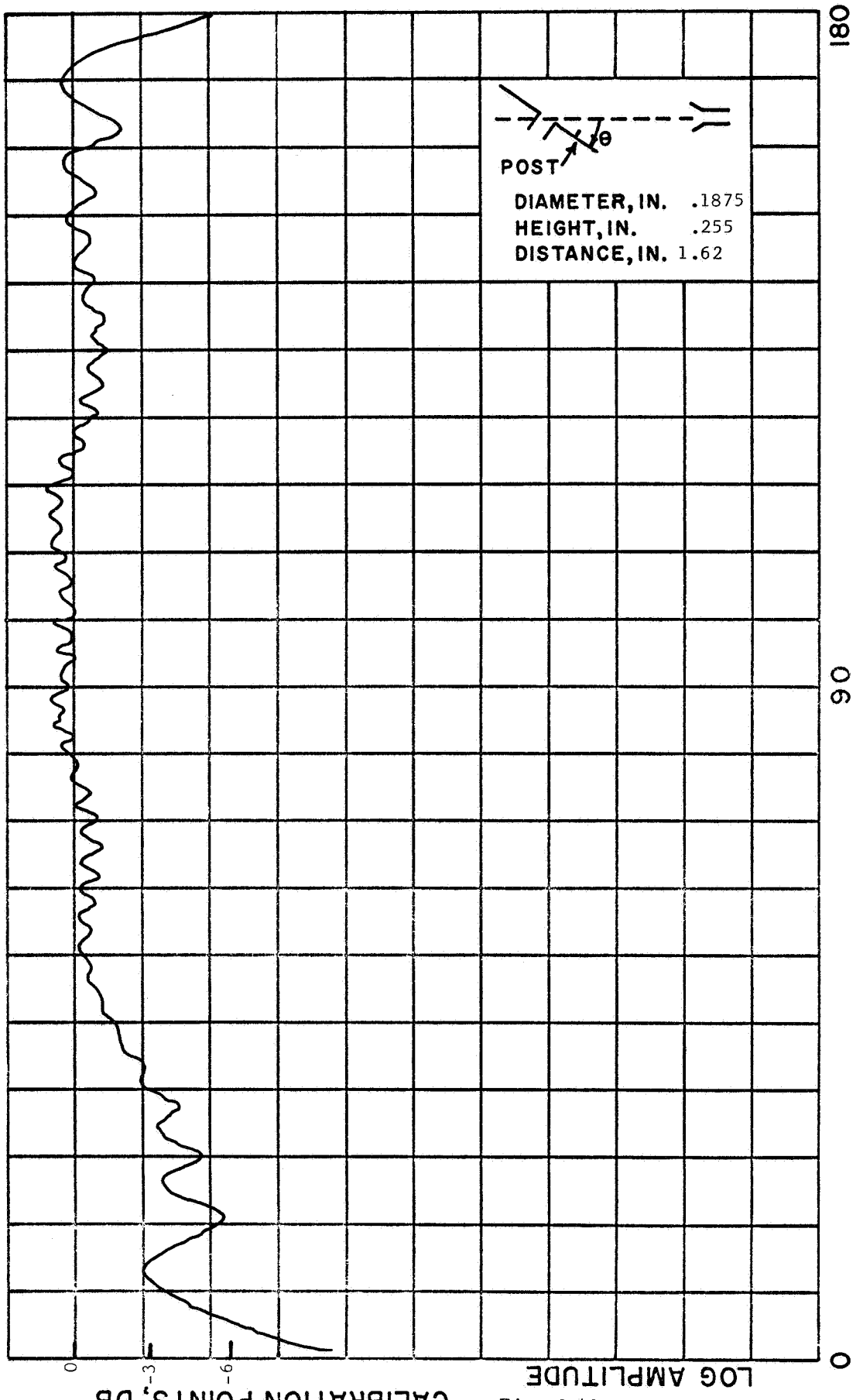
θ
POST
DIAMETER, IN. .1875
HEIGHT, IN. .255
DISTANCE, IN. 1.62
180
90
0
θ, DEGREES
LOG AMPLITUDE
0
-3
-6
CALIBRATION POINTS, DB

Fig. 2.41

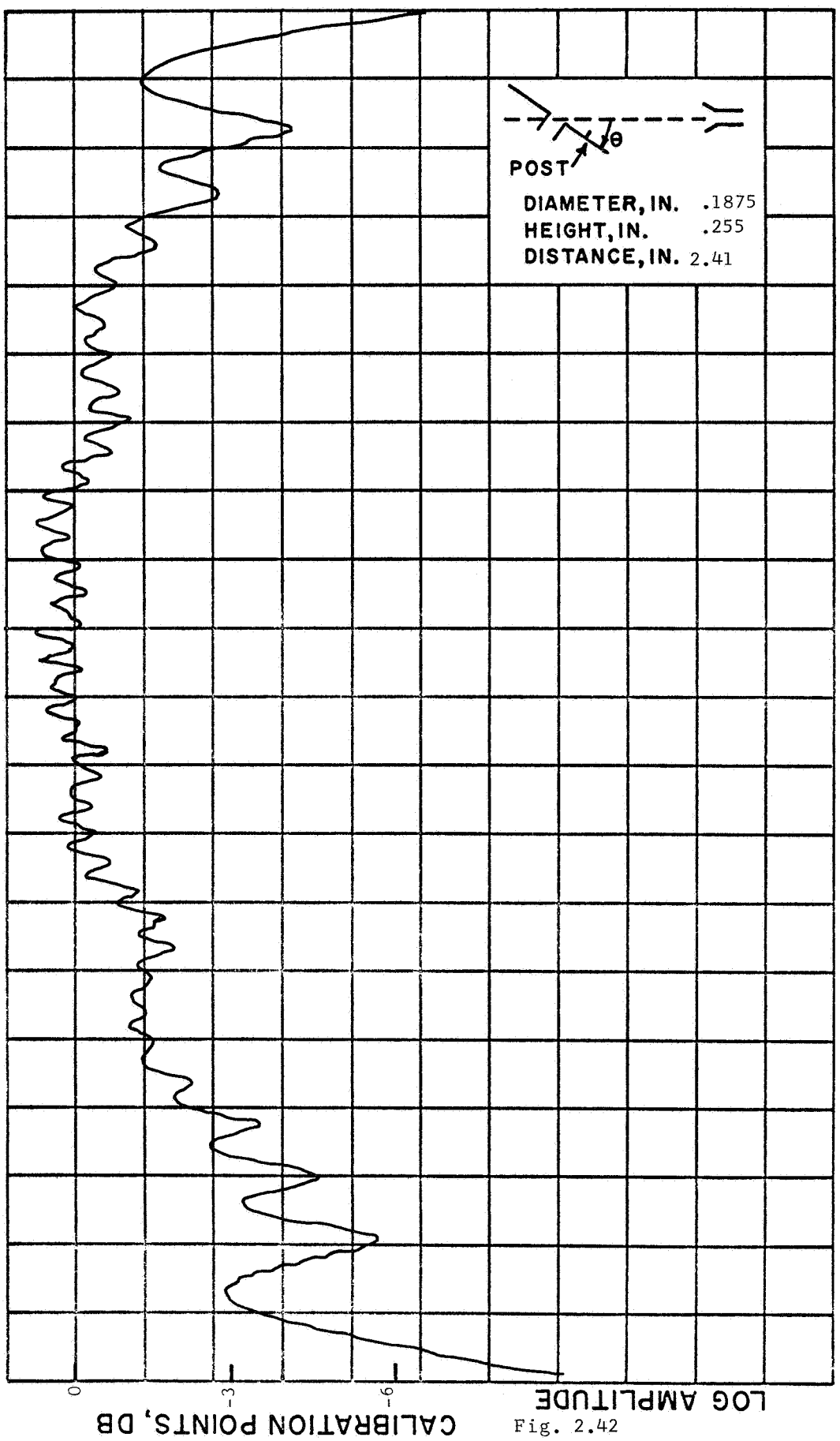
POST
θ
DIAMETER, IN. .1875
HEIGHT, IN. .255
DISTANCE, IN. 2.41
180
90
0
θ, DEGREES
LOG AMPLITUDE
0
-3
-6
CALIBRATION POINTS, DB

Fig. 2.42

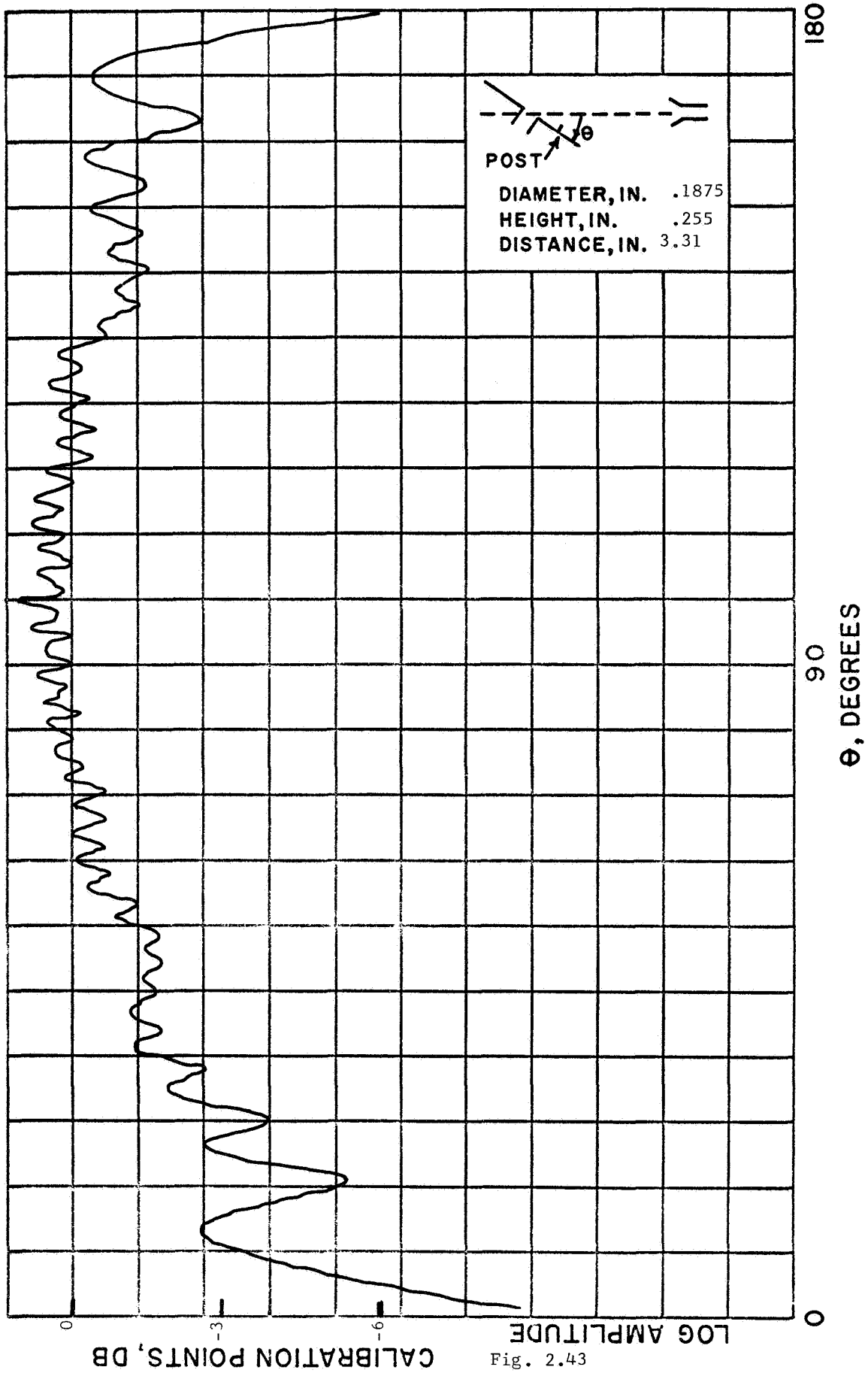
POST
θ
DIAMETER, IN. .1875
HEIGHT, IN. .255
DISTANCE, IN. 3.31
180
90
0
θ, DEGREES
LOG AMPLITUDE
0
-3
-6
CALIBRATION POINTS, DB

Fig. 2.43

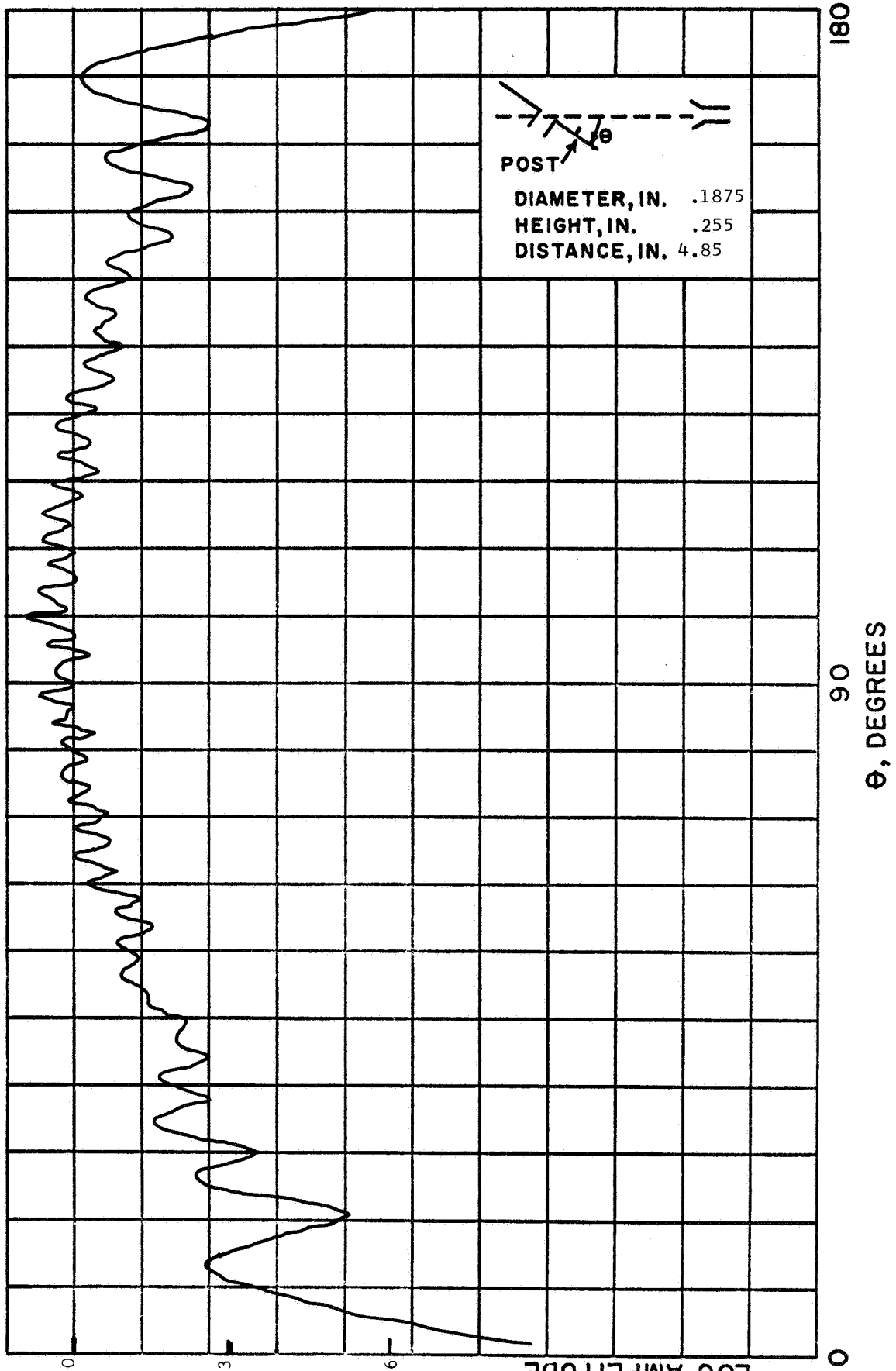
POST
DIAMETER, IN. .1875
HEIGHT, IN. .255
DISTANCE, IN. 4.85
θ
180
90
0
θ, DEGREES
LOG AMPLITUDE
0
-3
-6
CALIBRATION POINTS, DB

Fig. 2.44

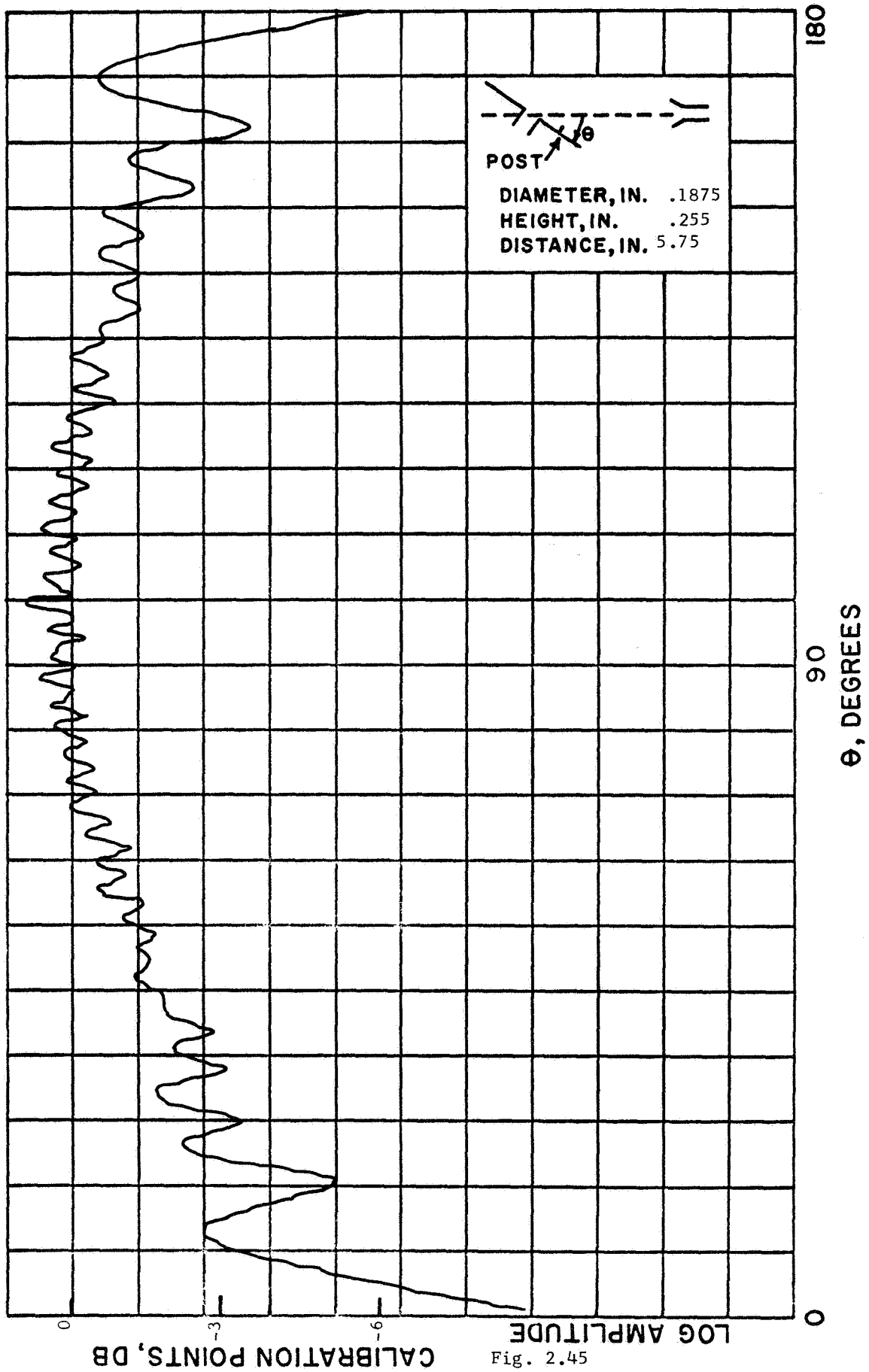
θ
POST
DIAMETER, IN. .1875
HEIGHT, IN. .255
DISTANCE, IN. 5.75
180
90
0
θ, DEGREES
LOG AMPLITUDE
0
-3
-6
CALIBRATION POINTS, DB

Fig. 2.45

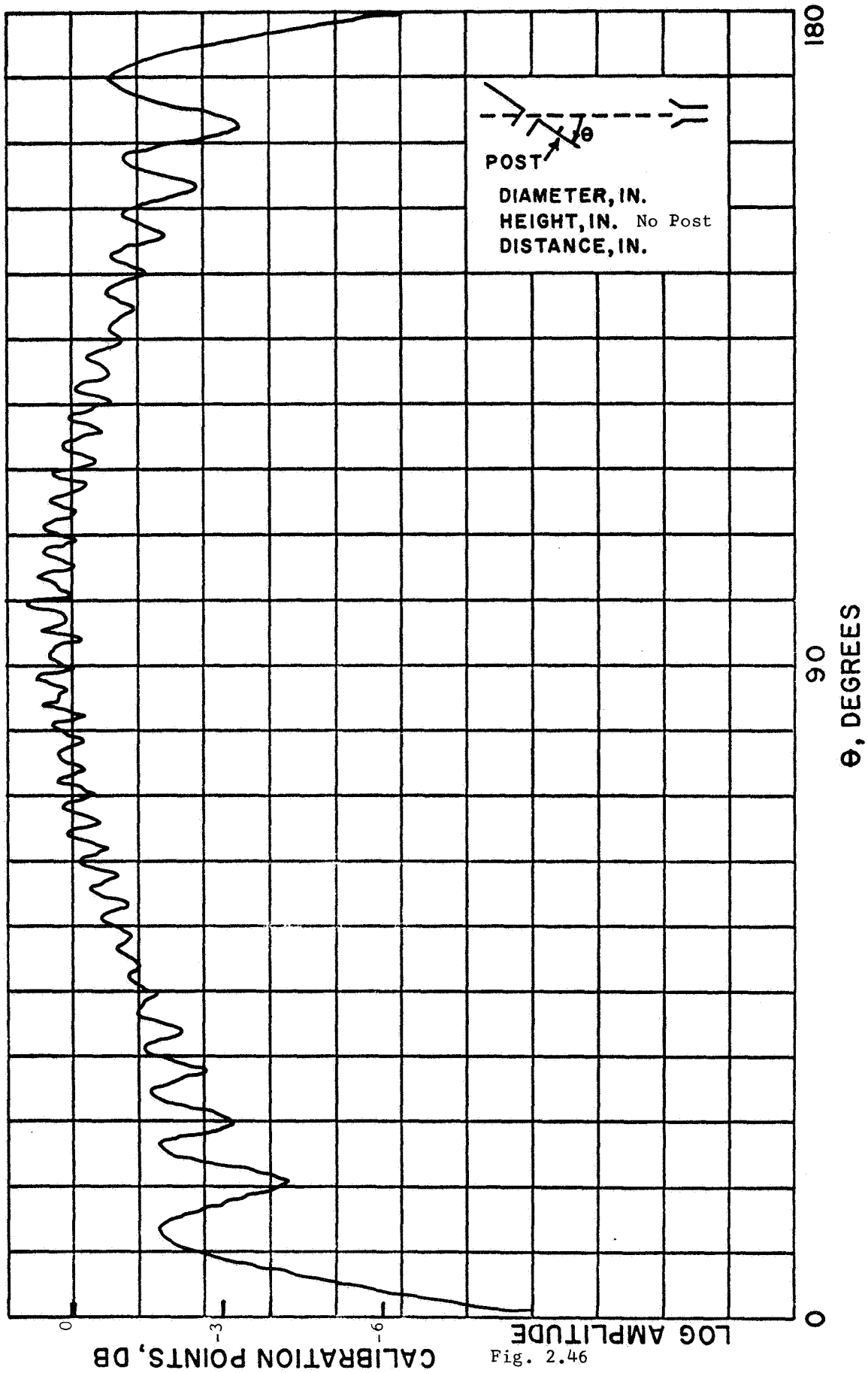
POST
θ
DIAMETER, IN.
HEIGHT, IN. No Post
DISTANCE, IN.
180
90
0
θ, DEGREES
LOG AMPLITUDE
0
-3
-6
CALIBRATION POINTS, DB

Fig. 2.46

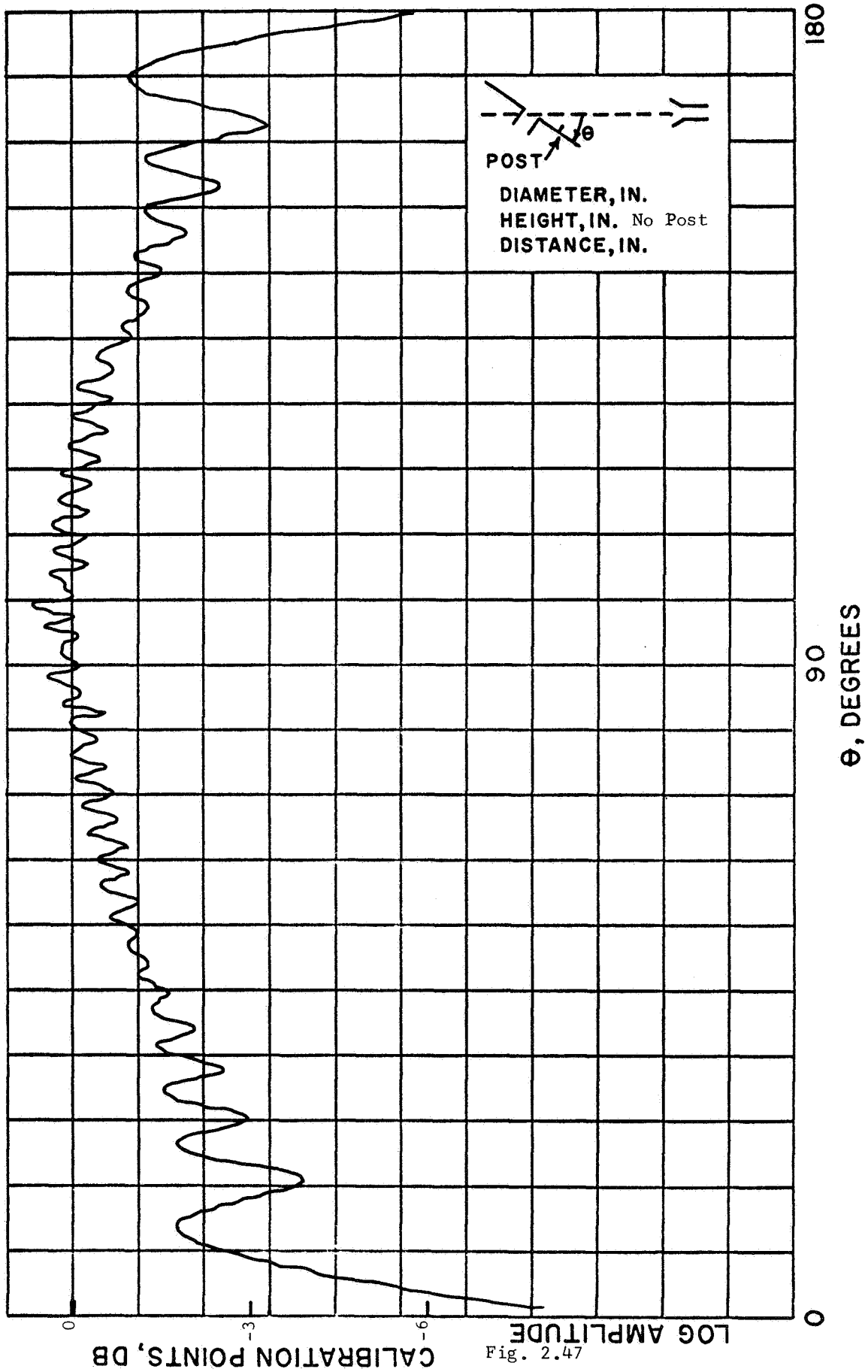
θ
POST
DIAMETER, IN.
HEIGHT, IN. No Post
DISTANCE, IN.
180
90
0
θ, DEGREES
LOG AMPLITUDE
0
-3
-6
CALIBRATION POINTS, DB

Fig. 2.47

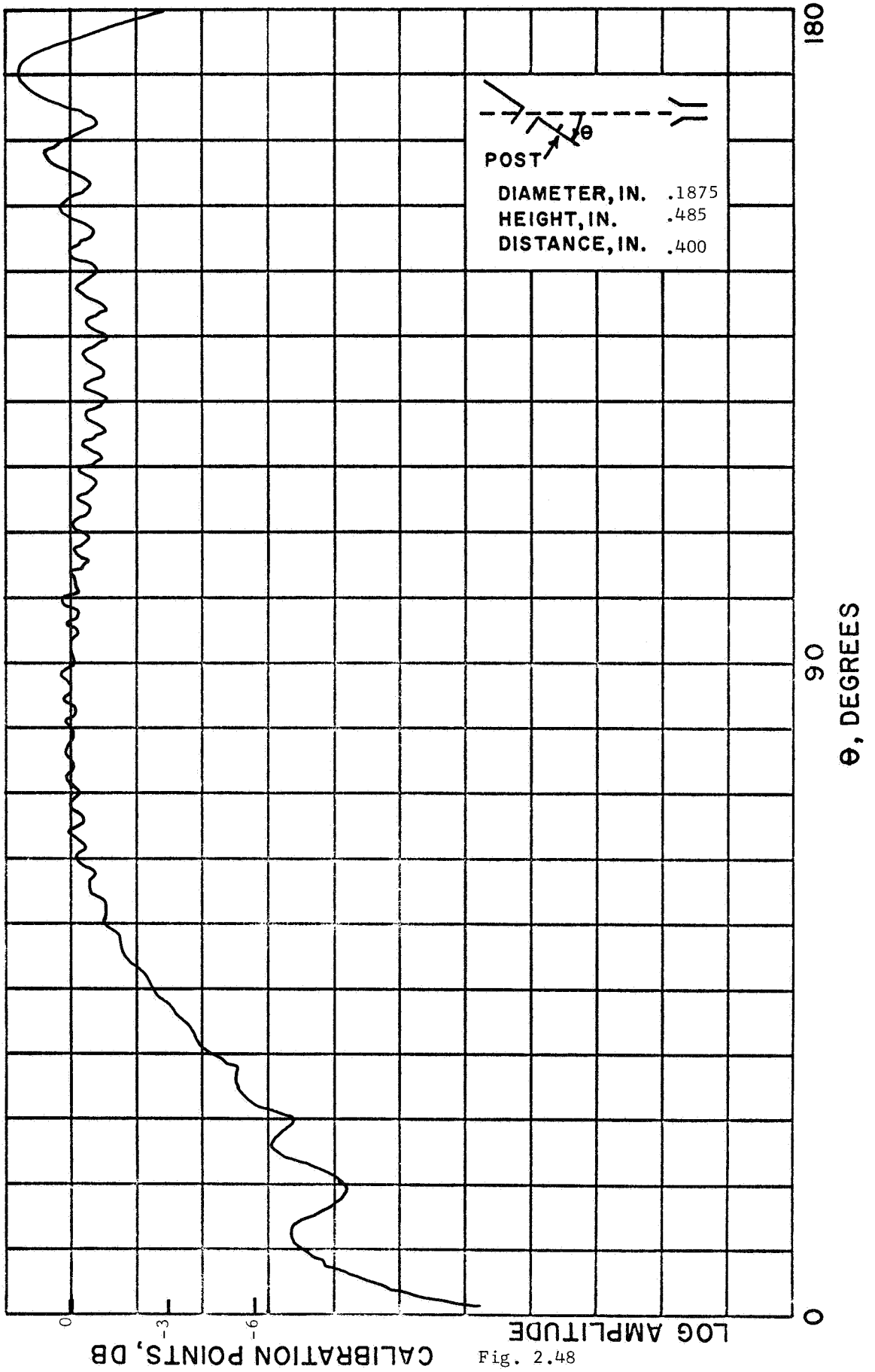
θ
POST
DIAMETER, IN. .1875
HEIGHT, IN. .485
DISTANCE, IN. .400
180
90
0
θ, DEGREES
LOG AMPLITUDE
0
-3
-6
CALIBRATION POINTS, DB

Fig. 2.48

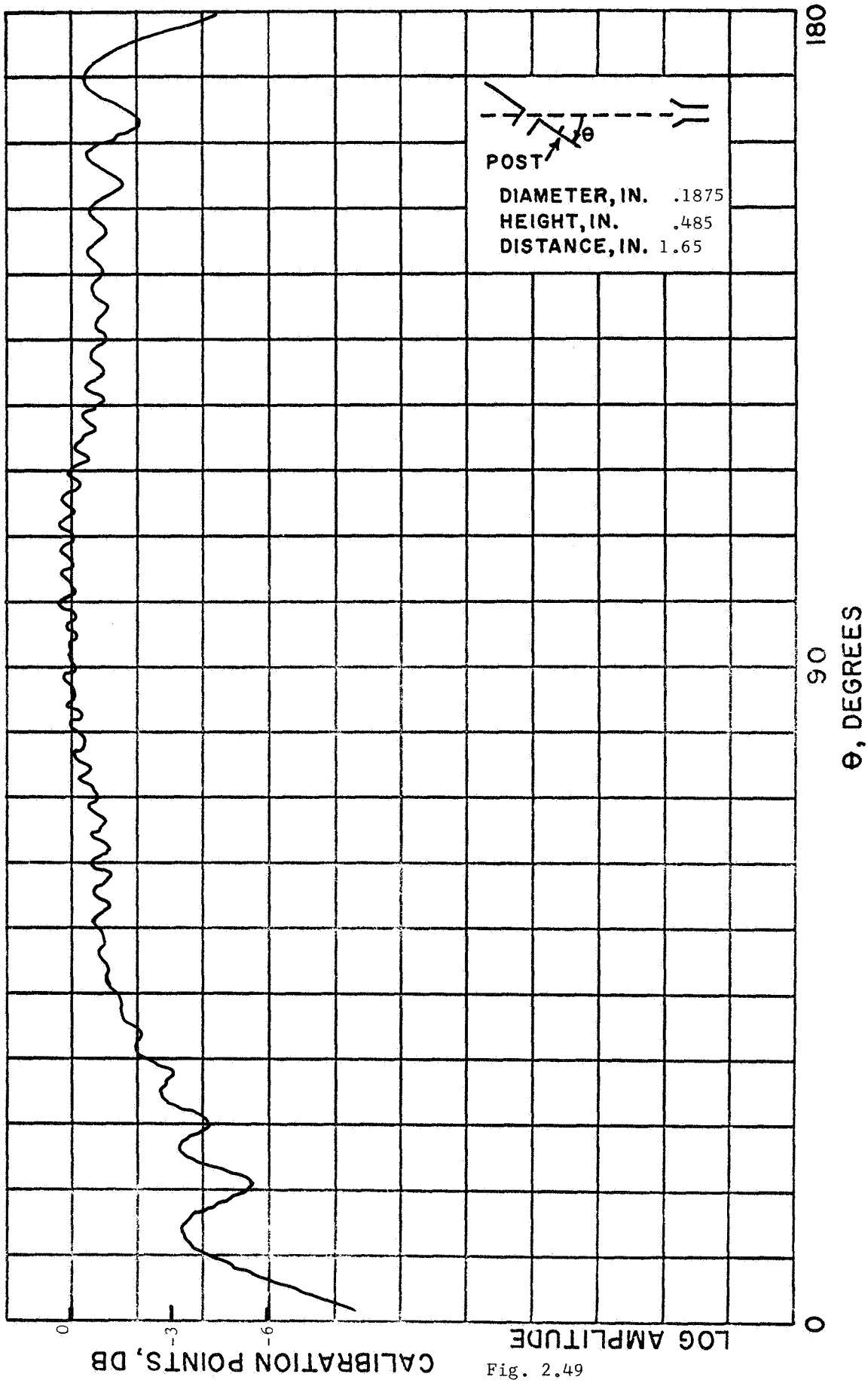
θ
POST
DIAMETER, IN. .1875
HEIGHT, IN. .485
DISTANCE, IN. 1.65
180
90
0
θ, DEGREES
LOG AMPLITUDE
0
-3
-6
CALIBRATION POINTS, DB

Fig. 2.49

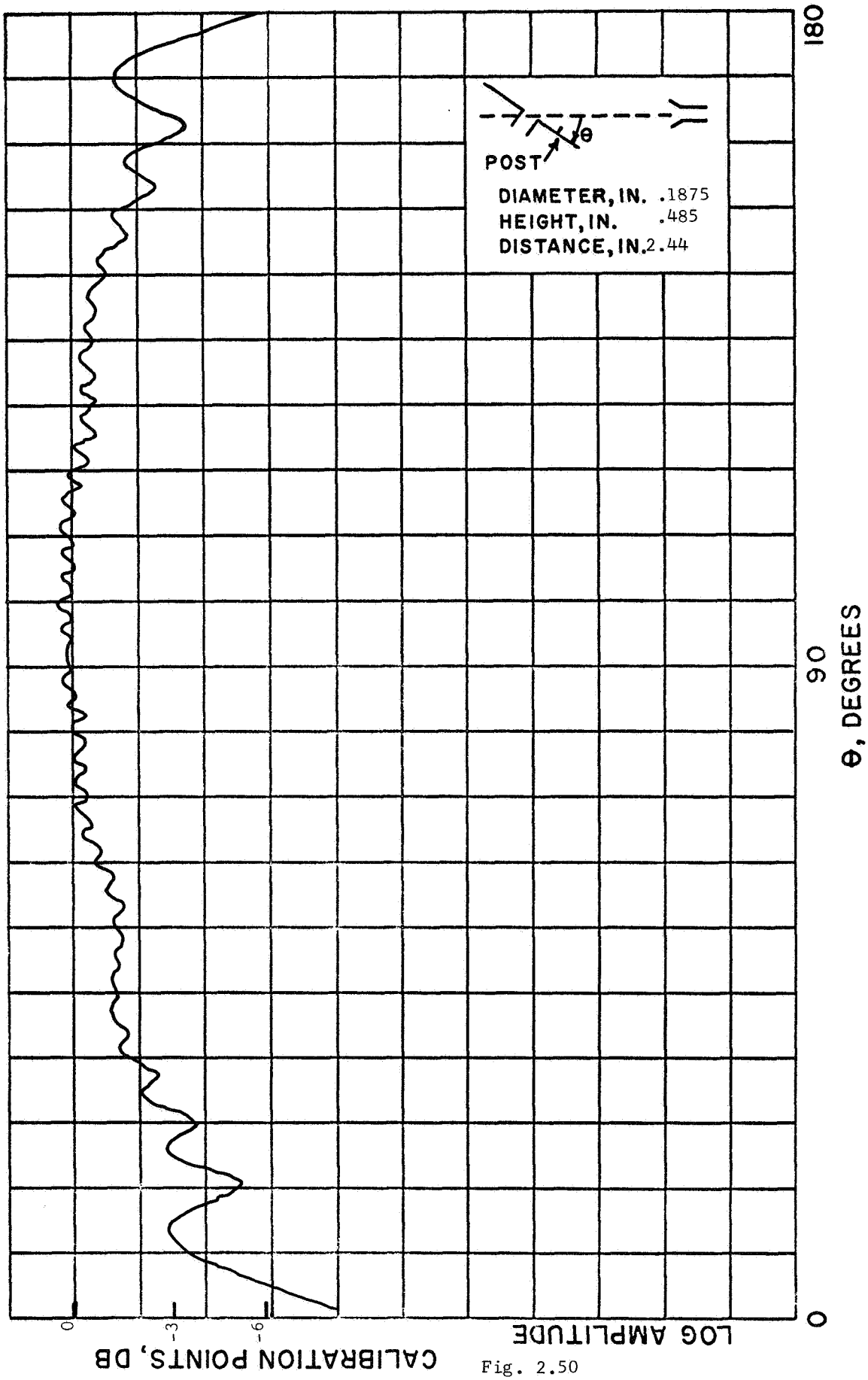
θ
POST
DIAMETER, IN. .1875
HEIGHT, IN. .485
DISTANCE, IN. 2.44
180
90
0
θ, DEGREES
LOG AMPLITUDE
0
-3
-6
CALIBRATION POINTS, DB

Fig. 2.50

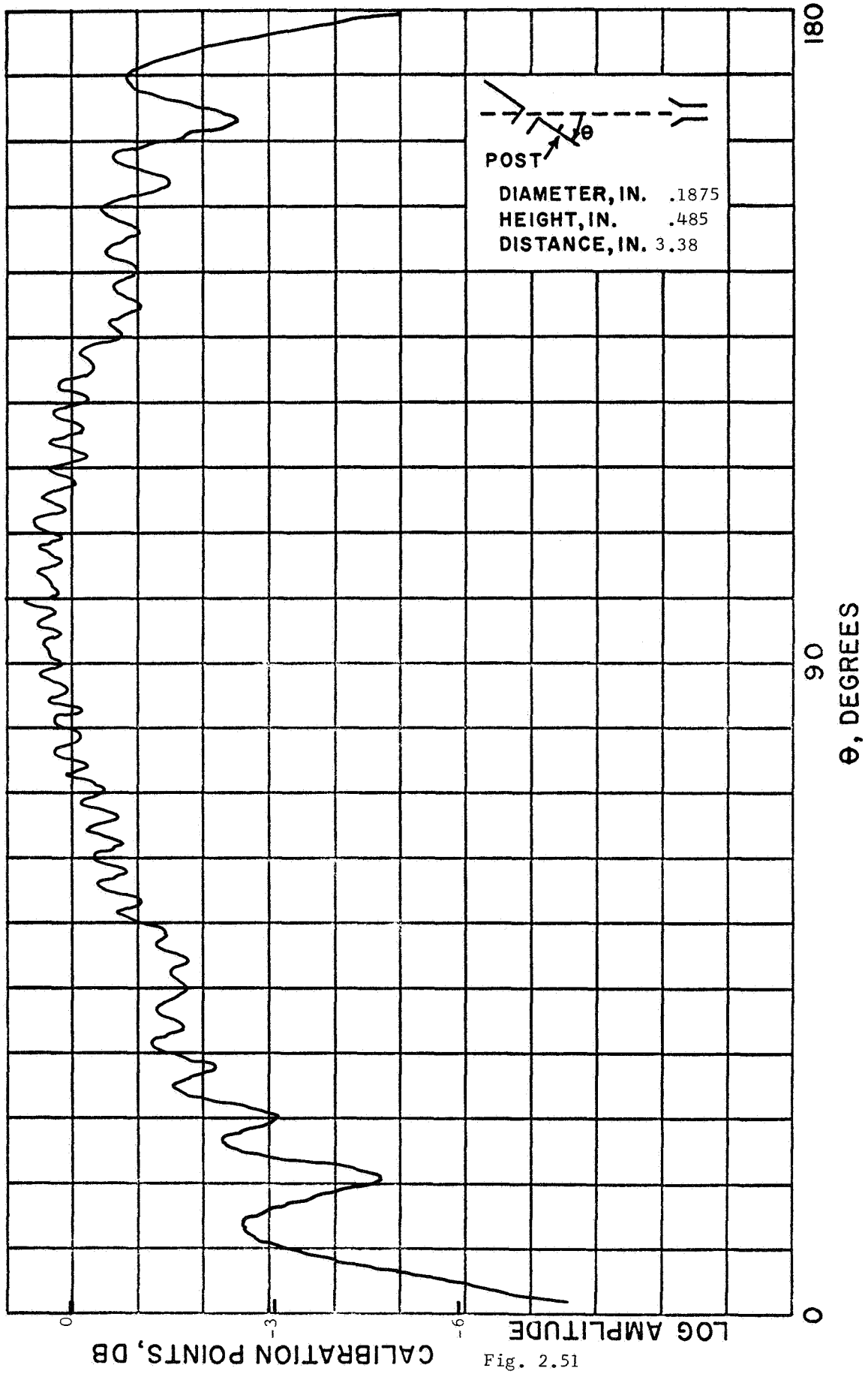
θ
POST
DIAMETER, IN. .1875
HEIGHT, IN. .485
DISTANCE, IN. 3.38
180
90
0
θ, DEGREES
LOG AMPLITUDE
0
-3
-6
CALIBRATION POINTS, DB

Fig. 2.51

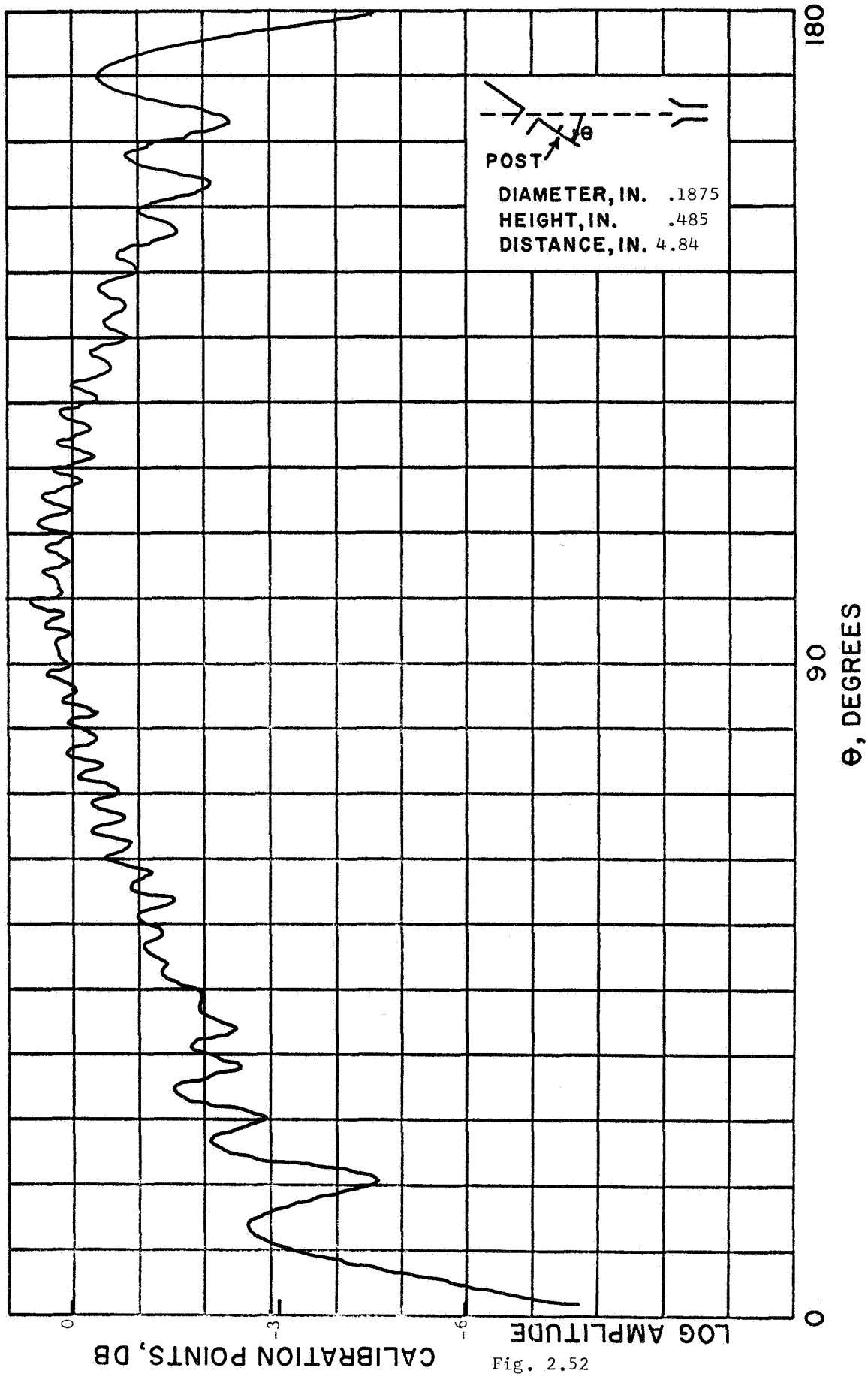
θ
POST
DIAMETER, IN. .1875
HEIGHT, IN. .485
DISTANCE, IN. 4.84
180
90
0
θ, DEGREES
LOG AMPLITUDE
0
-3
-6
CALIBRATION POINTS, DB

Fig. 2.52

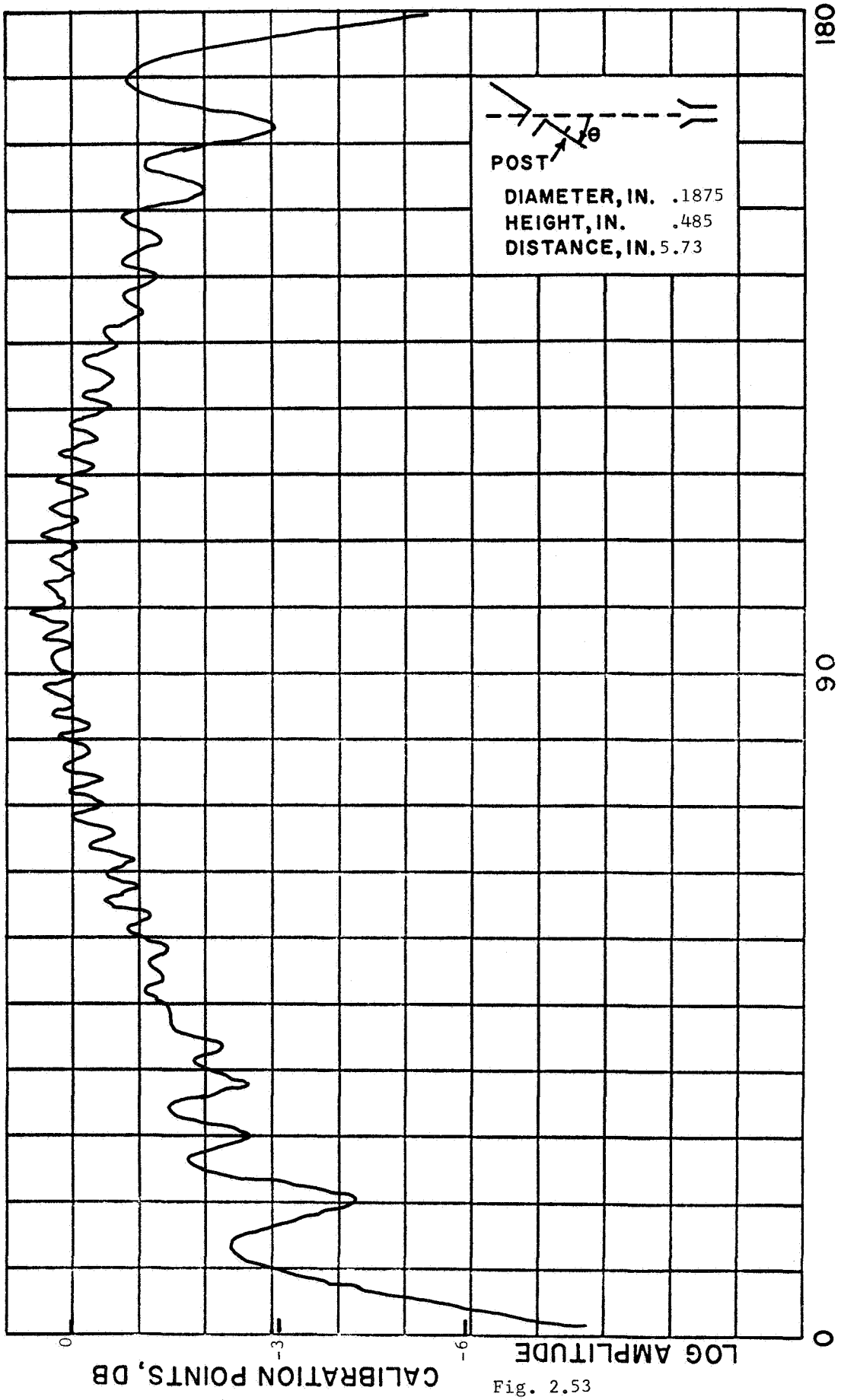
θ
POST
DIAMETER, IN. .1875
HEIGHT, IN. .485
DISTANCE, IN. 5.73
180
90
0
θ, DEGREES
LOG AMPLITUDE
0
-3
-6
CALIBRATION POINTS, DB

Fig. 2.53

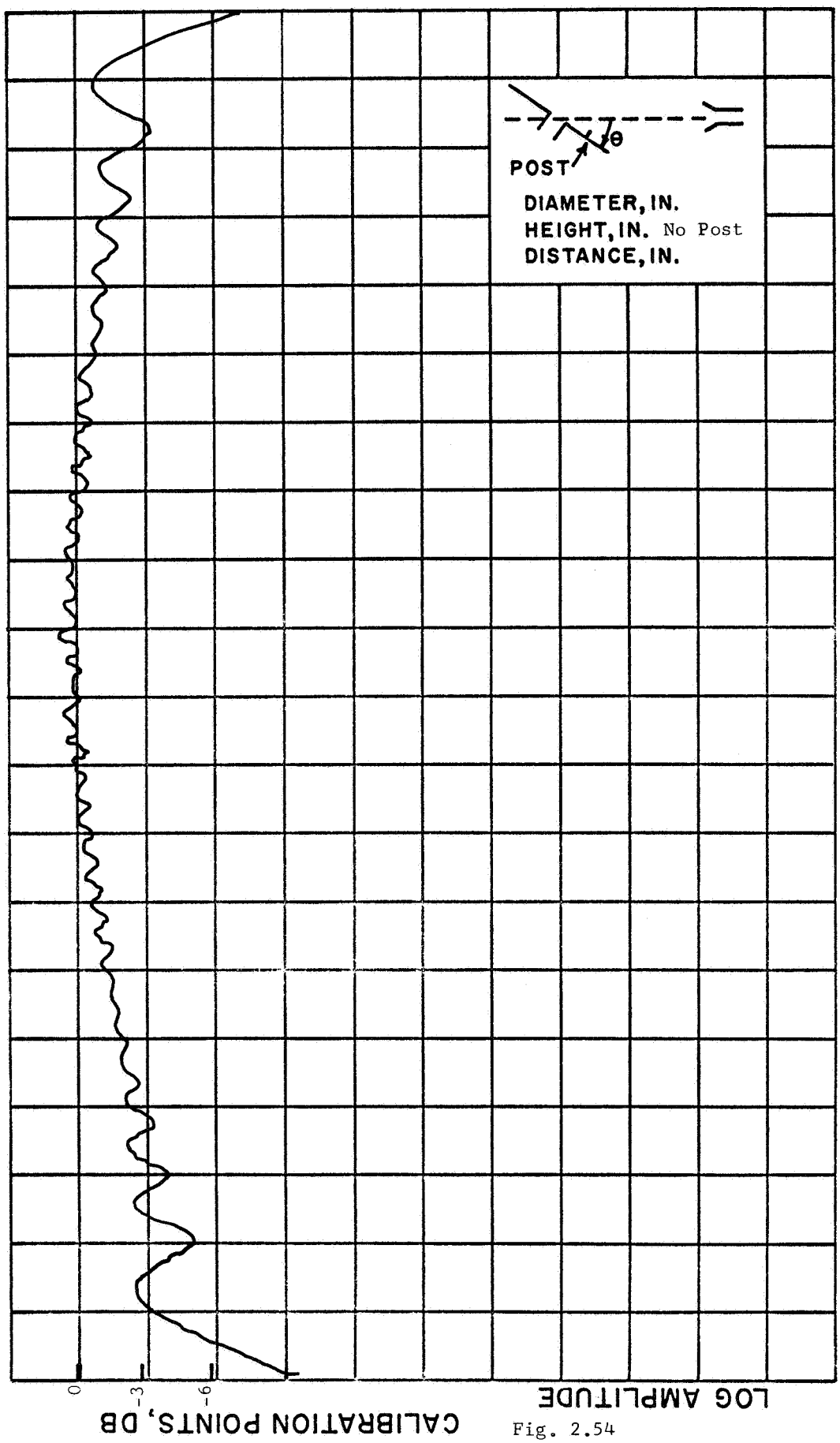
POST
θ
DIAMETER, IN.
HEIGHT, IN. No Post
DISTANCE, IN.
180
90
0
θ, DEGREES
LOG AMPLITUDE
0
-3
-6
CALIBRATION POINTS, DB

Fig. 2.54

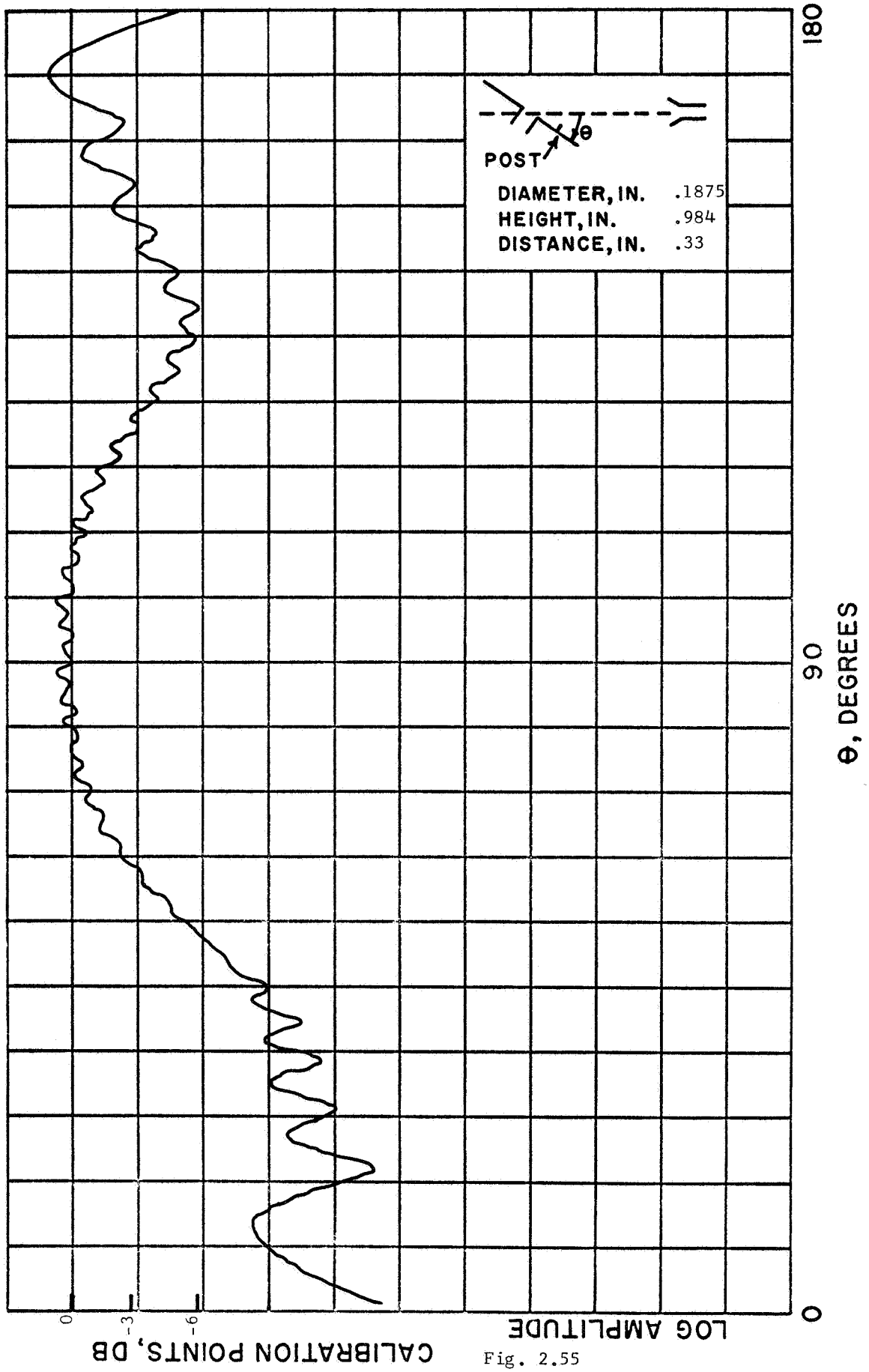
θ
POST
DIAMETER, IN. .1875
HEIGHT, IN. .984
DISTANCE, IN. .33
180
90
0
θ, DEGREES
LOG AMPLITUDE
0
-3
-6
CALIBRATION POINTS, DB

Fig. 2.55

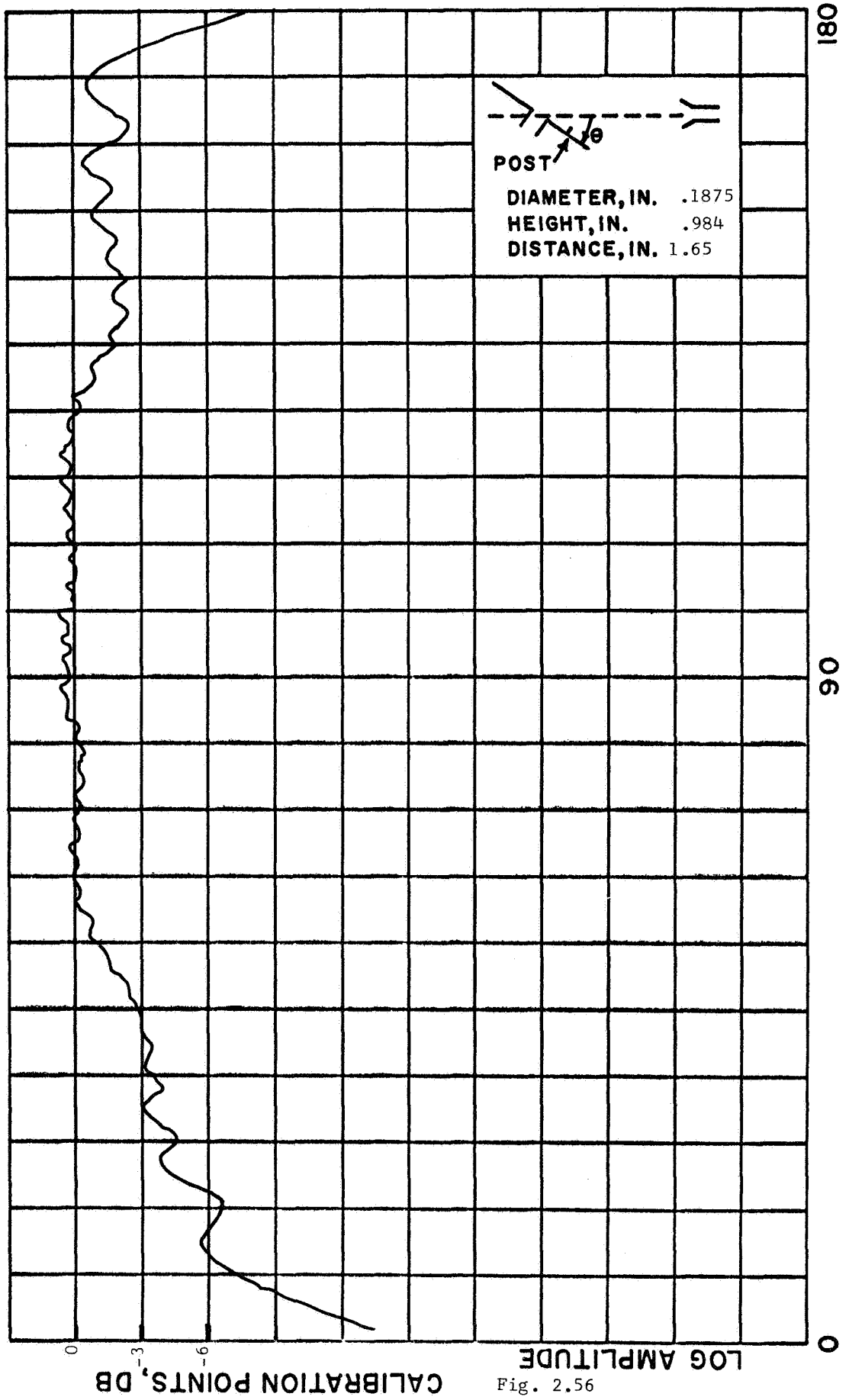
θ
POST
DIAMETER, IN. .1875
HEIGHT, IN. .984
DISTANCE, IN. 1.65
180
90
0
θ, DEGREES
LOG AMPLITUDE
0
-3
-6
CALIBRATION POINTS, DB

Fig. 2.56

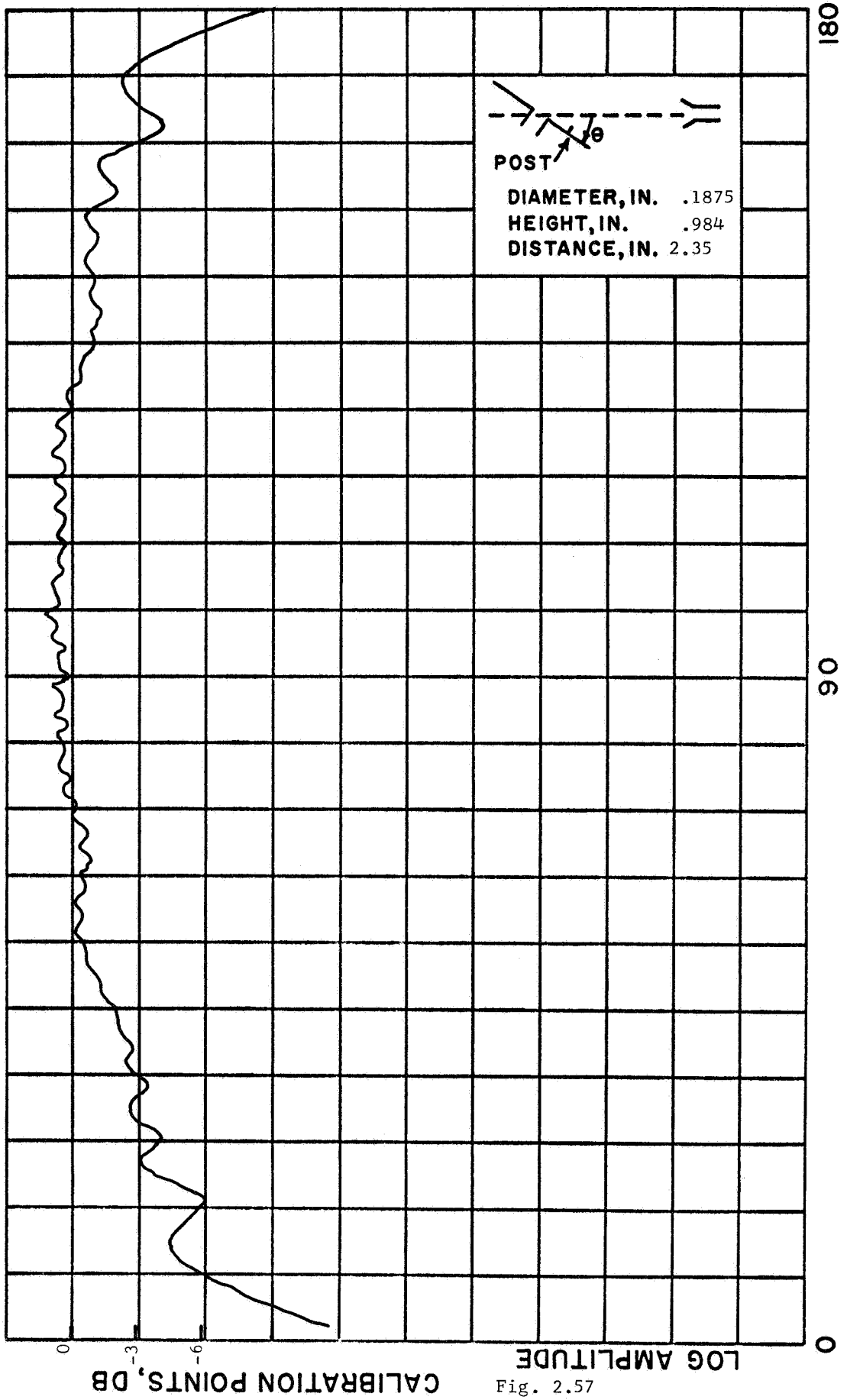
θ
POST
DIAMETER, IN. .1875
HEIGHT, IN. .984
DISTANCE, IN. 2.35
180
90
0
θ, DEGREES
LOG AMPLITUDE
0
-3
-6
CALIBRATION POINTS, DB

Fig. 2.57

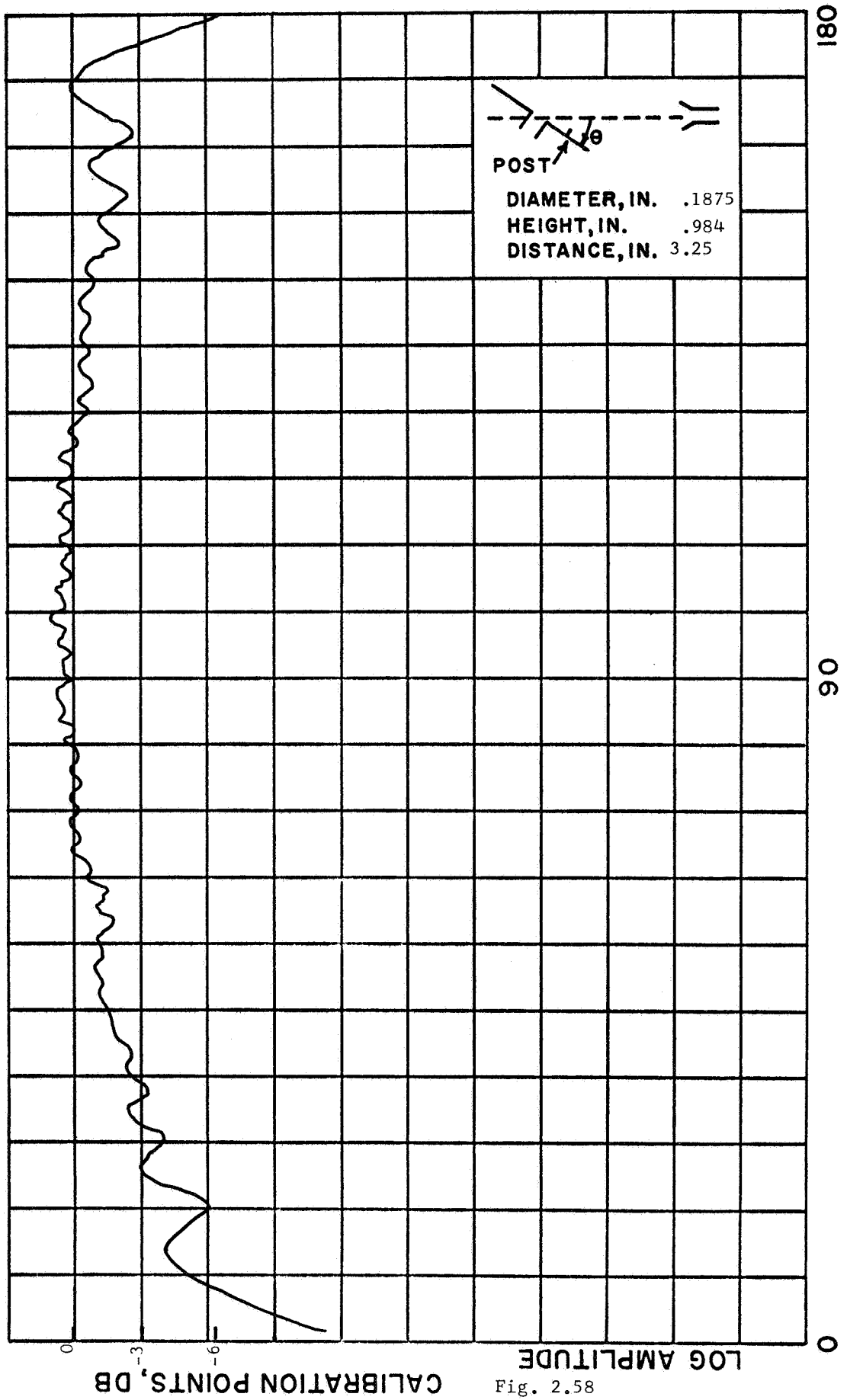
θ
POST
DIAMETER, IN. .1875
HEIGHT, IN. .984
DISTANCE, IN. 3.25
180
90
0
θ, DEGREES
LOG AMPLITUDE
0
-3
-6
CALIBRATION POINTS, DB

Fig. 2.58

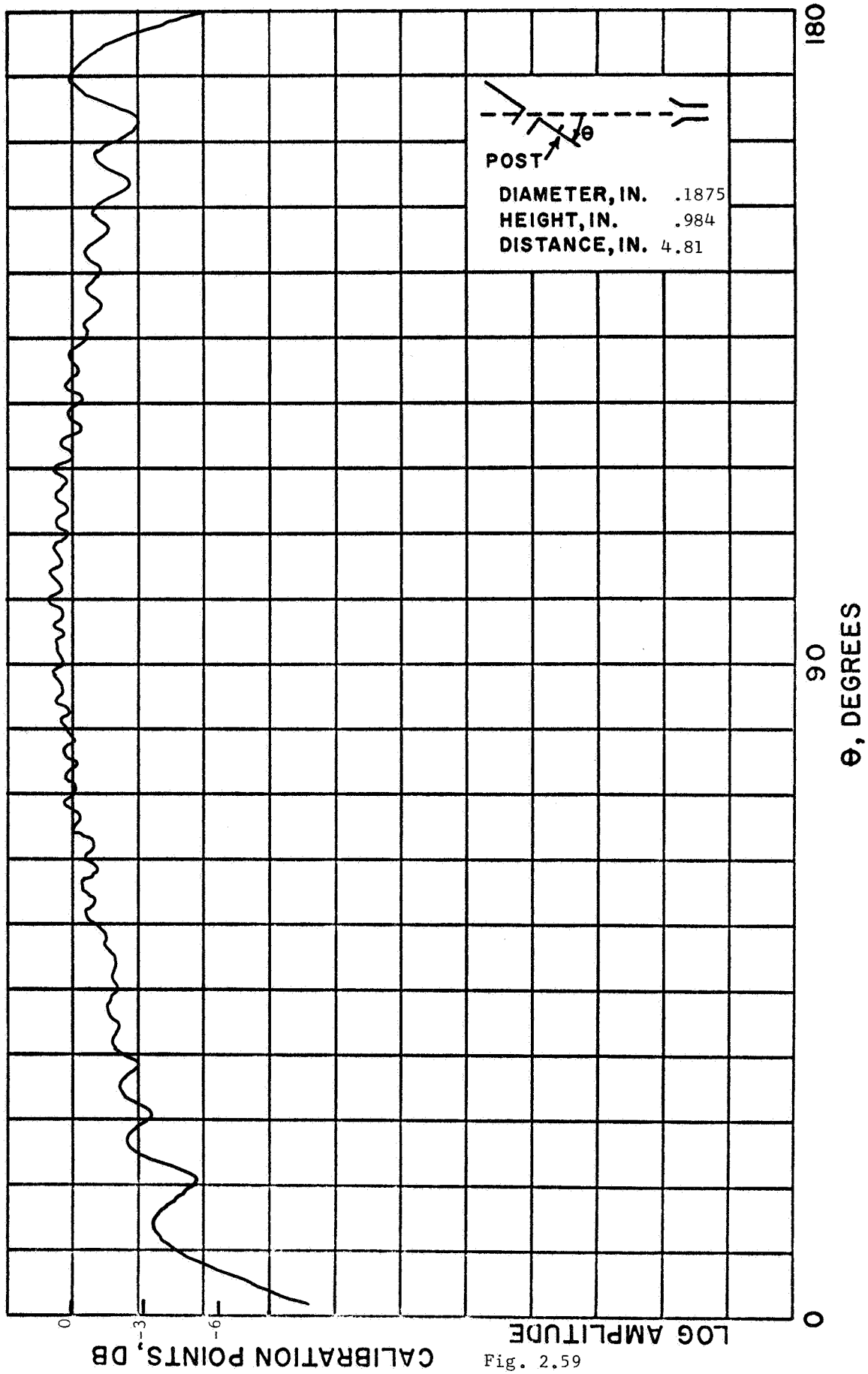
θ
POST
DIAMETER, IN. .1875
HEIGHT, IN. .984
DISTANCE, IN. 4.81
180
90
0
θ, DEGREES
LOG AMPLITUDE
0
-3
-6
CALIBRATION POINTS, DB

Fig. 2.59

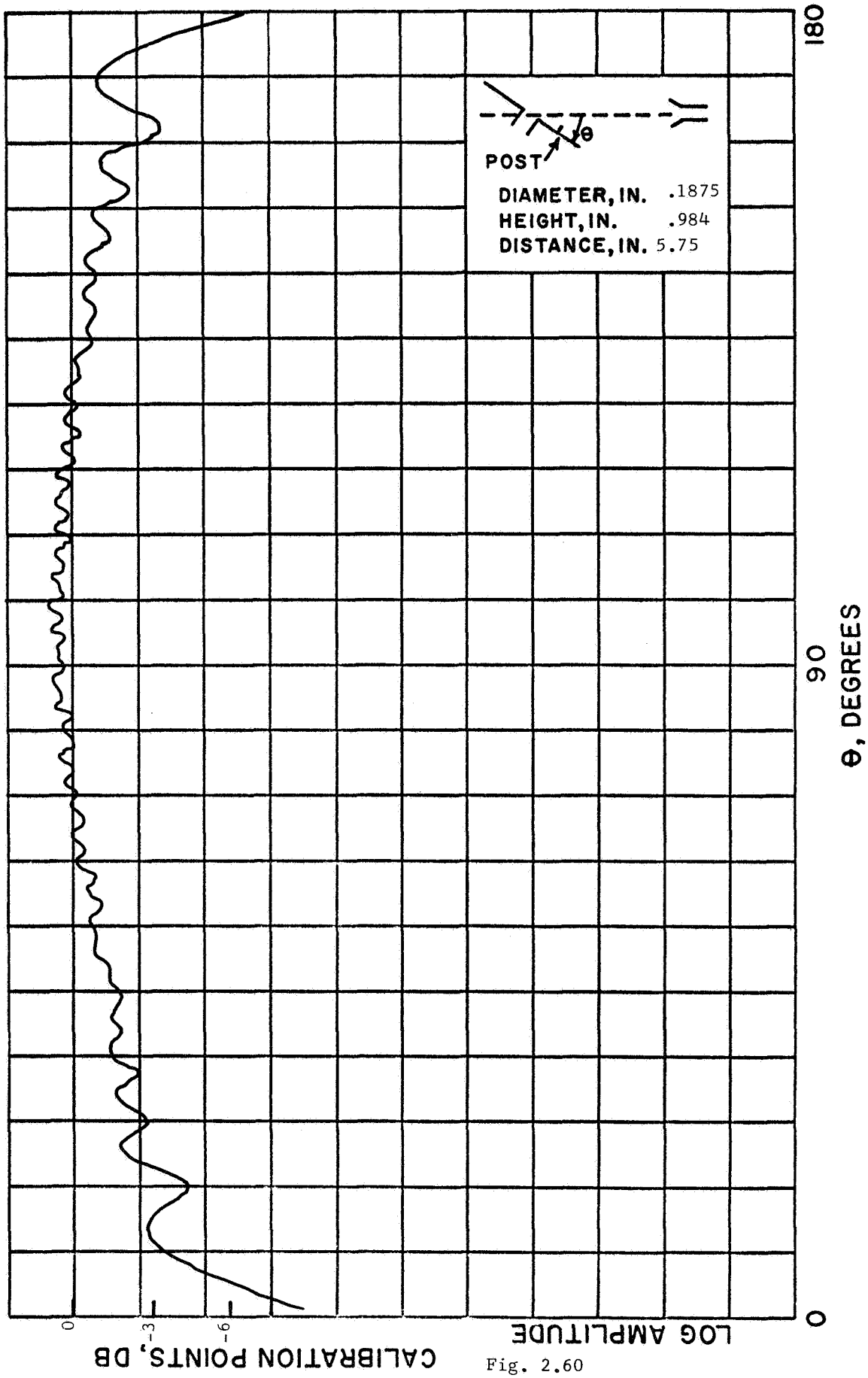
POST
DIAMETER, IN. .1875
HEIGHT, IN. .984
DISTANCE, IN. 5.75
θ
180
90
0
θ, DEGREES
LOG AMPLITUDE
0
-3
-6
CALIBRATION POINTS, DB

Fig. 2.60

Therefore, only rough agreement between measurement and theory could be expected. This agreement was noted in an examination of the patterns, particularly those patterns for the larger posts.

It was also noted that disturbance effects became very noticeable only for relatively large posts close to the slot. The previous development here indicated that the disturbance effect is generally most significant for directive antennas and is less important for omnidirectional antennas. While patterns for highly directive antennas were not made here, our measurements appear to confirm the prediction that isotropic antennas are less affected by disturbing objects.

Chapter 3

THE EFFECT OF CONDUCTIVITY ON FREQUENCY SCALING

Introduction

A requirement on scaling antennas in order to carry out measurements on a model rather than on the full-size antenna is that the frequency be scaled by the same factor as the length dimensions. Thus if

$$p = \frac{L}{L_m} \tag{3.1}$$

defines a scale factor where L is a length of the full-size antenna and L_m is a corresponding length of the model, then we must have also

$$p = \frac{f_m}{f} \tag{3.2}$$

where f and f_m are, respectively, the frequencies used for full-size and model antennas.

A second requirement is that conductivities, including that of air and metallic structures, must be scaled according to

$$p = \frac{\sigma_m}{\sigma} \tag{3.3}$$

Thus if the model is smaller than the full-size antenna and a higher frequency is used in making the model measurements then the conductivity of the model should be higher than that of the full-size antenna.

However, if σ for the metal structure is high enough, the metal may be considered to be a perfect conductor, and the conductivity need not be

scaled.[1]

It is necessary in frequency scaling to determine if the antenna structure conductivity is "high enough" so that it need not be scaled. Various standards can be used to make this determination. One such criterion arises naturally if we consider an antenna imaged in a ground plane, such as a dipole above a ground plane, or a slot in a ground plane. We can reasonably assume that conductivity is sufficiently high as long as image theory is applicable at the design frequency. Another test of the conductivity effects would be an examination of the surface impedance of the metal structure at the design frequency. If the power loss from a wave which strikes the surface is negligible, we would feel justified in neglecting any conductivity effects. We examine these two criteria for a scaling problem of interest, for which experimental measurements are discussed later. The antennas are of copper and aluminum. The lowest frequency used is 5 GHz and the highest 41.786 GHz.

Relaxation Time Effects

For an antenna with a metallic structure acting mainly as a ground plane in which the radiating structure is imaged, image theory requires an electron charge within the metal, or on its surface, to complement the charge on the radiating structure; that is, a positive charge on the radiating structure above the ground plane on the radiating structure above the ground plane is imaged by a negative charge below the ground plane surface. The result is a zero tangential electric field on the conductor. The physical process which occurs when a charge is placed above a conductor is a movement of electrons on the conductor surface in such a way as to cancel the tangential electric field which is initially

set up at the conductor surface by the charge placed above it.

If the charge above the conductor surface is time varying the electron charge on the surface must also vary with time in order to meet the surface boundary conditions. If the surface electron charge cannot change rapidly enough with time we would expect image theory to fail and conductivity to affect the antenna pattern appreciably.

In a conducting material, if an initial charge distribution ρ_o is established in some fashion it will redistribute itself in some fashion according to[2]

$$\rho = \rho_o \varepsilon^{-\frac{\sigma}{\varepsilon} t} \tag{3.4}$$

The relaxation time of this distribution is defined by

$$\tau = \varepsilon/\sigma \tag{3.5}$$

If τ is small compared to a period of the wave of interest, we would expect that any surface charge distribution can change rapidly enough with time to meet the necessary boundary condition on tangential electric field. Therefore, the tangential field will be negligibly small and the conductor acts as a perfect conductor.

The longest relaxation time involved in our problem is for the aluminum, for which

$$\tau_a \approx \frac{10^{-9}/36\pi}{3.54 \times 10^{7}} \approx 2.50 \times 10^{-19} \text{ sec}$$

At 41.786 GHz, the wave period

$$T \approx 2.39 \times 10^{-11} \text{ sec}$$

Since the relaxation time is much smaller than the wave period we expect that conductivity of the metal structure will not affect an antenna scaling problem at this frequency.

Surface Impedance

The surface impedance of a conductor, for a wave propagating normally into the conductor, is given by[3]

$$\eta_m = \sqrt{\frac{j\omega\mu}{\sigma + j\omega\varepsilon}} \tag{3.6}$$

and the surface resistance by

$$R = \mathrm{Re}\,(\eta_m) \tag{3.7}$$

The power loss per square meter of a wave incident normally on the conductor is

$$P_d = R\left|H_o\right|^2 \tag{3.8}$$

where H_o is the magnetic field strength. Now the power contained in the wave in air, per square meter, is

$$P = \eta\left|H_o\right|^2 = \sqrt{\frac{\mu}{\varepsilon}}\left|H_o\right|^2 \tag{3.9}$$

Then the ratio of dissipated power to incident power is

$$\frac{P_d}{P} = \frac{R}{\sqrt{\frac{\mu}{\varepsilon}}} = \frac{\mathrm{Re}\left(\sqrt{\frac{j\omega\mu}{\sigma + j\omega\varepsilon}}\right)}{\sqrt{\mu/\varepsilon}} \tag{3.10}$$

We might expect in antenna measurements that if this ratio is negligbly small the metal structure can be considered a "perfect conductor."

In modeling, if the ratio is negligibly small for all frequencies used, the metal conductivity will not appreciably affect the modeling problem. Table 3.1 gives values of R and P_d/P for two metals, copper and aluminum, and two frequencies, 5 and 41.786 GHz, which were the lowest and highest frequencies used in measurements to be discussed later.

	R		P_d/P	
f, GHz	Cu	Al	Cu	Al
5	0.0185	0.0236	4.90×10^{-5}	6.26×10^{-5}
41.786	0.0533	0.0684	1.41×10^{-4}	1.82×10^{-4}

Table 3.1

Surface Resistance and Power Dissipated

Table 3.1 shows clearly that for the highest frequency and the lowest conductivity used in this antenna scaling problem the ratio of power lost to power incident, in a plane wave normally incident on the conductor, is negligible. While this case does not fit our antenna problem exactly it nevertheless indicates that we can consider these conductors to be "perfect", that is to have no losses and therefore infinite conductivity. We then can reasonably expect that conductivity will not affect the frequency scaling of antennas until the frequency becomes much greater than the 41.786 MHz used in our measurements.

Pattern Measurements of Scaled Antennas

A program of measurements has been carried out to determine experimentally if antenna conductivity affects patterns in typical frequency

scaling problems. It was desired to use antenna structures having different conductivities, to scale by a relatively large factor, and to have the highest frequency at least 40 GHz. Since this would involve constructing several antennas a simple antenna was chosen, consisting of a slot in a ground plane.

Three antennas were built of 0.190" aluminum and three of 0.190" aluminum covered on the front surface with 16 oz. copper (approximately 1/32") bonded to the aluminum with a non-conducting cement. The skin depth of the copper was far less than 1/32", and the aluminum served merely as a stiffener. Each aluminum antenna had a corresponding copper antenna of the same size, except for the negligible added thickness of the copper. The ground plane for each antenna was slotted in the center to accept the exterior dimensions of a standard waveguide. The waveguide was cleaned of paint, coated with Eccobond 56C Liquid Solder, a conducting cement, and pushed through the ground plane from the back until it was flush with the front surface of the ground plane. For added strength and rigidity a flange on the waveguide was pressed against the back of the ground plane and cemented in place. The front surface of the ground plane, including the waveguide-ground plane joint, was polished with jeweller's rouge.

The guide sizes selected are given in Table 3.2.

Inner Dimension Inches	Guide Designation RG-97/U	RG-53/U	RG-49/U
Narrow	0.112	0.170	0.872
Broad	0.224	0.420	1.872

Table 3.2
Interior Waveguide Dimensions

The largest convenient ground plane size available was 36" x 36", so this was used with the largest waveguide. A problem exists in scaling this to the smaller sizes needed with the smaller guides since for standard waveguide sizes the narrow and broad dimensions do not have the same scale factor. For example, if we compare RG-53/U and RG-49/U we see that

$$\frac{0.872}{0.170} \neq \frac{1.872}{0.420}$$

Now we know that the E-plane pattern of a slotted ground plane will be most affected by the narrow dimension of the slot and not very much by the broad dimension. Similarly it will be affected most by the ground plane dimension measured in the pattern plane, that is the dimension measured parallel to the narrow dimension of the slot. The pattern will not be greatly affected by the ground plane dimension measured parallel to the broad dimension of the slot. The converse is true for the H-plane patterns. It was therefore decided to scale the ground plane sizes in the same ratio as the appropariate slot dimension. Thus the "height" of the ground plane, measured along the same line as a measurement of the narrow guide dimension, was scaled by the same factor used to scale the narrow slot dimension. The "width" of the ground plane was scaled

by the broad slot dimension factor. The ground plane sizes are given by Table 3.3.

Ground Plane Size, Inches	Guide Designation RG-97/U	RG-53/U	RG-49/U
Parallel to Narrow Slot Dimension	4.624	7.018	36
Parallel to Broad Slot Dimension	4.308	8.055	36

Table 3.3
Ground Plane Dimensions

In carrying out the scaling it is also clear that frequencies must be scaled differently. In agreement with the preceding discussion, since E-plane patterns are most affected by the narrow slot dimension, the frequencies for E-plane measurements were scaled by the narrow-slot-dimension factors, and the H-plane measurements according to the broad-dimension scaling. The frequencies used are given in Table 3.4.

Frequency, MHz	Guide Designation RG-97/U	RG-53/U	RG-49/U
E-plane Pattern	38.929	25.647	5
H-plane Pattern	41.786	22.286	5

Table 3.4
Frequencies Used in Pattern Measurements

The antennas described above were constructed on the University of Alabama campus and transported to Huntsville. Radiation patterns were made using the anechoic chamber and the facilities of the Astrionics

Laboratory of the Marshall Space Flight Center. Principal E- and H-plane patterns were made for each of the six antennas. These are shown in Figs. 3.1 through 3.12.

The antenna patterns are arranged in pairs, the pattern for the aluminum ground plane followed by that for the copper having the same frequency and same pattern plane. When one compares these pattern pairs for aluminum and copper, that is 3.1 and 3.2, etc. it is apparent that ground plane conductivity does not affect the pattern appreciably for any frequency used or for either pattern plane. The patterns 3.9 and 3.10 seem dissimilar in one respect. Rapid oscillations occur near 0° in one pattern and near 180° in the other. However, both patterns are asymmetrical, and this asymmetry could not be caused by conductivity effects. It is thought that these rapid oscillations were caused by energy feeding directly to the mixer or diffracted from the ground plane edge and leaking into the mixer. Such a pattern could easily be non-symmetric and also could be different near the edges for two different antennas. The more significant portions of patterns 3.9 and 3.10 show that they are nearly identical.

In addition to the necessary similarity of these patterns pair-by-pair just described, all the E-plane patterns for the different frequencies should be the same and all H-plane patterns should be the same. A comparison of the six E-plane patterns, Figs. 3.1 through 3.6, shows that this is substantially true, and a comparison of the H-plane patterns, Figs. 3.7 through 3.12, shows the same thing.

These conclusions were reached, with a high degree of confidence in the results, by overlaying patterns and comparing them. In addition a

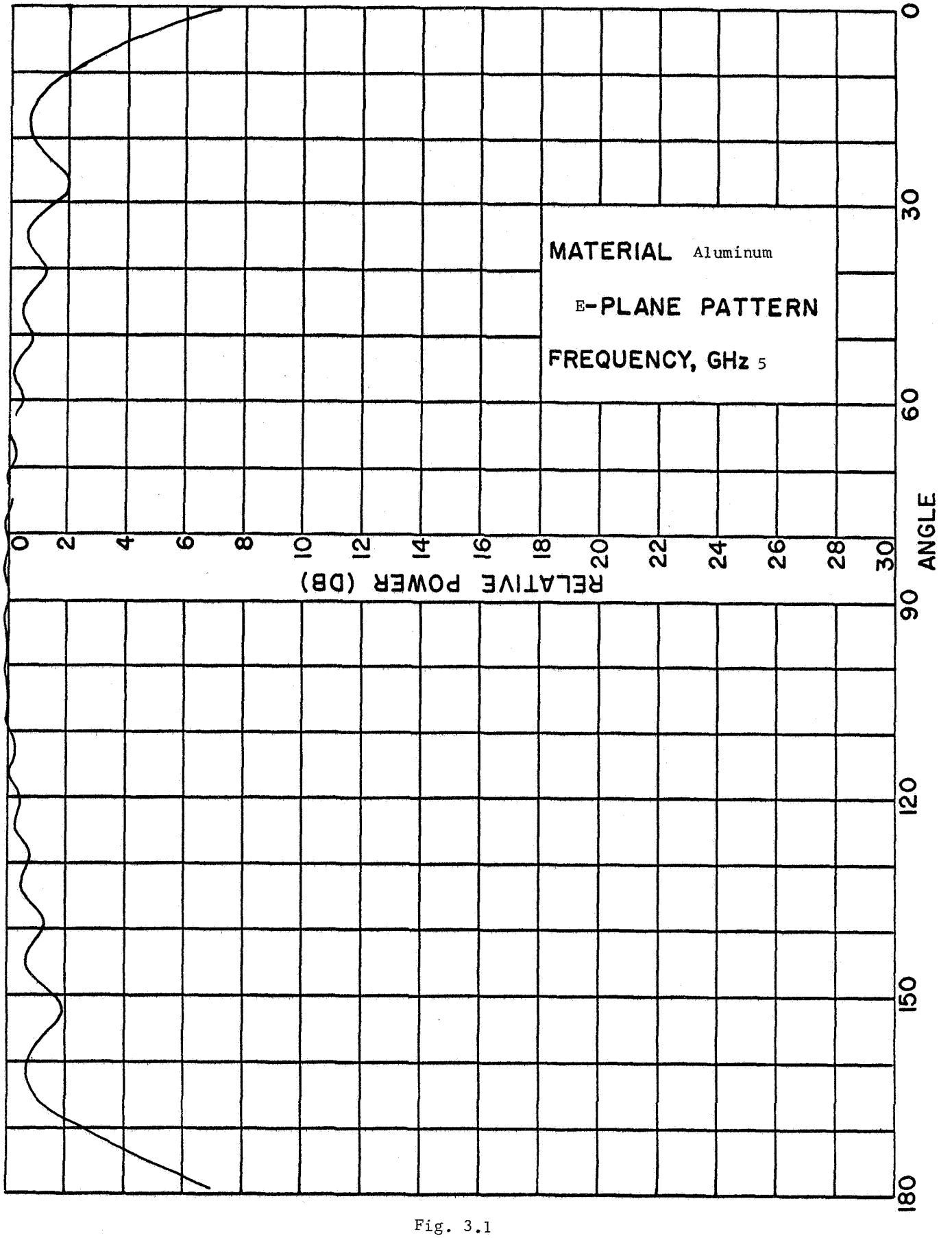
MATERIAL Aluminum
E-PLANE PATTERN
FREQUENCY, GHz 5
0 2 4 6 8 10 12 14 16 18 20 22 24 26 28 30
RELATIVE POWER (DB)
0 30 60 90 120 150 180
ANGLE

Fig. 3.1

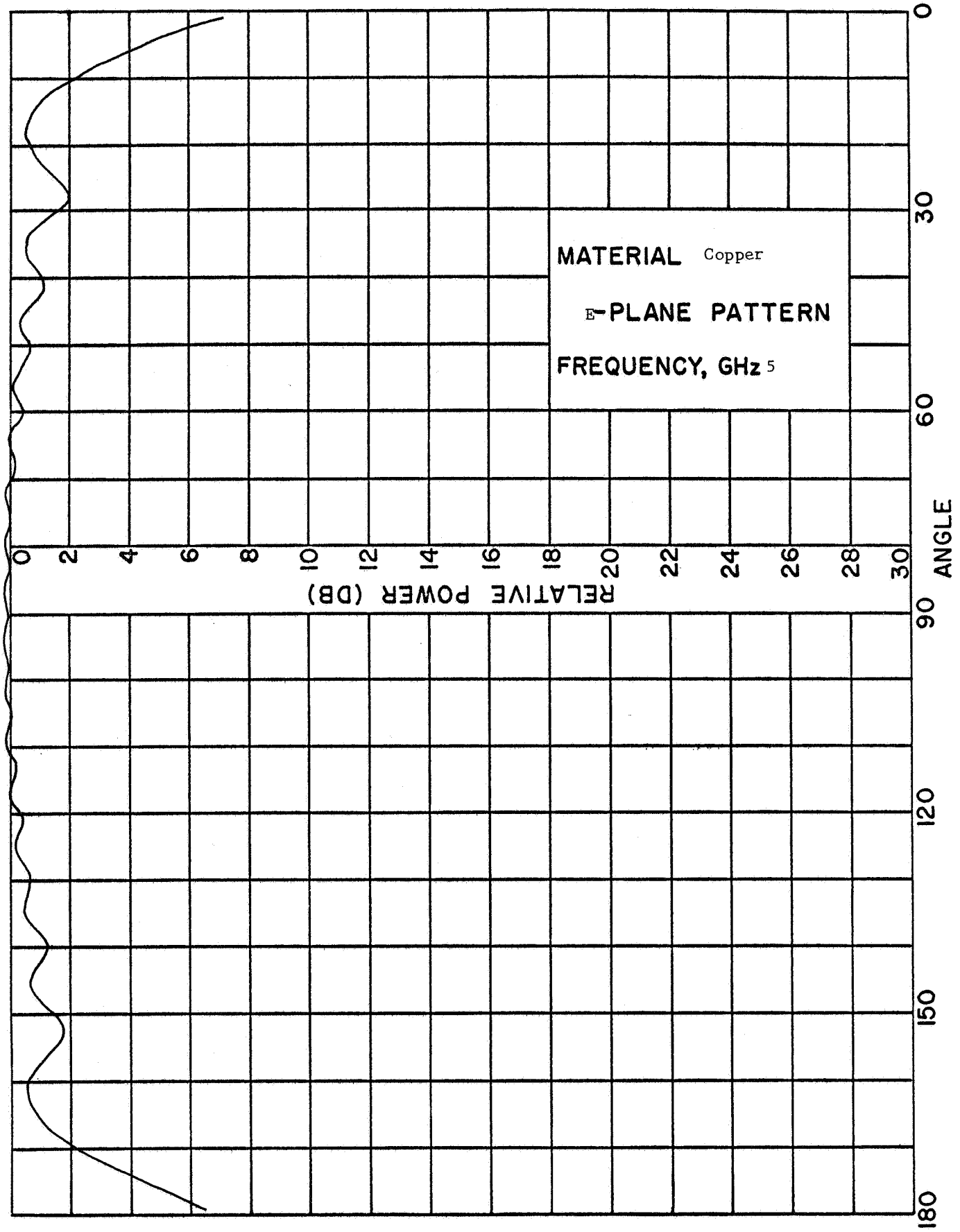
MATERIAL Copper
E-PLANE PATTERN
FREQUENCY, GHz 5
0 2 4 6 8 10 12 14 16 18 20 22 24 26 28 30
RELATIVE POWER (DB)
0 30 60 90 120 150 180
ANGLE

Fig. 3.2

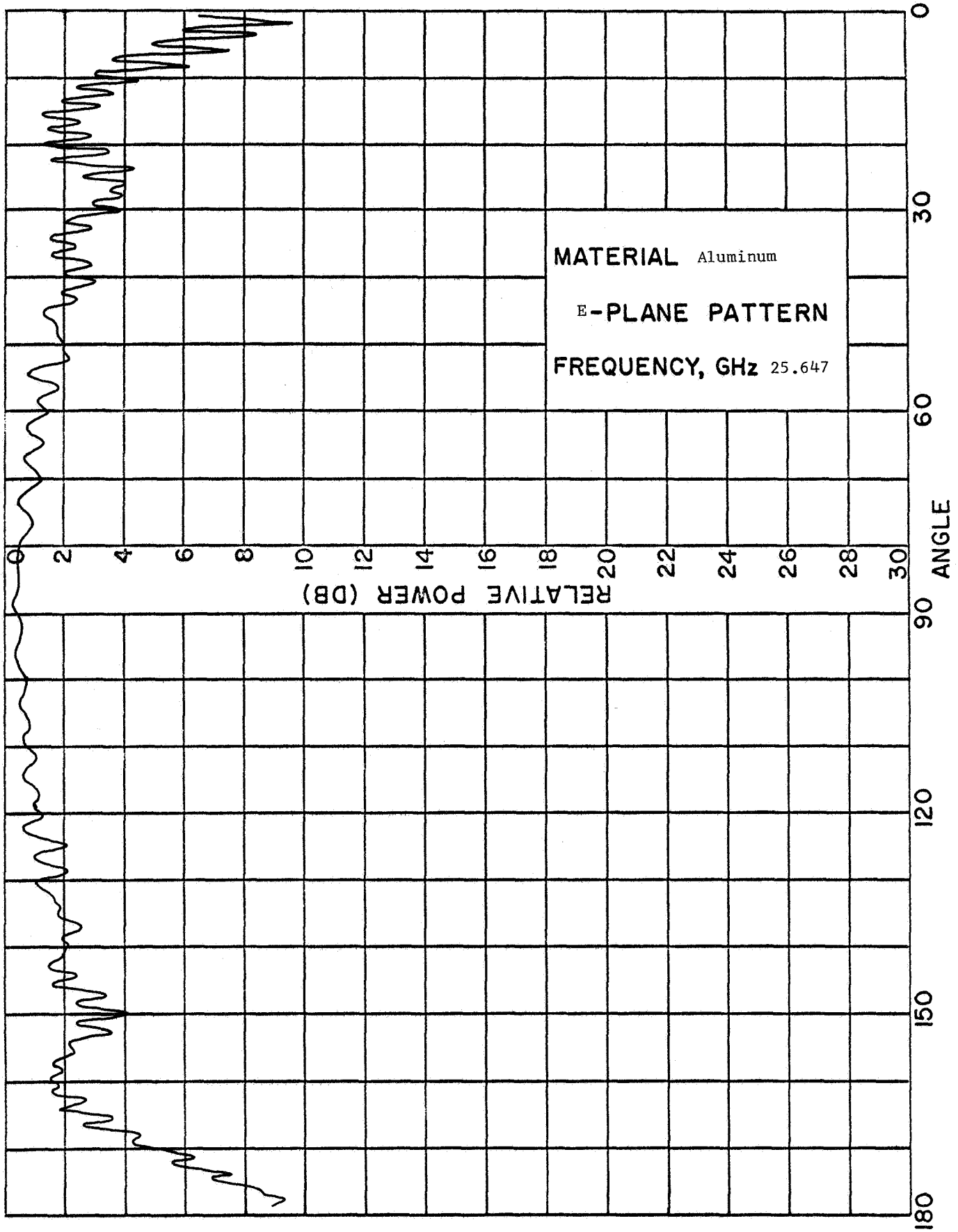
MATERIAL Aluminum
E-PLANE PATTERN
FREQUENCY, GHz 25.647
RELATIVE POWER (DB)
0
2
4
6
8
10
12
14
16
18
20
22
24
26
28
30
ANGLE
0
30
60
90
120
150
180

Fig. 3.3

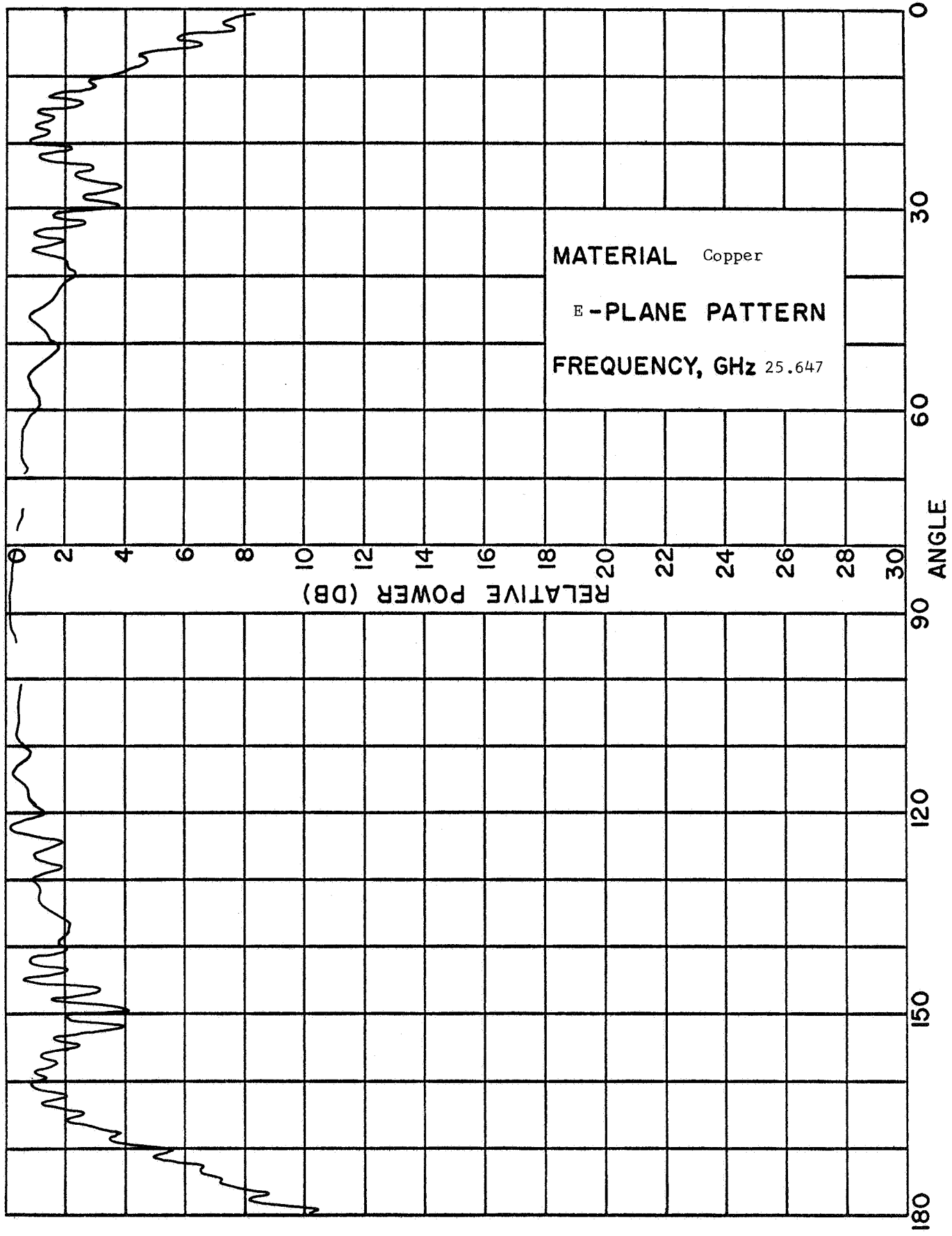
MATERIAL Copper
E-PLANE PATTERN
FREQUENCY, GHz 25.647
RELATIVE POWER (DB)
0
2
4
6
8
10
12
14
16
18
20
22
24
26
28
30
ANGLE
0
30
60
90
120
150
180

Fig. 3.4

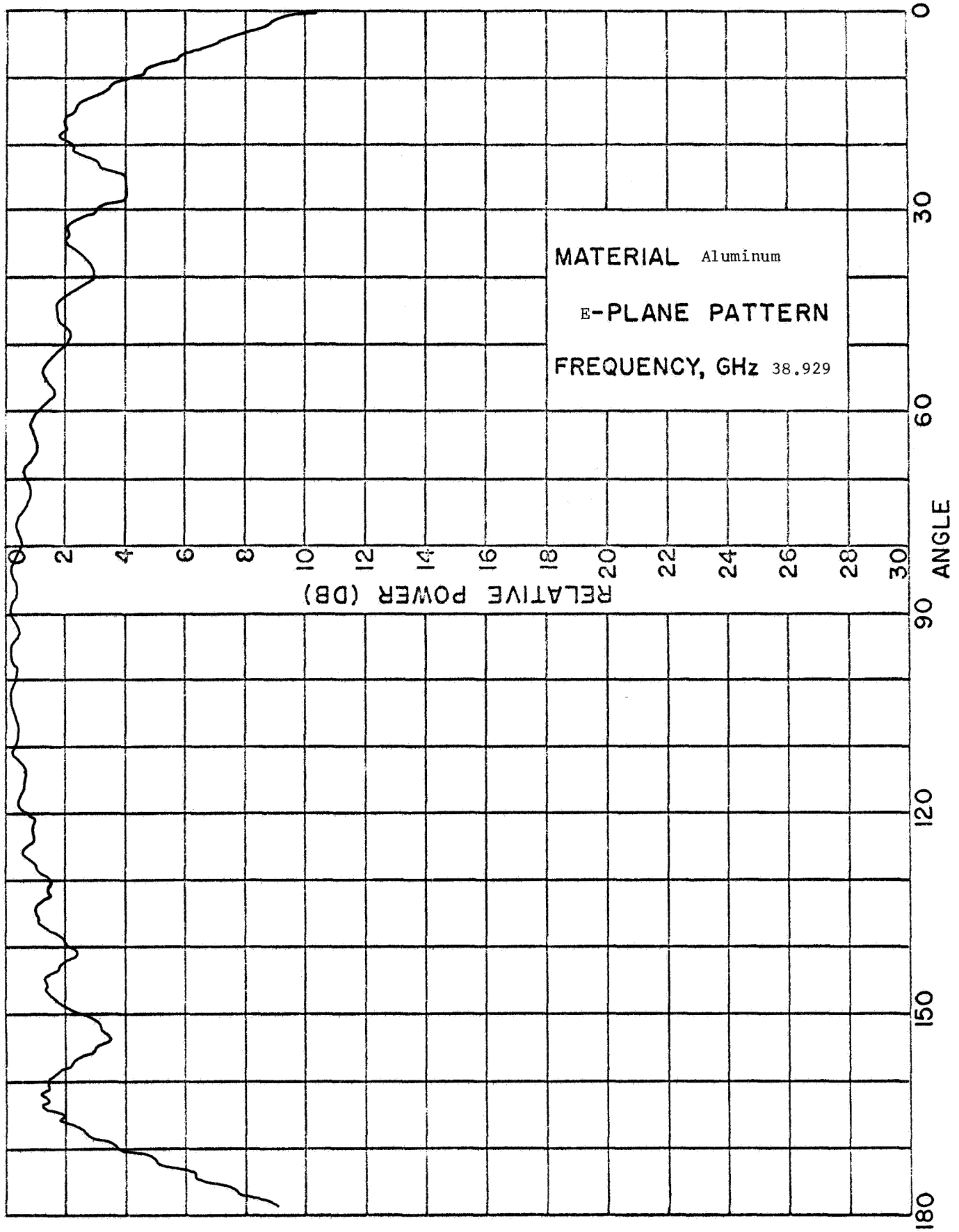
MATERIAL Aluminum
E-PLANE PATTERN
FREQUENCY, GHz 38.929
RELATIVE POWER (DB)
0
2
4
6
8
10
12
14
16
18
20
22
24
26
28
30
ANGLE
0
30
60
90
120
150
180

Fig. 3.5

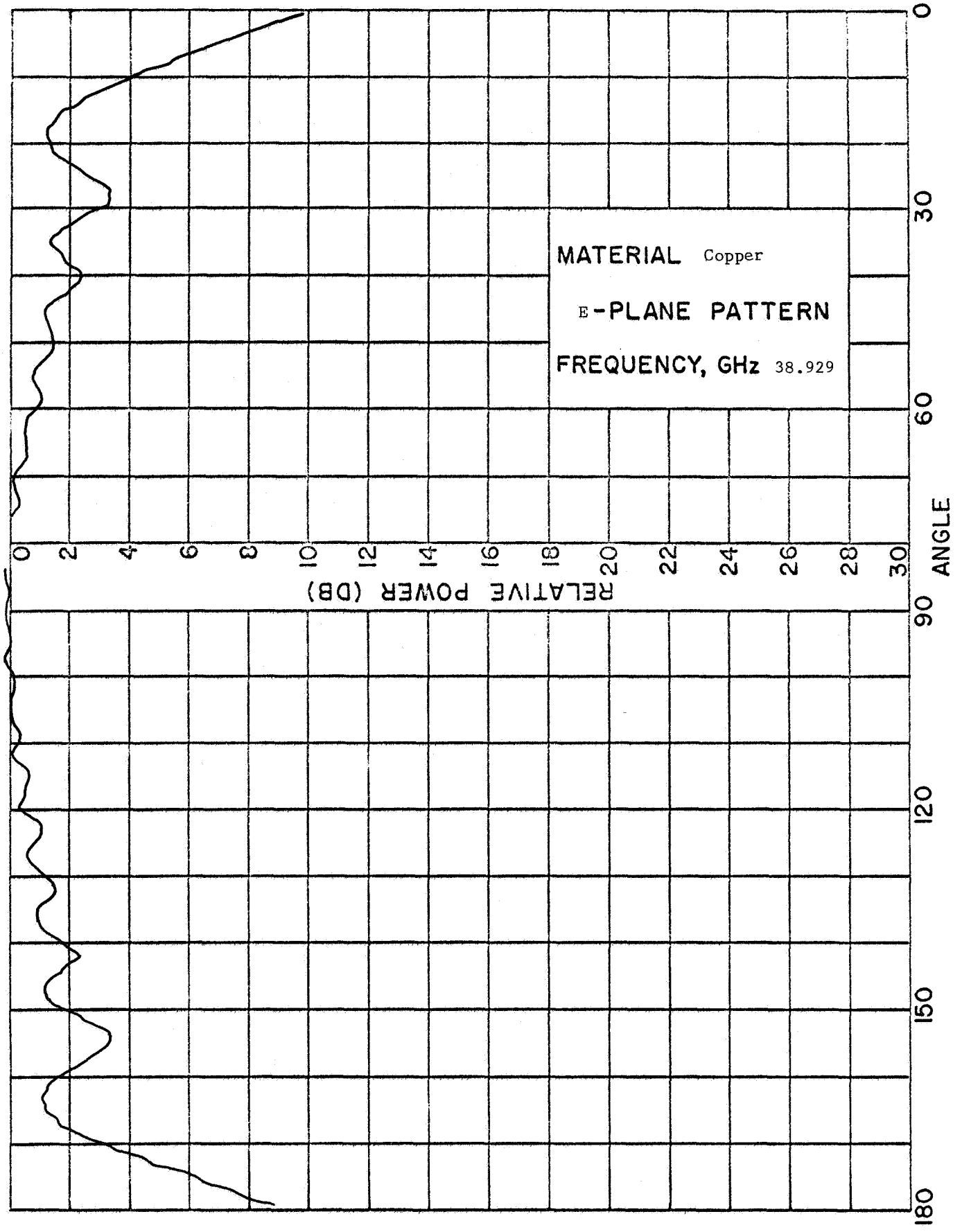
MATERIAL Copper
E-PLANE PATTERN
FREQUENCY, GHz 38.929
RELATIVE POWER (DB)
0
2
4
6
8
10
12
14
16
18
20
22
24
26
28
30
ANGLE
0
30
60
90
120
150
180

Fig. 3.6

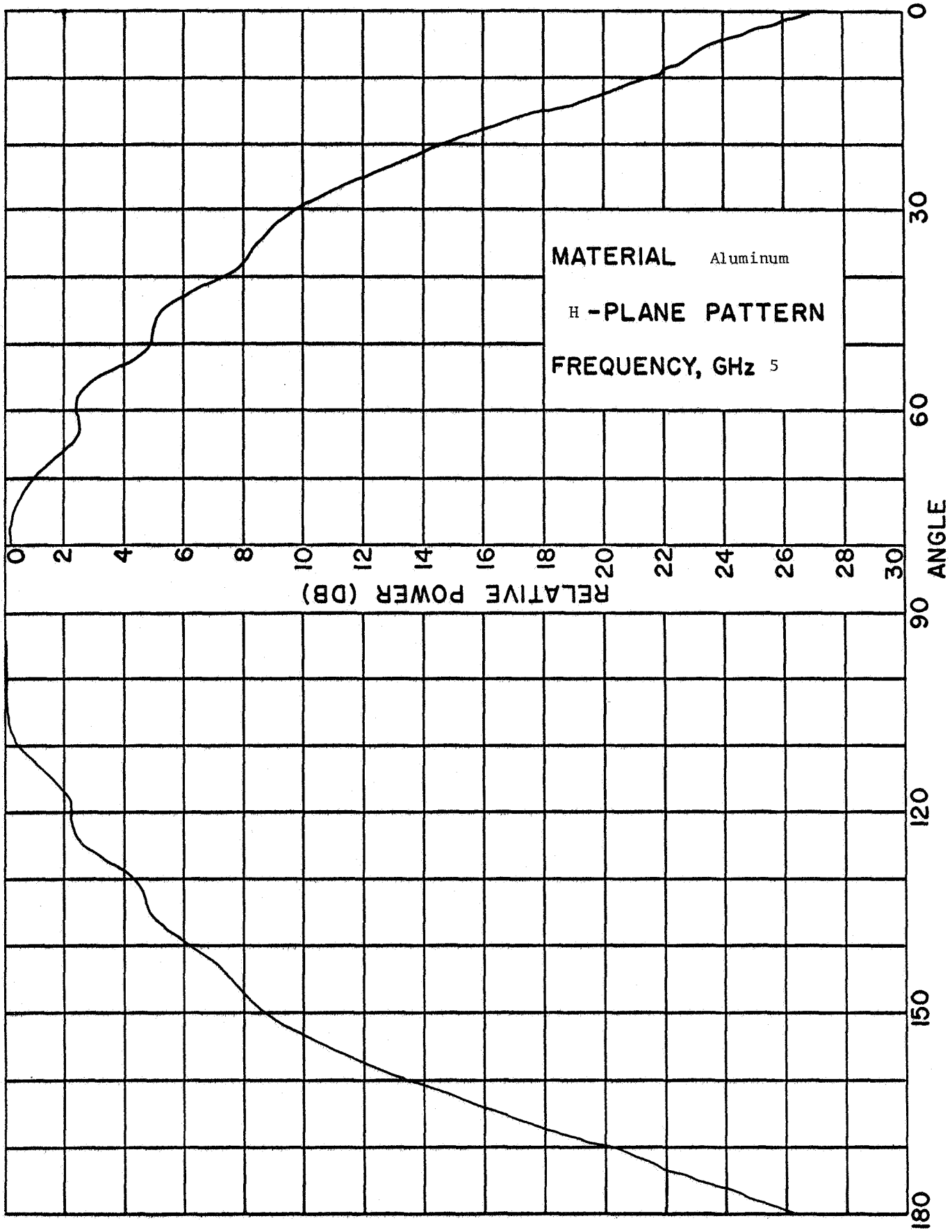
MATERIAL Aluminum
H-PLANE PATTERN
FREQUENCY, GHz 5
0
2
4
6
8
10
12
14
16
18
20
22
24
26
28
30
RELATIVE POWER (DB)
0
30
60
90
120
150
180
ANGLE

Fig. 3.7

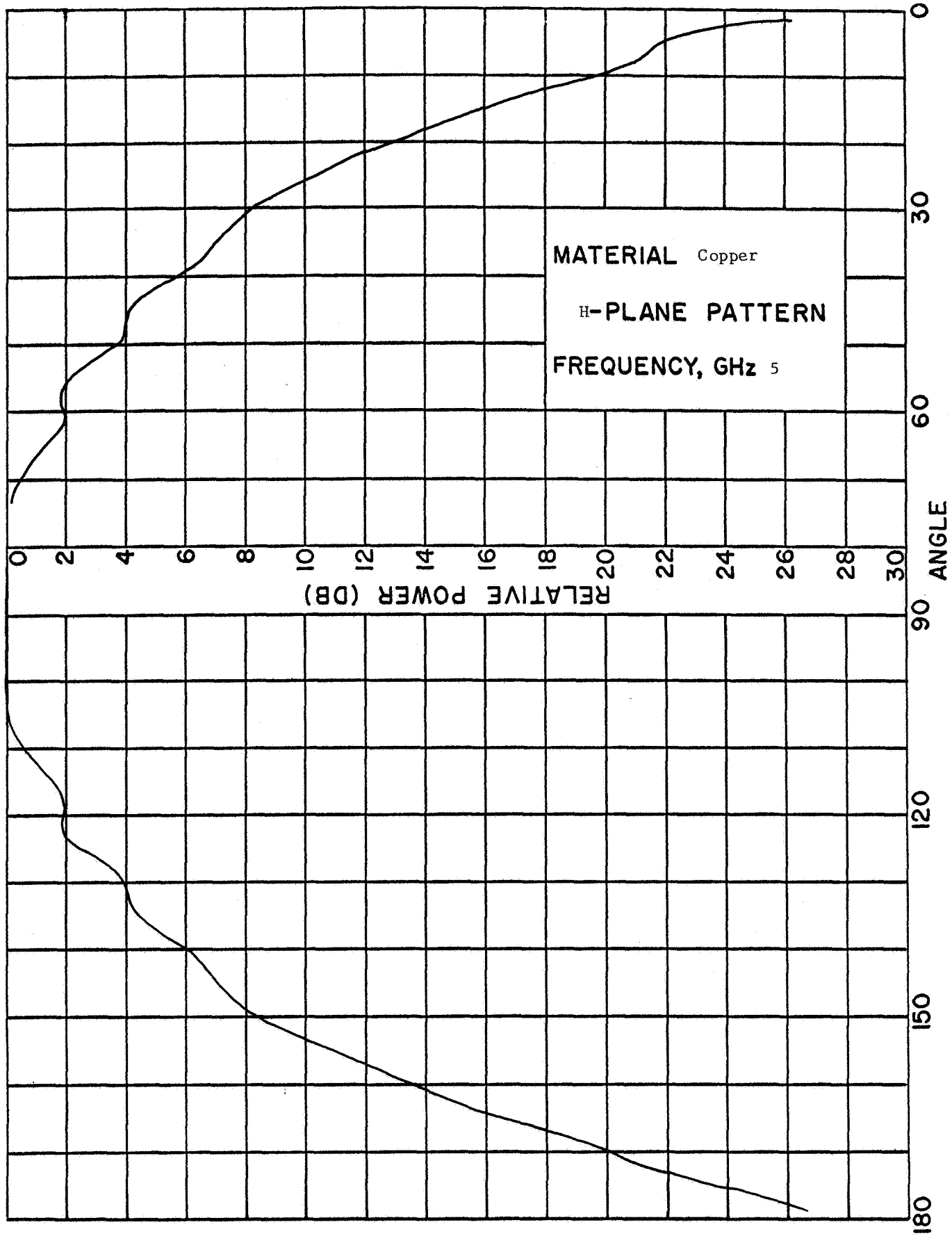
MATERIAL Copper
H-PLANE PATTERN
FREQUENCY, GHz 5
RELATIVE POWER (DB)
0 2 4 6 8 10 12 14 16 18 20 22 24 26 28 30
ANGLE
0 30 60 90 120 150 180

Fig. 3.8

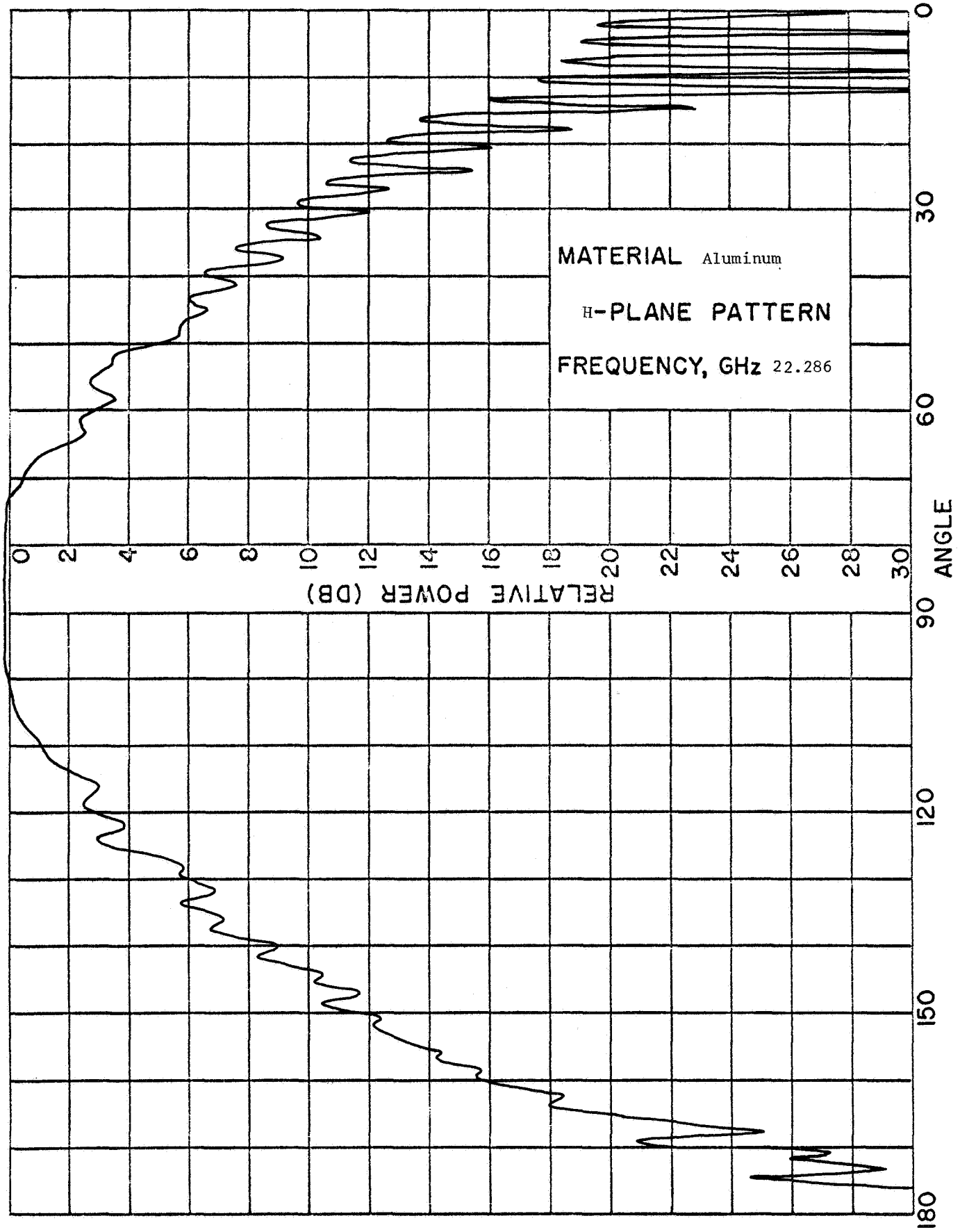
MATERIAL Aluminum
H-PLANE PATTERN
FREQUENCY, GHz 22.286
RELATIVE POWER (DB)
0 2 4 6 8 10 12 14 16 18 20 22 24 26 28 30
ANGLE
0 30 60 90 120 150 180

Fig. 3.9

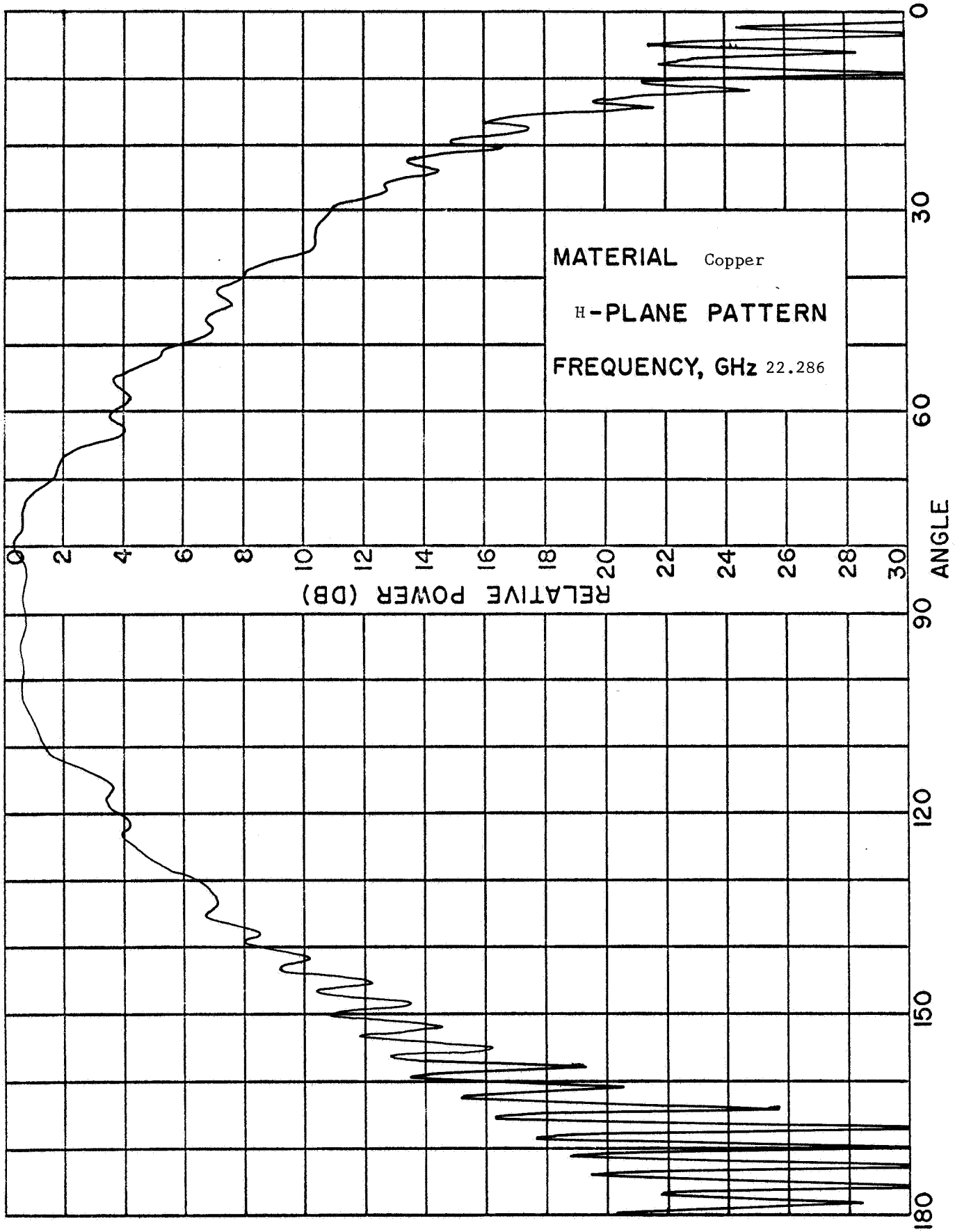
MATERIAL Copper
H-PLANE PATTERN
FREQUENCY, GHz 22.286
RELATIVE POWER (DB)
0
2
4
6
8
10
12
14
16
18
20
22
24
26
28
30
ANGLE
0
30
60
90
120
150
180

Fig. 3.10

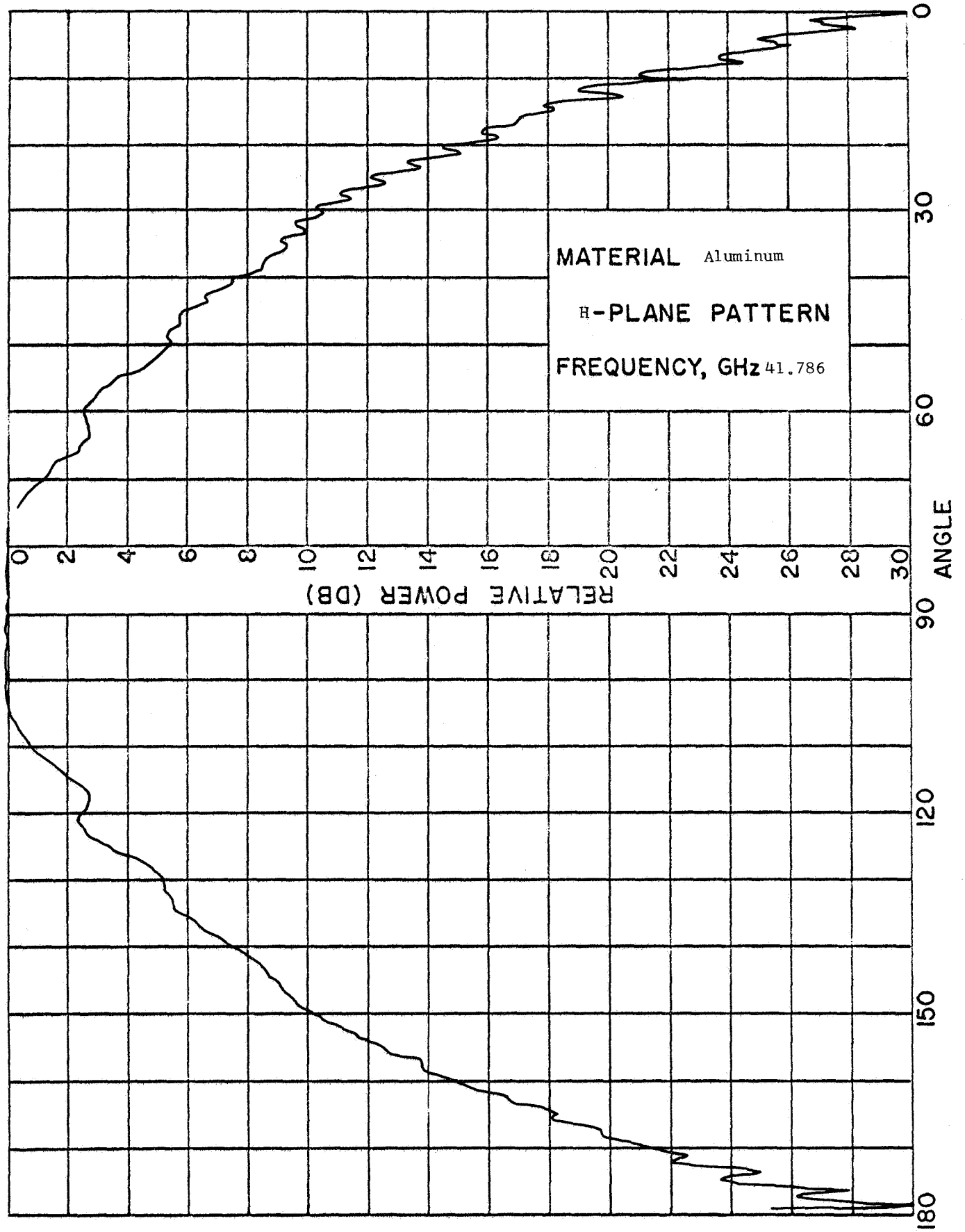
MATERIAL Aluminum
H-PLANE PATTERN
FREQUENCY, GHz 41.786
RELATIVE POWER (DB)
0
2
4
6
8
10
12
14
16
18
20
22
24
26
28
30
ANGLE
0
30
60
90
120
150
180

Fig. 3.11

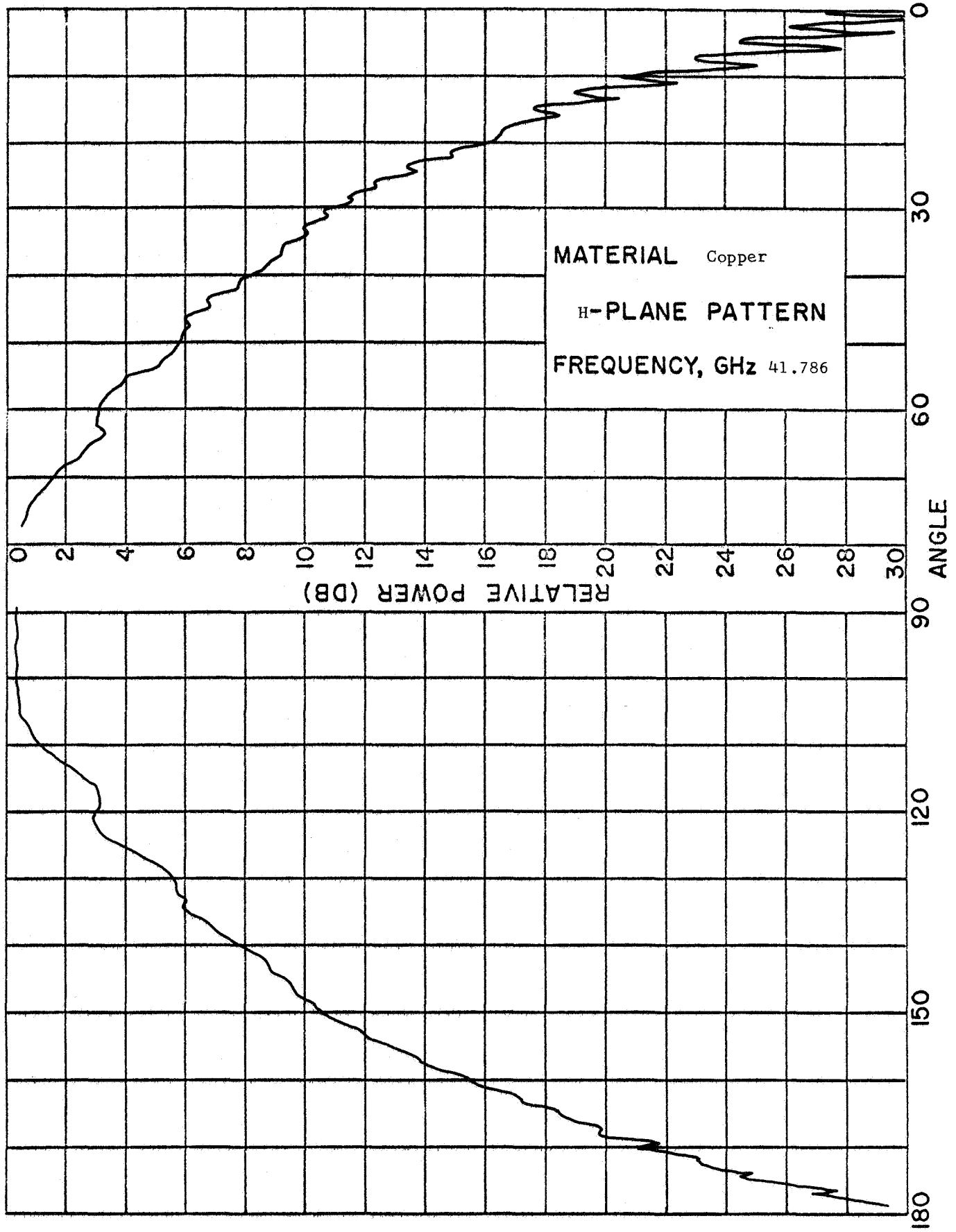
MATERIAL Copper
H-PLANE PATTERN
FREQUENCY, GHz 41.786
RELATIVE POWER (DB)
0
2
4
6
8
10
12
14
16
18
20
22
24
26
28
30
ANGLE
0
30
60
90
120
150
180

Fig. 3.12

relative directivity was obtained for all patterns by integrating to obtain the area under each of the twelve patterns. No significant differences in directivity among the six E-plane patterns, or among the six H-plane patterns, were noted.

It appears quite safe to conclude from the theoretical developments and the measurements described in this chapter that one is safe in frequency scaling antennas, certainly up to 40 GHz and probably even to much higher frequencies, in pattern measurements. It also appears that aluminum or copper may be used as desired without affecting the resulting patterns.

References for Chapter 3

1. J. D. Kraus, "Antennas," McGraw-Hill Book Company, Inc., New York, N. Y., 1950, pp. 485-486.

2. J. A. Stratton, "Electromagnetic Theory," McGraw-Hill Book Company, Inc., New York, N. Y., 1941, p. 15.

3. R. F. Harrington, "Time-Harmonic Electromagnetic Fields," McGraw-Hill Book Company, Inc., New York, N. Y., 1961, pp. 51-54.

Chapter 4

THE EFFECT OF SURFACE ROUGHNESS ON PATTERNS

Introduction

It was shown theoretically and experimentally in Chapter 3 that conductivity effects in frequency scaling are not significant for the slotted ground plane antenna using either copper or aluminum ground planes, frequencies up to 40 GHz, and frequency scaling factors up to 8; and probably, from the theoretical development, we can make the same statement for most antenna types with even higher frequencies and scale factors.

In this chapter we wish to consider briefly surface roughness effects on patterns. Beckmann and Spizzichino in discussing scattering from objects assert that "it is a well-known fact that the roughness of a surface modifies the scattered field for more than its electrical properties."[1] This brings out a problem which exists in connection with surface roughness effects. Much of the theoretical and experimental work on roughness described in the literature is concerned with scattering from rough objects or rough terrain, or propagation over rough terrain. In an extensive bibliography given by Beckmann and Spizzichino[1] no reference was discovered dealing with patterns radiated by antennas with rough surfaces. We are thus forced to make the reasonable assumption in this chapter that a degree of roughness that would produce a significant effect in the scattered field pattern of an object would also produce a significant effect in the total field if a primary radiator (such

as a slot) were located near or on the same surface.

Surface Roughness

Surface roughness is measured as an average deviation from a mean center line at the surface. It is commonly measured in microinches. It is a function of machining methods and materials used. Table 4.1 gives typical values of roughness which might be expected for various machining methods.[2]

Operation	Roughness (microinches), Range
Saw cut, Torch cut	1000 - 250
Turning, Shaping, Milling, Boring	500 - 16
Drilling	350 - 40
Reaming	250 - 18
Grinding	175 - 5
Honing	40 - 2.5
Lapping, Polishing	30 - 0.5

Table 4.1

Surface Roughness and Skin Depth

One criterion which can be applied to an antenna surface is that the surface roughness should be less than the skin depth. Table 4.2 gives the skin depth in microinches for copper and aluminum at 10 GHz and 40 GHz.

	10 GHz	40 GHz
Aluminum	33.4	16.7
Copper	26	13

Table 4.2

Skin Depth (microinches)

It may be seen that to meet this criterion even at 10 GHz one might find it necessary to lap and polish antenna surfaces. It has been reported[3] that in England the Defence Research Telecommunications Establishment has required the surface roughness of models to be better than 12 microinches, and similar requirements have been used by the Roay Radar Establishment and Royal Aircraft Establishment. At a later time this requirement was relaxed to 30 microinches at X-band by the RAE. A factor in this choice seems to have been the desire to keep the rms surface roughness amplitude smaller than the skin depth.

Back-Scattering of Rough Objects

It is reported by Senior[3] that Dawson of the Defence Research Telecommunications Establishment has stated that if model surface roughnesses exceeded 20 or 30 microinches a change in echoing area could be detected. On the other hand Senior,[3] and Hiatt, Senior, and Weston[4] found in measurements of rough spheres and cone-spheres that greater roughnesses can be used without significantly affecting the back-scattering cross sections.

Hiatt, et al,[4] measured the back-scattering from a quite rough 25 cm sphere, having a surface roughness of the order of 9000 microinches and a roughness width of about 3 mm, as a function of rotation angle of the

sphere. They found that at 2.87 GHz the roughness had no appreciable effect on cross-section; at 9.70 GHz deviations from smooth-sphere values were as great as 1.5 dB; at 22.97 GHz as great as 3.9 dB; and at 31.97 GHz as great as 6.4 dB[3]. At the highest frequency the ratio of surface roughness to wavelength is

$$\frac{\delta}{\lambda} \approx 0.024$$

In later measurements Senior[3] used a rough cone terminated by a portion of a rough sphere. The cone had a half-angle of 12.5° and the cap sphere a radius of about 4.5 cm. These measurements were made more difficult to interpret by faulty construction which resulted in a significant degree of asymmetry in the model, and Senior also stated that their data were not analyzed as completely as might be desired. Senior concluded that at X-band the back-scattering cross-section measured as a function of cone aspect angle changed by an average value of about 2 dB when compared to the smooth body curve. The value of these measurements was further decreased by a failure to give the value of surface roughness used in the measurements.

In summing up the measurements reported in Reference 3 and using the experience gained in previous measurements[4], Senior suggested that a high degree of surface finish is not essential for model scattering work. In his opinion a surface finish of the order of 10^{-3} wavelengths should affect the dominant back-scattering pattern (with the model oriented to produce maximum back-scattered energy) by less than one dB, and the minimum of the back-scatter pattern (model oriented to produce minimum back-scattered energy) by no more than one or two dB.

In Senior's opinion a similar tolerance on length dimensions of the model ($10^{-3}\lambda$) should be more than adequate.

Significant features of the measurements reported by Hiatt and by Senior are that they are back-scattering as a function of model aspect, and the cross-section as a function of aspect angle for the bodies used does not vary by more than a few dB. One might well find that bistatic cross-sections are seriously affected by surface roughness, particularly in deep pattern minima. One might also find that antenna radiation patterns are affected seriously by surface roughness, again perhaps most seriously at pattern minima.

It appears most appropriate to conclude from the preceding discussion that the effect of surface roughness on antenna patterns is at present not known very well. The safe course to follow in constructing antennas thus is to try to obtain the best surface finish possible within reasonable economic and time limits.

References for Chapter 4

1. P. Beckmann and A. Spizzichino, "The Scattering of Electronmagnetic Waves from Rough Surfaces," Pergamon Press (MacMillan), New York, N. Y., 1963, p. 5.

2. R. A. Lindberg, "Processes in Materials of Manufacture," Allyn and Bacon, Inc., Boston, 1966.

3. T. B. A. Senior, "Surface Roughness and Tolerances in Model Scattering Experiments," IEEE Transactions on Antennas and Propagation, vol. AP-13, no. 4, pp. 629-636, July 1965.

4. R. E. Hiatt, et al, "A Study of Surface Roughness and its Effect on the Backscattering Cross Section of Spheres," Proceedings of the IRE, vol. 48, no. 12, pp. 2008-2016, December 1960.

Chapter 5

EVALUATION AND USE OF ANECHOIC ROOMS

Introduction

It is well known that if it is desired to measure deep nulls in an antenna pattern the undesired reflections in an anechoic room must be kept extremely small when compared to the direct radiation from the transmitter. Buckley[1] points out, for example, that reflections must be 50 dB below the direct-ray level to allow -30 dB nulls to be measured to within $\pm$ 1.4 dB. Consideration of such examples quickly makes it clear that measurement of the quality of an anechoic room, which would involve measurements of -50 dB reflections (or smaller) in the presence of the direct ray, is exceedingly difficult for high-quality rooms. Various methods of evaluating anechoic room performance have been devised and presented in reports and in the literature. A good discussion of these measurements has been given by Buckley[1,2,3] and will not be repeated here.

Instead we present in this chapter a method, involving coding of the transmitted signal, which can be used for two purposes: (1) evaluating the quality of an anechoic room, and (2) decreasing the effect of undesired reflections while carrying out pattern measurements.

In this method the transmitted carrier is modulated with a binary sequence. The local oscillator signal is similarly modulated with the same binary sequence and delayed by an appropriate time. The coded carrier and local oscillator signals are then mixed at the receiving

antenna (whose pattern is being measured). If the time delay in the local oscillator path is chosen correctly the direct-ray signal and the local oscillator signal will mix properly to give an output 1F. However, signals reflected from the chamber walls, arriving at a different time and hence out of binary code phase (not RF phase) with the local oscillator signal, will be suppressed by the mixing action. Similarly a different choice of local oscillator path delay would lead to emphasis of the reflected waves in the chamber and suppression of the direct ray. This would allow measurements of the reflections.

Pattern Measurement and Chamber Evaluation System

Consider the system of Fig. 5.1. With the exception of the code generator and modulators this is a common system for measuring antenna patterns in an anechoic chamber. A CW signal is transmitted toward the receiving antenna whose pattern is being measured. The local oscillator is supplied to a mixer immediately following the receiving antenna, and the resulting 1F signal is amplified and detected. In the system of Fig. 5.1 the CW and LO signals are modulated by a binary sequence, and the LO signal is delayed in a controlled manner.

If the modulating signal produced by the code generator is

$$M(t)$$

the output of the upper balanced modulator is

$$M(t) \cos \omega_c t$$

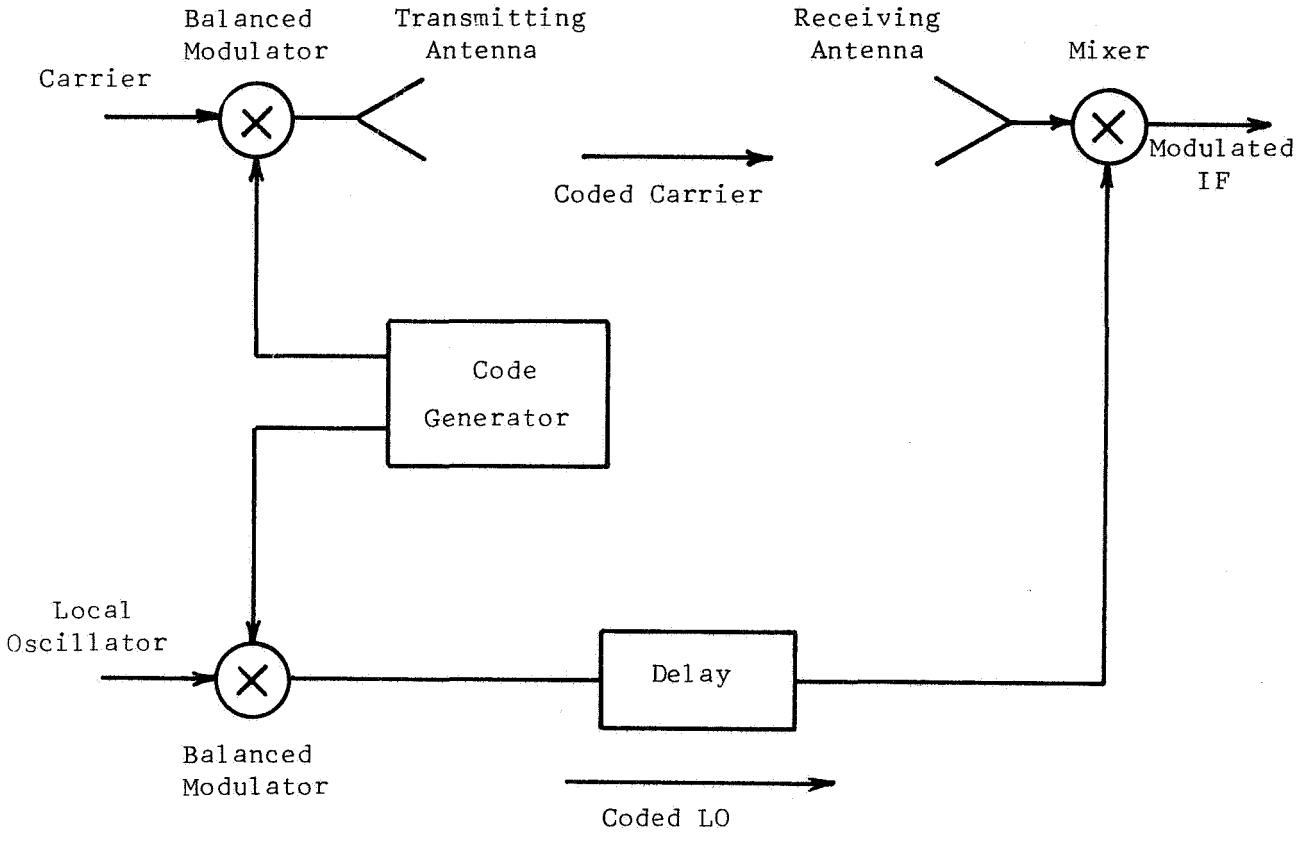

Fig. 5.1

System for Pattern Measurement and Chamber Evaluation

and the output of the lower modulator is

$$M(t) \cos \omega_{LO} t$$

where we neglect any phase angles in the CW and LO signals and any amplitude differences in the modulated signals.

After the time delays in the CW and LO paths the signals applied to the final mixer are

$$M(t) \cos \omega_c t$$

and

$$M(t+\tau) \cos \omega_{LO} t$$

and the output is

$$M(t)M(t+\tau) \cos (\omega_c - \omega_{LO})t$$

This is the modulated IF output of Fig. 5.1

Envelope detection and integration of this IF signal with a commonly used envelope detector such as would be available in any standard microwave receiver gives an output

$$V(\tau) = \int M(t)M(t+\tau)dt \qquad (5.1)$$

Now Eq. (5.1) is the autocorrelation function of the modulating waveform, and thus has a peak at $\tau = 0$, or if the modulating wave is periodic, peaks will occur for τ equal to a multiple of the period. The ideal choice of a modulating waveform is one which would have a very high peak in its autocorrelation function at $\tau = 0$ and low values for all other

values of τ. Then the direct wave from the transmitting antenna, arriving at the same time as the LO signal, would give a receiver output. On the other hand, waves reflected from the walls of the anechoic chamber, and thus delayed in time from the direct wave, would give a non-zero value of τ in Eq. (5.1) and thus a very small receiver output.

An example will illustrate this. Consider that the modulation of Fig. 5.1 is a rectangular pulse. For a properly chosen LO signal delay a pulse of the carrier arrives at the final mixer at the same time as a pulse of the LO, and an IF output is obtained. If the times of arrival differ by one pulse width or greater, as would be true for some waves reflected from chamber walls, the IF output is zero. Pulse modulation has the disadvantage of low average power, and a better modulation waveform is discussed in the next section.

Two disadvantages of this system must be mentioned. One is the increased bandwidth required for the antennas, of the order of hundreds of megacycles. The other is loss in the balanced modulators, perhaps 6 dB, which will decrease the S/N ratio at the receiver. If this is significant the modulation can be carried out before a final TWT amplifier.

The Pseudo-Random Binary Sequence

A typical modulating waveform suitable for our purposes is shown in Fig. 5.2. This is a periodic binary waveform with the example shown having a period of 7 bit-times. The autocorrelation function for the example waveform of Fig. 5.2 is shown in Fig. 5.3, assuming the amplitudes in Fig. 5.2 are $\pm$ 1. It is obvious that modulation of a carrier by this waveform changes only the carrier phase and thus does not decrease

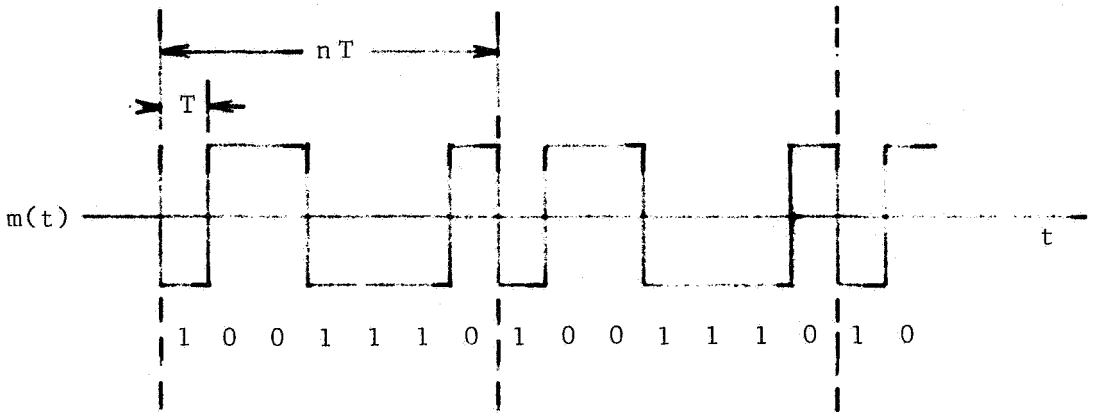

Fig. 5.2

Binary Modulating Sequence

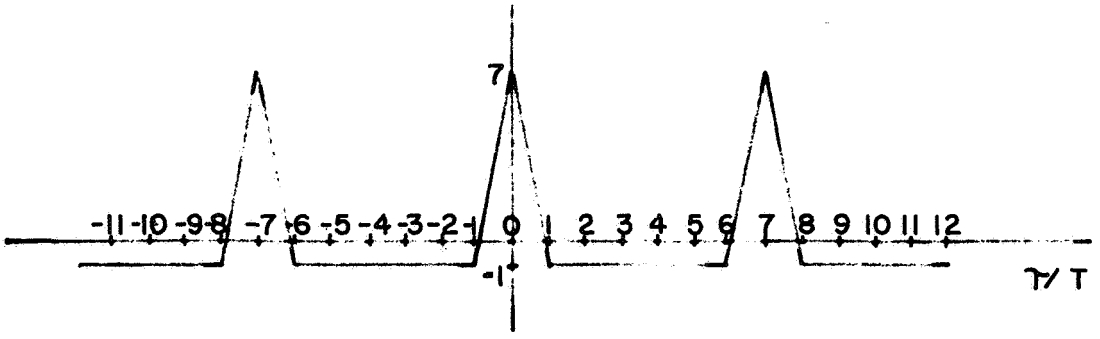

Fig. 5.3

Autocorrelation Function of m(t)

average power of the carrier, except for the modulator losses discussed earlier.

The waveform of Fig. 5.2 is a time waveform corresponding to a binary sequence of 1's and 0's, also given in Fig. 5.2. It is a 7-bit example of a maximum-length linear shift register sequence and because of various properties has been called a pseudo-noise code[4] or a pseudo-random code[5]. Highly significant properties of the time waveform corresponding to such a code are that the autocorrelation function of an n-bit code has a peak value of n, repeating at $\tau = nT$, and a minimum value of -1 first reached at $\tau = T$ and maintained until the next peak begins. This is illustrated in Fig. 5.3.

Consider a longer code than the 7-bit code of Fig. 5.2 as an example. Let this be a 127-bit code with a bit time of 10 nsec, corresponding to a bit rate of 100 MHz. Such a code is quite feasible. If we neglect the small negative value of the autocorrelation function we find that the voltage emphasis given to signals at the autocorrelation peak, compared to off-peak signals is

$$20 \log 127 = 42.1 \text{ dB}$$

Table 5.1 shows the off-peak suppression for various values of τ. These τ values are also related to path-length differences in air.

τ, nsec	path difference, ft.	suppression, dB
0	0	0
1	0.99	.9
2	1.97	1.9
3	2.96	3.1
4	3.94	4.5
5	4.92	6.1
6	5.91	8.1
7	6.89	10.6
8	7.88	14.2
9	8.87	20.6
10	9.85	42.1

Table 5.1

Suppression of Undesired Signals

Table 5.1 is calculated from the autocorrelation equation easily obtained from a generalization of Fig. 5.3.

$$V(\tau) = 20 \log \left(1 - \frac{\tau}{T} \frac{N+1}{N}\right)$$

where N is the number of bits in the binary sequence, τ is the time delay in nanoseconds, and T is one bit time in nanoseconds.

We can see from Table 5.1 that if the LO signal time delay is set properly to emphasize the direct ray from transmitter to receiving antenna a signal reflected from a chamber wall and arriving, for example, 8 nanoseconds later than the direct signal will be suppressed by 14.2 dB.

Consider an anechoic chamber which is 100 ft long and 40 ft wide. A single-bounce ray reflected from a side wall at the mid-way point of the chamber will have a path length of

$$2 \sqrt{50^2 + 20^2} \approx 108 \text{ ft.}$$

Table 5.1 shows that this single-bounce ray will be suppressed by an

amount between 14 and 20 dB.

Anechoic Chamber Evaluation

The preceding discussion was mainly concerned with the use of coded signals to emphasize the direct ray from transmitter to receiver and suppress wall-reflected rays. However, one could obviously change the delay introduced into the LO line and thereby suppress the direct ray. This would lead to a knowledge of chamber reflections as a function of time delay. If this is combined with directional information obtainable from a directive receiving antenna it appears to offer a very powerful method for evaluating anechoic chambers.

Generation of Maximum-Length Binary Sequences

Not all binary modulating sequences lead to waveforms having the desirable autocorrelation function typified by Fig. 5.3. However, as pointed out, such autocorrelation functions are properties of time waveforms described by maximum-length linear shift register sequences, allowing a binary 1 to represent a unit negative voltage and a 0 to represent a unit positive voltage. Such sequences have the properties that (1) in each period of the sequence the number of 1's differs from the number of 0's by at most 1, (2) among the runs of 1's and 0's in a period, one-half the runs of each kind are of length one, one-fourth are of length two, one-eight of length three, etc., and (e) if a period of the sequence is compared, term by term, with any cylic shift of itself, the number of agreements differs from the number of disagreements by at most 1.[4]

Fig. 5.4 shows a shift register capable of generating a 15 bit sequence

100010011010111

Each of the four stages of the shift register contains a 1 or a 0 and transfers this to the next stage at each clock pulse. The half-adder stage has an output according to the logic

x_3	x_4	Output
0	0	0
0	1	1
1	0	1
1	1	0

An n-stage shift register can generate a maximum length sequence of

$$p = 2^n - 1$$

bits.

The requirements of a sequence generator for anechoic chamber evaluation are quite severe for commonly available shift registers and half adders. In our laboratory an asynchronous variation of the system of Fig. 5.4 has been built and tested. The synchronously-operating shift register was replaced by a TWT amplifier and delay line. This required the use of a carrier (in our case at X-band) inserted by a mixer prior to the first "stage." The half-adder of Fig. 5.4 was replaced by a mixer. This system generates a 127-bit code with a bit-time of about 7 nanoseconds. This code is well-suited for chamber evaluation or for suppression of reflected rays in a chamber.

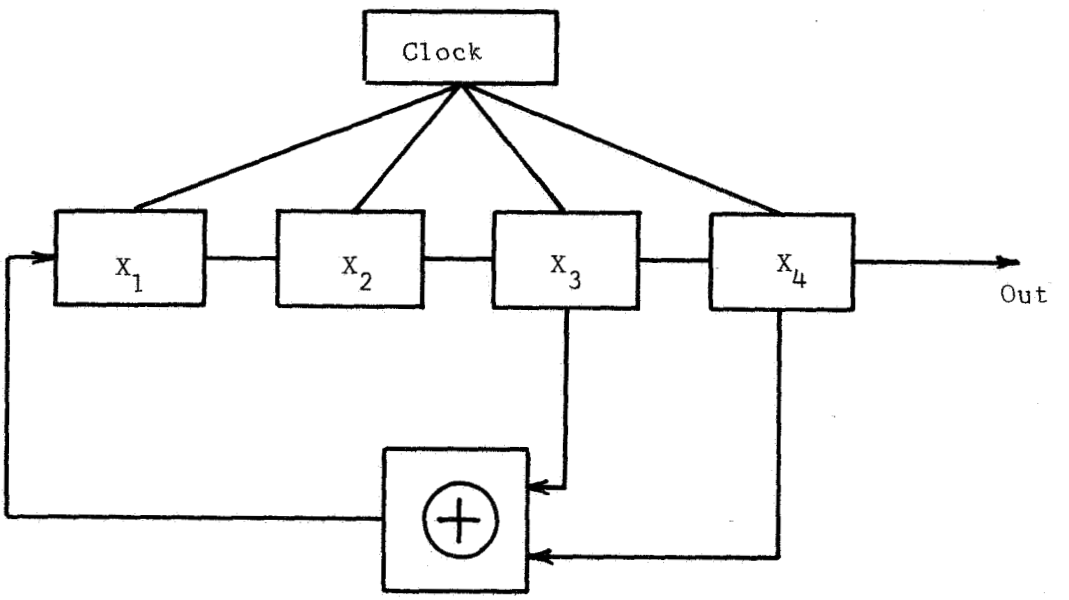

Fig. 5.4

Shift-Register Sequence Generator

Another code generator, which has been considered (and experimentally developed for a 3-bit code) utilizes a repetitive pulse and a tapped delay line, as indicated by Fig. 5.5. It appears feasible to build such a delay line code generator for the sequence lengths necessary for anechoic chamber evaluation.

Conclusions

The foregoing discussions have shown the great advantages of using a pseudo-random binary modulating signal in using an anechoic chamber for pattern measurements and in evaluating the chamber reflections. The major advantage is in suppressing wall reflections when the system is being used to measure patterns and in suppressing the direct transmitter-receiver ray when the system is used to evaluate chamber reflections. This system is useful for both indoor and outdoor ranges.

References for Chapter 5

1. E. F. Buckley, "The Design and Evaluation of Microwave Anechoic Chambers," paper presented at joint meeting of IRE Professional Groups, PGME, PGMTT, and PGAP, Chicago, Illinois, April 8, 1960.

2. E. F. Buckley, "Microwave Reflectivity Measurements -- Theory and Practice," Electronics Design, March 15, 1962.

3. E. F. Buckley, "Outline of Evaluation Procedures for Microwave Anechoic Chambers," Microwave Journal, vol. 6, no. 8, pp. 69-75, August 1963.

4. S. W. Golomb, "Digital Communications," Prentice-Hall, Inc., Englewood Cliffs, N. J., 1964.

5. R. S. Berkowitz, "Modern Radar," John Wiley and Sons, Inc., New York, N. Y., 1965.

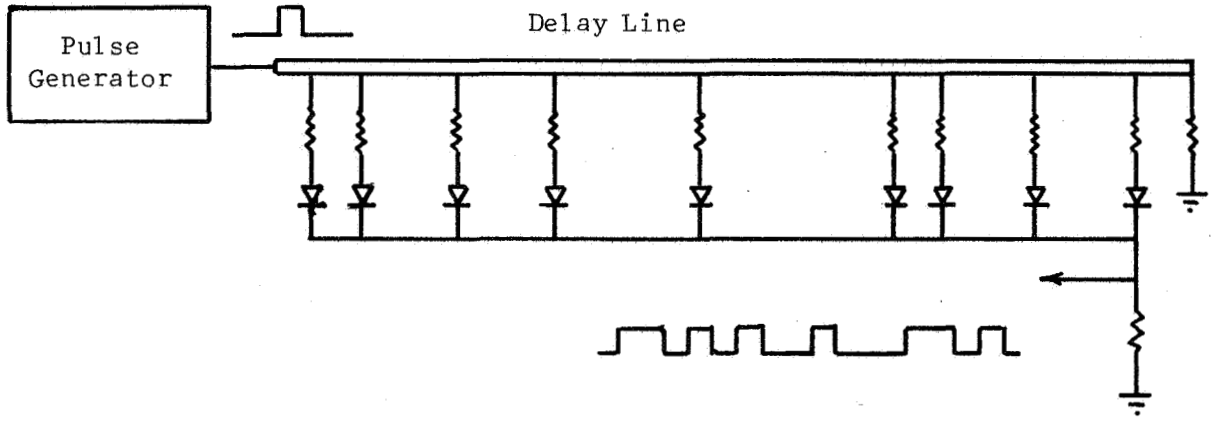

Fig. 5.5

Delay-Line Sequence Generator